MODELING OLEFIN POLYMERIZATION USING MONTE CARLO SIMULATION: DETAILED COMONOMER DISTRIBUTION

by

Mohammad A. Al-Saleh

A thesis

presented to the University of Waterloo

in fulfillment of the

thesis requirement for the degree of

Master of Applied Science

in

Chemical Engineering

Waterloo, Ontario, Canada, 2006

I hereby declare that I am the sole author of this thesis. This is a true copy of the thesis, including any required final revisions, as accepted by my examiners.

I understand that my thesis may be made electronically available to the public.

Abstract

In recent years there have been many efforts to develop and expand the ability of mathematical models capable of describing polymerization systems. Models can provide a key competitive advantage for the industry and research in terms of production and technology development. As new resins are continuously produced to meet the requirement of final applications and processability, it is imperative to pursue strong polymer characterization with special attention to detailed analysis of polymer microstructure. The microstructure of polyolefin is defined by its distribution of molecular weight, chemical composition, branching topology, and stereoregularity.

In this work, a Monte Carlo simulation model was developed to describe the polymerization mechanisms of olefin homopolymerization and copolymerization using single-site coordination catalyst. The mathematical model is meant to describe molecular weight and chemical composition distribution in copolymerization system. More specifically, this research work gives a detailed study of the molecular structure for ethylene-α-olefin copolymer.

The chemical and physical properties of copolymers are influenced not only by their average composition, but also by the monomer sequence distribution along the polymer chains. Predicting the molecular weight and comonomer distributions can lead to a better understanding of the possible morphology in solid stated because they are considered to be the main structural parameters that affect the crystallinity of polymeric materials. As a consequence, final physical properties such as the tensile properties of a copolymer could be controlled by the ratio of crystalline species in the polymer.

This work is considered to be a useful tool that enables us to understand and explore specific polymerization catalytic system. Being able to describe the short chain branching and the monomer sequence distribution as a function of chain length enables us to have a better control over semi-batch polymerization reactors.

Acknowledgments

I am grateful to all of you that have surrounded me with their love and care. I thank my family for their courage and patience to overcome all the problems blended with new flavor in this short trip of our lives.

I am grateful and thankful to my friend and supervisor Prof. Leonardo C. Simon. I thank him for giving me the opportunity to learn from him and become one of his students. Prof. Simon has a dedicated professional personality with a bright vision of the future. I am confident that his creativity will always direct him to elite.

I thank Prof. Thomas Duever and Prof. Joao Soares for their comments and inputs. Prof. Soares is a well known icon in the polymer research and I am glad that I had the chance to meet with him to discuss my work. Prof. Duever is a very open minded person with a lot of knowledge and experience. Once I first talked with him I discovered a man who is full of love and care. His position and professional career did not affect his personality when you talk to him you find a man who is down to earth and that's how scientists should be.

Dedication

To my precious,

Jasmine and Haneen

Table of Content

vii

List of Figures

List of Tables

Selected Abbreviations

A = transition metal center

L = ligands

X = halogen

AlR_3 = alkylaluminum cocatalyst

R = alkyl group

C = catalyst

Al = co-catalyst

C^* = active site

M = monomer

n = number of active-site types in a multiple-site catalyst

$P^*_{r=1}$ = growing polymer with one monomer insertion of chain length r = 1

$P^*_{r=1+n}$ = growing polymer of chain length r, where (r = 1+n) and (n) is the number of monomer insertions into the polymer chain after first insertion to the active site

H_2 = hydrogen

P^*_r = growing polymer of chain length r

P^*_{rH} = active site with hydrogen atom formed via chain transfer by β-hydride elimination

P^*_{rMe} = active site with methyl group formed via chain transfer by β-methyl elimination

P^*_H = active site with hydrogen atom formed via a chain transfer to hydrogen

P^*_{rM} = active site formed via a chain transfer to monomer

P^*_{Al} = active site with alkyl group formed via a chain transfer to cocatalyst

D_r = dead chain with a saturated end

$\overline{\overline{D}}_r$ = dead polymer chain containing a terminal vinyl unsaturation

D_{Al} = dead polymer chain formed via a transfer to cocatalyst reaction

Cd = Deactivated catalytic site

[A] = Concentration of monomer A

[B] = Concentration of comonomer B

$[P_r^*]$ = Concentration of the active species

k_{pA} = Propagation reaction constant for monomer A

k_{pB} = Propagation reaction constant for monomer B

k_{tA} = Termination reaction constant for monomer A

k_{tB} = Termination reaction constant for monomer B

P_p = Probability of propagation

r_n = Number average chain length for branched copolymer

P_B = Probability of adding monomer B

Chapter 1 – Introduction

1.1 Research Capability

Polyolefins which include large volume materials such as polyethylene (PE), polypropylene (PP) and specialty materials are the largest volume commodity plastics with important applications in several sectors of our modern economy: energy, transportation, information technology, packaging and health care.

Control of molecular weight and chain branching has a direct effect on processing and final physical properties – thermal and mechanical. The production of polyolefin resins with coordination catalysts (Ziegler, Philips, single-site metallocene or late-transition metal systems) allows advanced control over the molecular structure.

It is very crucial for catalyst and product development for polymers to understand and analyze the microstructure of the polymers produced. This would allow us to take the necessary steps towards the needed modification in the process or the conditions of a catalytic system so that we reach to the desired final product specifications.

The model proposed here focuses on the homopolymerization of ethylene (monomer A) and on the copolymerization of ethylene (monomer A) and α-olefins (comonomer B). The objective is to predict the chemical composition of the polymeric chains produced by analyzing: a) chain length distribution; b) polydispersity; c) average comonomer (B) composition; d) comonomer composition distribution as function of chain length; e) monomer (A) and comonomer (B) segment length distribution as function of chain length; f) average triads distribution; g) triad distribution as a function of chain length; and h) the distribution of monomer and comonomer as a function of segment length.

The Monte Carlo model developed in this work was used to simulate steady state homopolymerization and copolymerization reactions in semi-batch reactors.

1.2   Thesis Outline

The thesis is divided into five main chapters. We start with the introduction followed by a literature review. Then we talk about the model description. After that we discuss the simulation results and end up with conclusions and recommendations.

Chapter 1   Focuses on the model capability and the parameters that would be predicted in the model.

Chapter 2   Presents a literature review for mainly coordination polymerization simulations with Monte Carlo modeling. This chapter emphasizes the importance of polyolefin polymerization and the importance of microstructure determination.

Chapter 3   Explains and describes the mathematical model of this thesis. It focuses on the homopolymer and copolymer models and how they were built. It will describe the logic for the model flow charts and explain how the parameters were calculated.

Chapter 4   Discusses the simulation results for the homopolymer model and copolymer model. Examples of the compositional drifts in which four semi-batch reactors were simulated are demonstrated.

Chapter 5   Gives general conclusions and future recommendations.

Chapter 2 -Literature Review

2.1 Polyolefins and Olefin Polymerization

2.1.1 Polyolefins

Olefin polymerization to produce polymers with different microstructure and properties is one of the most investigated areas in the industry and academia. Polyolefins are made from simple and easily available monomers and they contain only carbon and hydrogen (Pasch, 2001).

Polyolefins include large volume materials such as polyethylene (PE), polypropylene (PP) and specialty materials such as ethylene–propylene elastomers (EPR), ethylene-propylene-diene (EPDM), and polybutene-1 (PB). The major reasons behind the successful growth of the polyolefin industry are: their versatility with respect to physical and mechanical properties and application, the energy savings during their production and use in comparison with other materials and their low cost and the readily available raw materials (Galli and Vecellio, 2004).

2.1.2 Olefin Polymerization

Catalysis is the key to many chemical transformations. For successful industrial implementation of a catalyst certain prerequisites have to be fulfilled. The ideal catalyst has to combine high efficiency (i.e. effective use of starting materials, and minimal waste emission), high selectivity (i.e. optimal conversion to the desired product), and high total turnover (i.e. amount of product formed per given amount of catalyst) with durability, low toxicity, and low overhead expenditure (i.e. cheap catalyst, and little maintenance). Understanding how the catalyst structure and properties can affect these parameters, combined with chemical curiosity, is and will be the driving force for the future improvement and development of catalysis.

In 1935 Perrin discovered that ethylene could be polymerized at very high pressure into a semi crystalline solid. This discovery at the ICI laboratories led to the commercialization of low-density polyethylene (Whiteley, 2002).

In 1950 Hogan and Banks at the Phillips Petroleum Company discovered that highly crystalline polyethylene could be produced at moderate temperature and pressure with a catalyst containing chromium oxide on a silica support (Whiteley, 2002).

The industrial Ziegler-Natta catalyst has a long history that extends for more than four decades. The work on the olefin polymerization by Karl Ziegler in Germany and by Giulio Natta in Italy had a striking impact on the academic and scientific role of macromolecular chemistry as discipline, and on the great development of the polymer industry. Natta's work results focused on the relationship between the crystal structure of titanium chlorides and the overall activity and selectivity of the catalysts (Cerruti, 1999). In the 1950s the first commercial catalysts for the industry were introduced because of discoveries of $TiCl_3$ catalysts by Ziegler and Natta. The catalyst activities and stereospecificities were low and improvements had to be achieved. In 1968, the discovery of an $MgCl_2$-supported $TiCl_4$ catalyst brought about a breakthrough and led to innovative improvement of the properties of the polyolefins and significant cut in the production costs (Kashiwa, 2004).

Metallocene catalysts are able to make polyolefins at very high yields and with a degree of microstructural control not possible by using conventional Ziegler-Natta catalysts. In the 1950s metallocene catalysts were known. Work on zirconium metallocene-methylalumoxane catalysts was contributed by Kaminsky (Bubeck, 2002). The polymers produced with metallocene catalysts have narrower molecular weight distributions and more uniform incorporation of co-monomers than those produced by Phillips or Ziegler-Natta systems. Figure 2.1 shows the structure of metallocene catalyst which consists of a positively charged metal ion sandwiched between two negatively charged cyclopentadienyl anions.

4
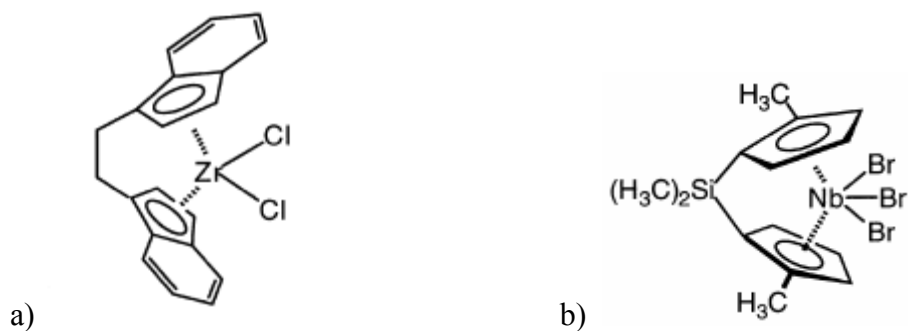
Figure 2-1 Typical metallocene catalyst structures, a) dichloro[1,2-di(η^5-inden-1-yl)ethane]zirconium b) tribromo[2,2'-(dimethylsilanediyl)-di(η^5-cyclopentadienyl)niobium (Salzer, 1999)

The continuous product property improvements have been boosted by technology development still very much in progress. Figure 2.2 shows the progress of technology in the development of polyethylene.
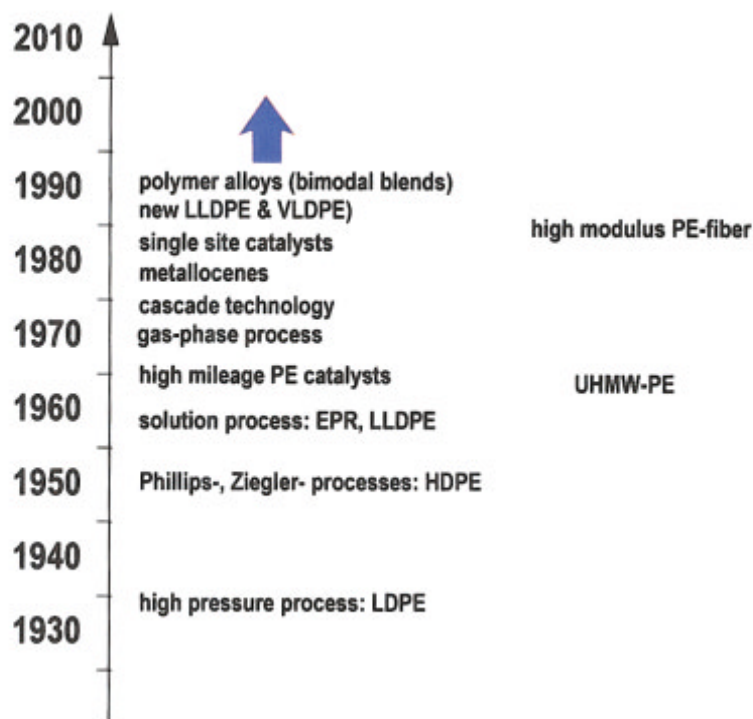
Figure 2-2 Polyethylene evolution (Galli and Vecellio, 2004)

2.1.3 Product Characteristics and Catalyst Consumption for Ti, Cr & Metallocene Catalysts

The properties of product such as polyethylene depend on the parameters of the polymerization process and on the type of the catalyst used in the manufacturing process. Ziegler catalysts (titanium based) usually yield chains with a small number of unsaturations, while the concentration of such functional groups is significantly higher when Phillips type catalysts (chromium based) are used. Metallocene catalysts make possible the production of a polymer with predetermined molecular structure and very low number of unsaturations (Epacher et al., 2000). The following (Table 2.1) lists the main catalyst types available commercially in the market. Figure 2.3 shows different types of catalysts for polyethylene commercial production and their global proportion in 2001.

Table 2-1 Examples of commercial catalyst types and general characteristics

Catalyst	Transition Metal	Characteristics
Metallocene	Zirconium	• Narrow molecular weight distribution
		• Co-catalyst required
		• Hydrogen as chain transfer agent
Ziegler	Titanium	• Relatively narrow molecular weight distribution
		• Aluminum alkyl co-catalyst required
		• Hydrogen is used for molecular weight control
Phillips	Chromium	• Relatively broad molecular weight distribution
		• Co-catalyst not required
		• Hydrogen is not used for molecular weight control
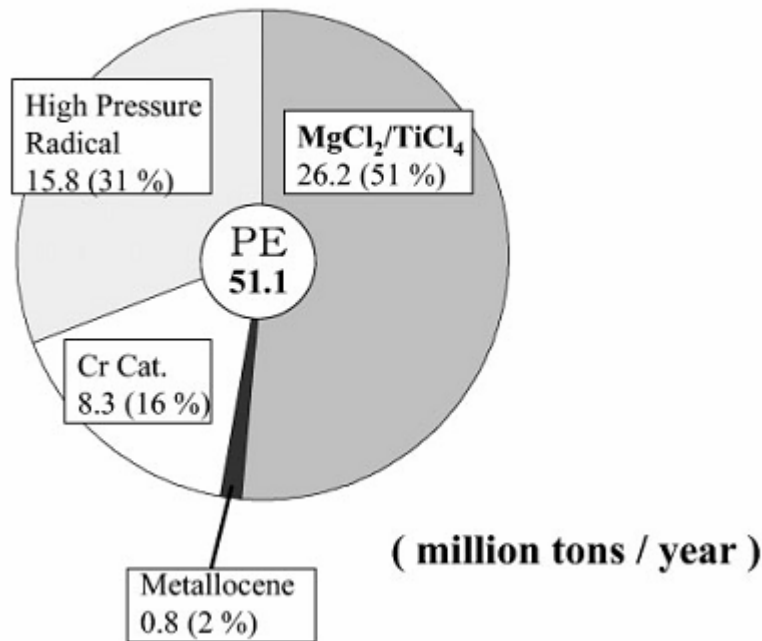
Figure 2-3 Catalysts for global PE production (Kashiwa, 2004)

2.1.4 Polyethylene (LDPE, LLDPE, HDPE)

Polyethylene (PE) is a high molecular weight hydrocarbon. Polyethylene includes low-density; linear low-density and high-density polyethylene. Polyethylene is produced by the polymerization of ethylene which results in an essentially straight chain, high molecular weight hydrocarbon. There are different ways of classifying PE. The polyethylenes are classified according to molecular weight and the relative degree of branching in their molecular structures, which can be controlled with selective catalysts.

Low-density polyethylene (LDPE) has more extensive branching, resulting in a less crystalline material. High-density polyethylene (HDPE) has minimal branching, which makes it more rigid and less permeable than LDPE. Linear low-density polyethylene (LLDPE) combines the toughness of low-density polyethylene with the rigidity of high-density polyethylene.

The largest tonnage plastic material produced worldwide is polyethylene which is produced commercially using free-radical initiators, Phillips-type catalysts, Ziegler-Natta catalysts, and more recently, metallocene catalysts. By combining several polyethylene made with metallocene catalysts, tailored end-use properties can be manufactured. This explains why metallocenes are playing a more and more important role in the polyethylene industry (Kou et al., 2005).

2.2 Coordination Reaction Mechanism and Kinetic Equations

Most industrial processes today still use heterogeneous Ziegler-Natta catalysts, although the market share of metallocene resins is increasing due to the enhanced properties of polyolefins made with these catalysts and the fact that polymerization process that were originally designed to use Ziegler-Natta catalysts can be converted to operate with metallocenes with minimal changes in the process.

Although traditional heterogeneous and homogeneous Ziegler-Natta catalysts are commonly used as the standard example of coordination polymerization, coordination catalysts include any complex of transition metals and organic ligands. Phillips catalysts are heterogeneous, chromium-based complexes that are not classified as Ziegler-Natta catalysts. Metallocenes are complexes of a transition metal - in most cases an early transition metal - and cyclopentadienyl or cyclopentadienyl-derivative ligands; late transition metal catalysts may have a variety of ligands containing heteroatoms such as phosphorous, nitrogen, or oxygen directly bonded to the transition metal.

The active site in coordination catalysts for olefin polymerization is a transition metal surrounded by ligands. The catalytic properties depend on the fine tuning between the transition metal and ligands in terms of geometry and electronic character. In most cases the active site is produced by the activation of a complex called pre-catalyst, or catalyst precursor. The creation of the active site by reaction of the pre-catalyst with an activator or cocatalyst is made just prior to its injection in the polymerization reactor or inside the polymerization reactor itself. The activator alkylates the pre-catalyst complex to form the

active sites and stabilizes the resulting cationic active site. Common activators are based on organoaluminum or organoborane compounds. Because the activator works as a Lewis acid (electron acceptor) it is also used to scavenge polar impurities from the reactor. These impurities are electron donors such as oxygen, sulfur, nitrogen compounds and moisture (water, oxygen, mercaptans) that poison the cationic active site. Figure 2.4 shows a simplified chemical equation for the activation mechanism and the correspondent equation.

$$\left(\begin{array}{c}L \\ L\end{array}\!\!>\!\!A\!\!<\!\!\begin{array}{c}X \\ X\end{array}\right) \quad + \quad AlR_3 \quad \longrightarrow \quad \left(\begin{array}{c}L \\ L\end{array}\!\!>\!\!\overset{\oplus}{A}\!\!-\!\!R\right) \quad + \quad AlR_2 X_2^{\ominus}$$

$$C \quad + \quad Al \quad \longrightarrow \quad C^*$$
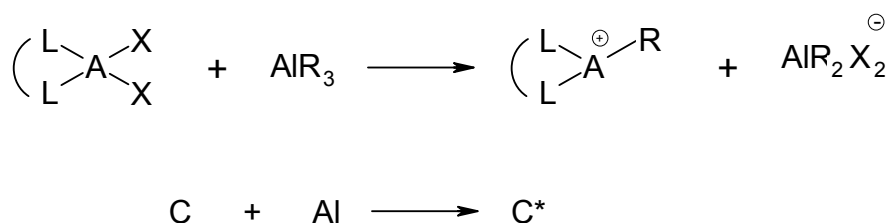
A = transition metal center (Ti, Zr, Ni,...)

L = ligands

X = halogen (Cl, Br)

AlR_3 = alkylaluminum cocatalyst

R = alkyl group (methyl, ethyl)

C = catalyst

Al = co-catalyst

C^* = active site

Figure 2-4 Catalyst activation by reaction of pre-catalyst and cocatalyst.

Polymerization with coordination catalysts proceeds via two main steps: monomer coordination to the active site and monomer insertion into the growing polymer chain, as illustrated in Figure 2.5. Prior to insertion, the double bond in the olefin monomer coordinates to the coordination vacancy of the transition metal. After the olefin is inserted into the growing polymer chain, another olefin monomer can coordinate to the vacant site and the process of insertion is repeated to increase the size of the polymer chain by one monomer unit at a time until chain transfer takes place. In the case of copolymerization,

there is a competition between the comonomers to coordinate to the active sites and to be inserted into the growing polymer chains. Different rates of coordination and insertion of comonomers determine the final chemical composition of the copolymer chain (Soares and Simon, 2005).
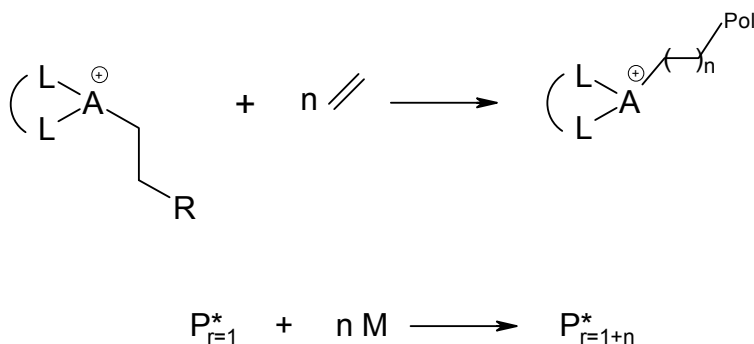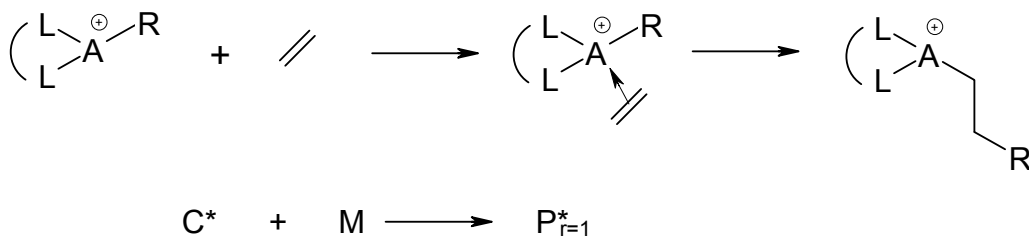
$$C^* \quad + \quad M \longrightarrow P^*_{r=1}$$

$$P^*_{r=1} \quad + \quad n\,M \longrightarrow P^*_{r=1+n}$$

M = monomer

n = number of active-site types in a multiple-site catalyst

$P^*_{r=1}$ = growing polymer with one monomer insertion of chain length r = 1

$P^*_{r=1+n}$ = growing polymer of chain length r, where (r = 1+n) and (n) is the number of monomer insertions into the polymer chain after first insertion to the active site

Figure 2-5 Monomer coordination and insertion

Several chain transfer mechanisms are operative in coordination polymerization: a) transfer by β-hydride elimination, b) transfer by β-methyl elimination, c) transfer to

10

monomer, d) transfer to cocatalyst, and e) transfer to chain transfer agent – commonly hydrogen - or other small molecules. The type of termination reaction determines the chemical group bound to the active site and the terminal chemical group in the polymer chain. The first three types produce unsaturated chain ends, while the last two types produce saturated chain ends. Figure 2.6 illustrates these five transfer mechanisms.

Chain transfer by β-hydride elimination

$$P_r^* \longrightarrow P_{rH}^* + \overline{\overline{D}}_r$$

Chain transfer by β-methyl elimination

$$P_r^* \longrightarrow P_{rMe}^* + \overline{\overline{D}}_r$$

Chain transfer to hydrogen

$$P_r^* + H_2 \longrightarrow P_H^* + D_r$$

Chain transfer to monomer

$$P_r^* + M \longrightarrow P_{rM}^* + \overline{\overline{D}}_r$$

11

Chain transfer to cocatalyst

$$P_r^* + Al \longrightarrow P_{Al}^* + D_{Al}$$

H_2 = hydrogen

P_r^* = growing polymer of chain length r

P_{rH}^* = active site with hydrogen atom formed via chain transfer by β-hydride elimination

P_{rMe}^* = active site with methyl group formed via chain transfer by β-methyl elimination

P_H^* = active site with hydrogen atom formed via a chain transfer to hydrogen

P_{rM}^* = active site formed via a chain transfer to monomer

P_{Al}^* = active site with alkyl group formed via a chain transfer to cocatalyst

D_r = dead chain with a saturated end

$\overline{\overline{D_r}}$ = dead polymer chain containing a terminal vinyl unsaturation

D_{Al} = dead polymer chain formed via a transfer to cocatalyst reaction

Figure2-6 Chain termination mechanisms

Reaction of the active site with polar impurities deactivates the catalyst. Due to the cationic nature of the active sites, nucleophilic groups with a lone pair of electrons (generally substances containing oxygen, nitrogen or sulfur) can coordinate irreversibly with the active site, causing irreversible catalyst deactivation. Bimolecular catalyst deactivation happens when two active sites form a stable complex that is inactive for monomer polymerization. This type of bimolecular intermediate is favored at high catalyst concentrations and is reversible. Figure 2.7 shows chemical equations for this catalyst deactivation mechanism.
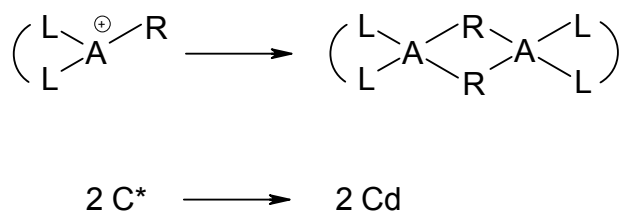
Cd = Deactivated catalytic site

Figure 2-7 Catalyst deactivation by bimolecular reactions.

The catalytic cycle is a convenient graphical way to describe the central role played by the active site in the mechanism of polymerization. Changes in the nature of the active site will affect the catalytic mechanism and consequently the activity and the selectivity of the polymerization. Changes in the polymerization reactor conditions, such as temperature and monomer concentration, play a vital role in the catalyst mechanism because they affect the rate constants of each of these steps. Figure 2.8 shows a catalyst cycle for olefin polymerization with coordination catalysts.
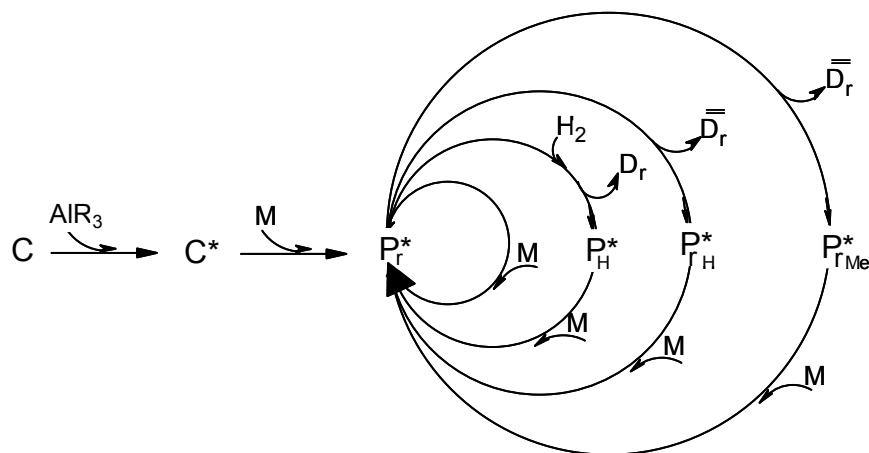
Figure 2-8 Catalytic cycle for polymerization

2.3 Polymer Microstructure Determination

New resins are produced to meet the requirements of the final application and processability. Accurate polymer characterization is required to analyze polymer microstructure which determines the polyolefin properties. The microstructure of polyethylene is defined by its distribution of molecular weight, chemical composition and long chain branching. Gel permeation Chromatography (GPC), temperature rising elution fractionation (TREF), crystallization analysis fractionation (Crystaf), differential scanning calorimetry (DSC), nuclear magnetic resonance spectroscopy (NMR), and Fourier-transform infrared spectroscopy (FTIR) are some of the techniques used to characterize polyolefins.

Gel permeation chromatography is an important analytical tool; it separates polymer chains by size, and therefore provides an indirect measure of the polymer molecular weight distribution.

Differential scanning calorimetry is a common method to locate phase transitions of materials to determine the associated transition enthalpy. The differential power to maintain a given temperature for two pans containing the material and a reference sample is recorded. Endotherm or exotherm peaks are indicated by a discontinuous phase transition which results in changes in the differential power supplied to the sample. The thermal properties obtained from DSC analysis would include the glass transition temperature, crystallization temperatures and endothermic or melting reactions.

Crystallization analysis fractionation and temperature rising elution fractionation use a unique approach to monitor the solution crystallization of polyolefins that will allow the calculation of the overall short chain branching distribution. The analysis is carried out by monitoring the polymer solution concentration during crystallization by temperature reduction. As the temperature decreases the most crystalline fraction composed of molecules with zero or few branches will precipitate first therefore resulting in a steep decrease in the solution concentration. This is followed by precipitation of the fraction

with decreasing crystallinity, hence an increase in the number of branches. The last data point corresponds to the material which has the highest number of branches and which will therefore still be soluble.

Nuclear magnetic resonance is a spectrometric technique for determining chemical structures. When an atomic nucleus with magnetic moment is placed in a magnetic field, it tends to align with the applied field. By determining the energy levels of transition for all of the atoms in a molecule, it is possible to determine the type of protons or carbons in the polymer chain. It is the fundamental technique for identification of type of branching, chain ends, and chemical composition. The technique is limited to the identification of a sequence of 5 carbon atoms.

Fourier transform infrared spectroscopy is simply the absorption measurement of different infrared (IR) frequencies by a sample positioned in the path of an IR beam. The main goal of the analysis is to determine the chemical composition of the sample.

2.4 Carbon-13 Nuclear Magnetic Resonance (^{13}C-NMR)

Nuclear Magnetic Resonance spectroscopy is a very powerful technique for polymer characterization that can be used to determine branching, the sequence of comonomer units in the copolymer chain. It is not only the overall composition that influences the chemical and physical composition of the copolymer but also the microcomposition and monomer sequence distribution along the polymer chain (Mohammadi et al., 2005).

To allow proper identification of different carbon structures in branched polyethylene, it is necessary first to adopt a nomenclature. Small changes in the type, number and relative position of short branches can change the final properties of polyethylene. The nomenclature shown in Figure 2.9 were first described by Randall and by Carman and Wilkes and later extended by others (Seger and Maciel, 2004). The Greek letters are used to denote the positions of a given backbone carbon site relative to methine carbons and side-chain carbons ("B" for branch) are labeled using the format *n*B*m*, where *m*

represents the length of the side chain and *n* refers to the position of the carbon in question, as counted from the *end* of the side chain.
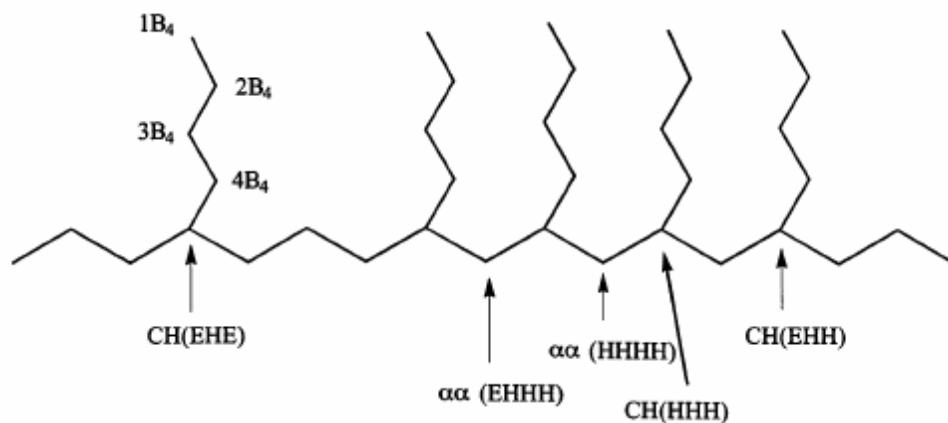
Figure 2-9 Nomenclature examples for poly(ethylene-co-1-hexene) substructures

The identification of short chain branches in polyethylene produced by copolymerization of ethylene and α-olefins is well established in the literature. This methodology will be explained here using the example of ethylene-1-hexene copolymer. The ^{13}C-NMR spectrum of ethylene-1-hexene copolymer containing 17.3 mol% 1-hexene is shown in Figure 2.10. Different triad and tetrad arrangements are observed for ethylene and 1-hexene. Table 13 is a tabulation of the chemical shifts and assignments.
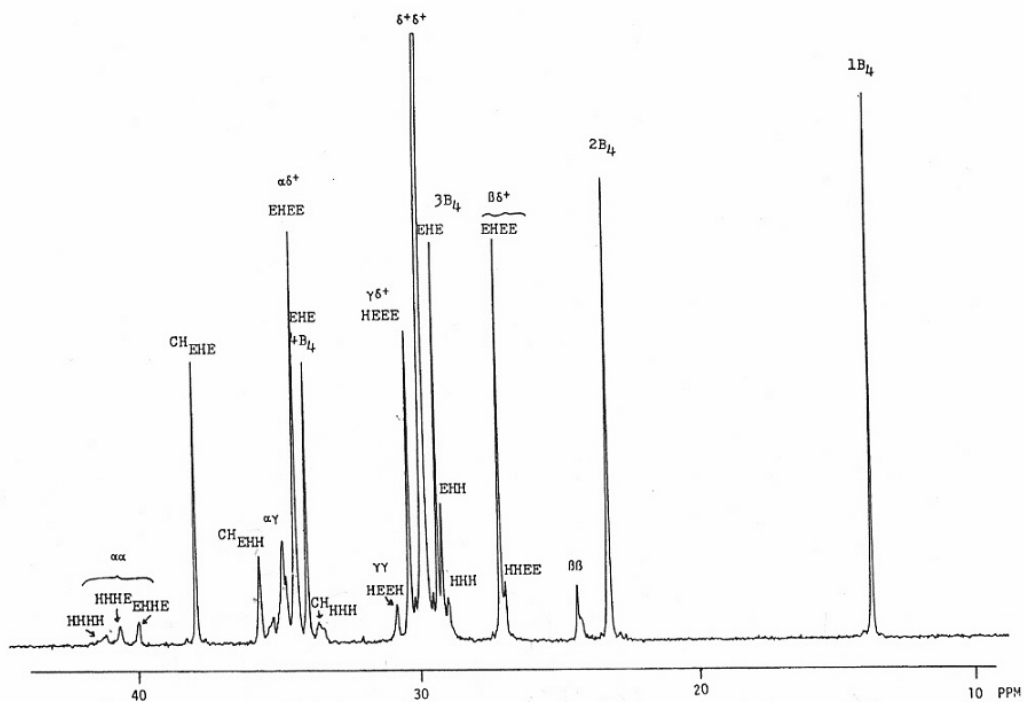
Figure 2-10 Carbon-13 NMR spectrum of ethylene-1-hexene copolymer at 125°C in 1,2,4-trichlorobenzene, obtained with 50.3 MHz (Randall, 1989)

Chemical Shift ppm, TMS			
TCB	TCE-d2	Carbon Assignment	Sequence Assignment
41.4		αα	HHHH (mmm)
40.86		αα	HHHE+EHHH (mm)
40.18		αα	EHHE (m)
38.13	38.22	Methine	EHE
35.85	35.92	Methine	EHH+HHE (m)
35.37		$4B_4$	HHH (mm)
35	35.1	αγ	HHEH+HEHH (mm)
		αγ	EHEH+HEHE (m)
34.9	35.02	αδ+	HHEE+EEHH
		$4B_4$	EHH+HHE (mm)
34.54	34.62	αδ+	EHEE+EEHE
34.13	34.21	$4B_4$	EHE
33.57		Methine	HHH (mm)
30.94	30.94	γγ	HEEH
30.47	30.48	γδ+	HEEE+EEEH
29.98	29.98	$\delta^+\delta^+$	(EEE)n
29.51	29.58	$3B_4$	EHE
29.34	29.41	$3B_4$	EHH+HHE (m)
29.18	29.24	$3B_4$	HHH (mm)
27.28	27.31	$\beta\delta^+$	EHEE+EEHE
27.09	27.13	$\beta\delta^+$	HHEE+EEHH (m)
23.37	23.39	$2B_4$	EHE+EHH+HHE+HHH
14.12	14.21	Methyl	EHE+EHH+HHE+HHH

Table 2-2 Carbon-13 chemical shift assignments at 50.3 Mhz for ethylene-1-hexene copolymers containing principally isotactic 1-hexene sequences and no inverted 1-hexene repeat units. The samples were prepared at 10% by weight in 1,2,4-trichlorobenzene (tbc) with perdeuterobenzene added and at 15% by weight in terachloroethane-d2 (tce-d2). The spectra were obtained at 125 ^{o}C. The δ+δ+ peak is set at 29.98 ppm with respect to an internal tetramethylsilane standard (Randall, 1989)

Ethylene-1-hexene copolymer spectrum can be divided into eight spectral regions as indicated by the chemical shift data in Table 2.2 and the ^{13}C-NMR spectrum in Figure 2.9. Carbon-13 NMR Spectrum of ethylene-1-hexene copolymer is shown with the respective eight spectral regions in Figure 2.11. Each region is descried below in terms of its range in ppm, contributing carbon atoms. The final intensity equations for each region

are defined by triads only. The intensity equations and the chemical shift assignments are summarized in Table 2.3.

Region "A" Range: 39.5-42 ppm

Contributing carbons: αα, Methylene

$$T_A \quad = \quad k(\text{HHHH} + \text{HHHE} + \text{EHHH} + \text{EHHE})$$

$$\quad = \quad k(\text{HH})$$

$$\quad = \quad k(\text{HHH} + (1/2) [\text{HHE} + \text{EHH}])$$

Region "B" Range: 38.1 ppm

Contributing carbons: (Methine)$_{\text{EHE}}$

$$T_B \quad = \quad k(\text{EHE})$$

Region "C" Range: 33-36 ppm

Contributing carbons: (Methine)$_{\text{EHH+HHE}}$, (Methine)$_{\text{HHH}}$, 4B$_4$, αγ, αδ$^+$

$$T_C \quad = \quad k(\text{EHEH} + \text{HEHE} + \text{HHEH} + \text{HEHH} + \text{EHEE} + \text{EEHE} + \text{HHEE} + \text{EEHH} +$$
$$\text{EHE} + 2\text{HHH} + 2[\text{EHH} + \text{HHE}])$$

$$\quad = \quad k(\text{HE} + \text{EH} + \text{EHE} + 2\text{HHH} + 2[\text{EHH} + \text{HHE}])$$

$$\quad = \quad k(\text{EHE} + 2[\text{EHH} + \text{HHE}] + 2\text{HHH} + 2\text{HEH} + [\text{HEE} + \text{EEH}])$$

Region "D" Range: 28.5-31 ppm

Contributing carbons: δ$^+$δ$^+$, 3B$_4$, γγ, γδ$^+$

$$T_D \quad = \quad k(2\text{EEE} + (1/2) [\text{HEE} + \text{EEH}] + \text{EHE} + \text{EHH} + \text{HHE} + \text{HHH})$$

Region "E" Range: 26.5-27.5 ppm

Contributing carbons: βδ$^+$

$$T_E \quad = \quad k(\text{EHEE} + \text{EEHE} + \text{HHEE} + \text{EEHH})$$

$$\quad = \quad k(\text{HEE} + \text{EEH})$$

Region "F" Range: 24-25 ppm

Contributing carbons: $\beta\beta$

T_F = $k(\,HEH\,)$

Region "G" Range: 23.4 ppm

Contributing carbons: $2B_4$

T_G = $k(\,EHE + EHH+HHE + HHH\,)$

Region "H" Range: 14.1 ppm

Contributing carbons: $1B_4$

T_H = $k(\,EHE + EHH+HHE + HHH\,)$

The correctness of the above equations can be established by summing the triad equations for T_A through T_H, whish is

$\sum T_x$ =   NMR total area   = $2k(\,E\,) + 6k(\,H\,)$
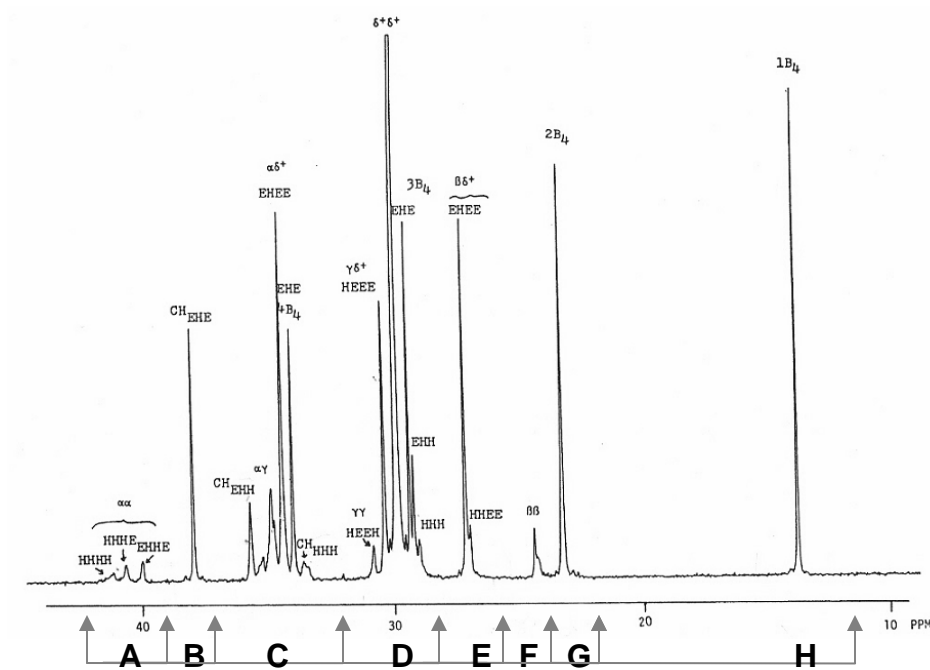
Figure 2-11 Carbon-13 NMR Spectrum of ethylene-1-hexene copolymer at 125°C in 1,2,4-trichlorobenzene with the eight spectral regions indicated in Table 2.2 (Randall, 1989)

Table 2-3 Intensity equations and respective chemical shift assignments

Region	Range (ppm) from	to	Contributing Carbons	Intensity Equation
A	39.5	42	αα, Methylene	TA = k(HHH + (1/2) [HHE+EHH])
B	38.1		(Methine)$_{EHE}$	TB = k(EHE)
C	33	36	(Methine)$_{EHH+HHE}$, (Methine)$_{HHH}$, 4B$_4$, αγ, αδ	TC = k(EHE + 2[EHH+HHE] + 2HHH + 2HEH + [HEE+EEH])
D	28.5	31	δ$^+$δ$^+$, 3B$_4$, γγ, γδ$^+$	TD = k(2EEE + (1/2) [HEE + EEH] + EHE + EHH+HHE + HHH)
E	26.5	27.5	βδ$^+$	TE = k(HEE+EEH)
F	24	25	ββ	TF = k(HEH)
G	23.4		2B$_4$	TG = k(EHE + EHH+HHE + HHH)
H	14.1		1B$_4$	TH = k(EHE + EHH+HHE + HHH)

2.5 Structure-Properties Relationship: Molecular Weight and Branching

Increasing the average molecular weight or the degree of polymerization of thermoplastics, such as polyethylene, leads to an increase in the tensile strength, impact toughness, creep resistance, wear resistance, and melting temperature. As the average molecular weight increases the melting temperature increases too, resulting in making material processability more difficult. The density, stiffness and strength of polymers are controlled by branching and packing the chains (Askeland and Phule, 2003). Therefore, linear low density polyethylene (LLDPE), which has more branches, is weaker than high density polyethylene (HDPE).

The stiffness of polyethylene depends on the amount of crystallinity, which in turn is determined by the ability of segments in the polymer chain to crystallize. A linear polyethylene is highly crystalline. Addition of small side-groups (methyl) to a linear polyethylene decreases the crystallinity. Longer or bulky (norbornene) side-groups have a better ability to decrease crystallinity (Ohshima and Tanigaki, 2000).

Qualitative relationships between molecular properties and polymer properties and processability of polymer are described in Table 2.4. The molecular structure and molecular weight distribution directly affects end-user properties.

Table 2-4 Relationship between molecular structure and properties of polyethylene (Ohshima and Tanigaki, 2000)

	Molecular structure	Molecular weight (Mw)	Molecular weight distribution	Branching chemicals	Degree of branching	Degree of branching distribution	Long-chain branching (LCB)
Mechanical and chemical property	Transparency	o	o	o	o	o	
	Tensile Strength	o	o	o	o	o	o
	Impact strength	o	o	o	o	o	o
	Rigidity				o	o	
	Heat resistance				o	o	
	Cold resistance	o	o	o	o	o	
	Chemical resistance	o	o	o	o	o	o
	Heat seal	o	o	o	o	o	
Processability	Bubble stability	o	o				o
	Draw down	o	o				o
	Extrusion torque	o	o				o

2.6 Technology-Product Relationship

The continuous growth and demand in the polyolefins market and especially for polyethylene and polypropylene required aggressive research efforts to achieve improved product properties. The scientific and technological developments aimed at a proper combination of the catalyst and the process to achieve the best polymer structure-property design (Figure 2.12) tailored to produce specialty materials for specific end-user application (Galli and Vecellio, 2004).
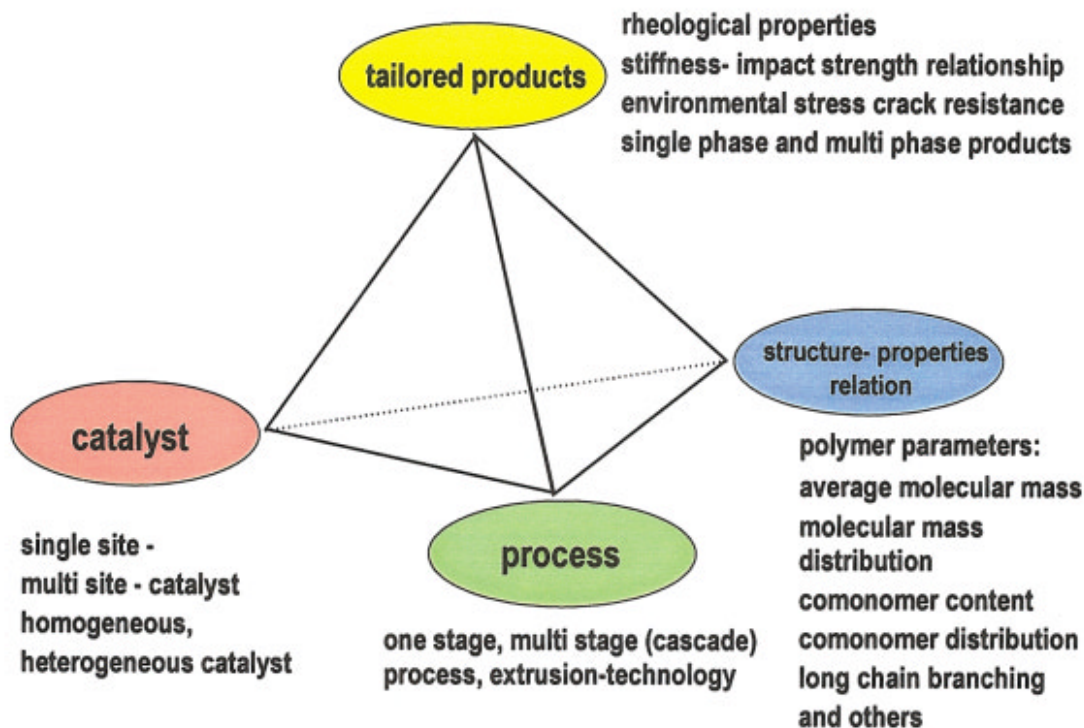
Figure 2-12 Technology-product relationship (Galli and Vecellio, 2004)

2.7 Monte Carlo Simulation and Applications

Monte Carlo simulation is a method that solves a probabilistic model of physical and chemical process through the use of random number generator. The observations generated are then analyzed usually using statistical methods, such as means, modes, variances and distributions, to produce useful information concerning the probabilistic model that underlies the simulated random experiment. It was named by Ulam, who in 1946 became the first mathematician to dignify this approach with a name, in honor of a relative having a propensity to gamble (Hoffman, 1998). Nicolas Metropolis also made important contributions to the development of such methods.

In macromolecular chemistry and physics, Monte Carlo methods can be applied to molecular dynamic simulations which calculate the spatial movement of molecules or molecular segments. Also Monte Carlo can be used for the calculation of product

distributions of polymerization reactions, such as chain length distribution, sequence length distribution and molecular weight distribution. In the case of very complex reaction schemes where conventional methods require a high level of sophistication and include many simplifying assumptions, Monte Carlo methods seem to be a simple and flexible alternative (Platkowski and Reichert, 1999).

2.8 Literature Review of Monte Carlo Modeling of Olefin Polymerization

Monte Carlo simulation has been used to study the kinetics and mechanism of polymerizations and the structure of polymer chains, such as the distribution of molecular weight, branching, stereoregularity and chain topology in different polymer systems.

2.8.1 Coordination Polymerization

Bruce and co-authors presented a method for simulating the microstructure of atactic-isotactic stereoblock polypropylene. A computer program was used to generate stereosequences based on alternating blocks of isotactic and atactic stereosequences. The simulations revealed that two polymers with identical observable isotactic pentad distributions may have very different microstructures which lead to different physical properties. The results of the simulations implied that the microstructure of a stereoblock polymer cannot be fully determined from the ^{13}C NMR spectrum at pentad resolution (Bruce and Waymouth, 1998).

Ling and co-authors applied Monte Carlo method to gas a phase polymerization system. The kinetics of gas phase polymerization of 1,3-butadiene catalyzed by rare earth complex with trialkylaluminum was discussed. Both absorption and diffusion of monomer in polymer particles were considered. According to the results of Monte Carlo simulation, three reasonable polymerization rates versus time curves coincide with experiments with errors between 0.91 and 5.78%. Two kinds of chain transfer reaction

contained similar possibilities but played different roles in polymerization (Ling et al., 2000).

Tobita and Hamashima used a Monte Carlo method to simulate the elution curves of size exclusion chromatography for nonlinear polymers formed through random branching and crosslinking of long polymer chains. In both randomly branched and crosslinked systems, the light scattering method gave good estimates. The authors concluded that the light scattering method is considered to be a promising technique to obtain the true molecular weight distributions for nonlinear polymer systems (Tobita and Hamashima, 2000).

Simon and co-authors correlated the polymerization temperature and ethylene concentration with parameters used in a Monte-Carlo model for polymerization and chain-walking mechanism with Ni-diimine catalysts. It was possible to fine-tune the polyethylene molecular architecture by the proper choice of the polymerization temperature and ethylene concentration. With a suitable value for each polymerization condition the Monte-Carlo model can be used to predict the corresponding short chain branch and can be, therefore, a useful tool for process and product control of polyolefins made with these catalysts (Simon et al., 2001).

Simon and Soares studied the formation of long-chain branches during ethylene polymerization with a combination of catalysts by Monte Carlo simulation. The model described polymerization with a non-branching catalyst that produces linear macromonomers, and a branching catalyst that produces linear and branched macromonomers. Three types of chain topology obtained during the synthesis were discussed in this work; linear, comb-branched, or hyperbranched. The results showed how the chain length distribution and the number of long-chain branches change according to the ratio between the two catalysts present in the reactor. The ratio hyperbranched/comb-branched was defined to evaluate the system composition and the contribution of each catalyst (Simon and Soares, 2002).

Costeux and co-authors presented analytical solution for Monte Carlo simulations of the microstructure of ethylene/α-olefin copolymers synthesized using single site catalysts. The authors derived the bivariate distribution and the longest ethylene sequence distributions in number and weight for the proposed system. The results were expected to be a first step in simulation of separation processes in temperature-rising elution fractionation and crystallization analysis fractionation (Costeux et al., 2002).

Beigzadeh developed a Monte Carlo model in which he used dual site catalyst system to polymerize ethylene with long-chain branching. A kinetic model was developed for a CSTR at steady state to simulate the polymerization process. He proposed a methodology for the calculation of the seven required Monte Carlo model probabilities from the kinetic model. The Monte Carlo model complemented the kinetic model results by providing detailed information about the chain microstructure and modeling the polymerization reactor. Beigzadeh work leads to the production of tailor-made polymers for any specific application (Beigzadeh, 2003).

Ling and co-authors used Monte Carlo method to simulate bulk polymerization of styrene with coordination mechanism. Initiation, propagation, deactivation and three chain transfer reactions and macro-monomer (polymer containing double bond end) insertion into active chain were considered. The simulation indicated that β-hydrogen elimination and transfer to monomer were the main chain transfer reactions in the whole polymerization. The possibility of macro-monomer insertion was less than monomer propagation but it plays an important role in late stage of polymerization (Ling et al., 2001).

Ling and co-authors used Monte Carlo simulation to study the deactivations and initiations of gas phase polymerizations of 1,3-butadiene. The influence of polymerization temperature has been studied. Monte Carlo modeling of polymerization kinetics and mechanism was confirmed by the agreement of experimental data and simulation results of polymerization run with a temporary evacuation of monomer. The

balance of catalysts and active chains was established by both initiation and chain transfer reactions with cocatalyst (Ling et al., 2003).

Costeux and co-authors extended statistical model which described the polymerization of branched ethylene homopolymers formed by single site catalyst for continuous stirred tank reactor to include a mixture of single site catalysts. An analytical solution was proposed to predict (linear chains/free arms/inner backbones) and the molecular weight distribution for any combination of single-site catalysts. The study showed the optimization of shear and extensional properties requires good control of the extent of vinyl termination and of the size of the segments between branch points (Costeux, 2003).

Haag and co-authors used Monte Carlo simulation to analyze the microstructure of polyolefinic thermoplastic elastomers made with a combination of two single-site catalysts. The crystallized fraction for both long-chain branched polypropylene and long-chain branched ethylene/α-olefin copolymers were described by the model and similar comonomer incorporation levels at 7.5%, considering same reaction probabilities. It was demonstrated that changing the propagation probability for linear catalyst also changes the symmetry of the branched chains. The authors proposed a mathematical correlation between the linear and long chain branching catalyst probabilities to ensure production of symmetrical branched chains (Haag et al., 2003).

Iedema and Hoefsloot presented Monte Carlo algorithms for the virtual synthesis of polyethylene catalyzed by one branch forming constrained geometry metallocene catalyst (CGC, 1C-system) or by a mixture of CGC and linear metallocene catalyst (2C-system) in a continuous stirred tank reactor. They found that 2C molecules feature a stronger comb-like topology than 1C molecules. The authors concluded that mixing catalyst is a good option to create more comb-like structures. The algorithms developed enabled understanding branched architectures in relation to kinetics and reactor conditions (Iedema and Hoefsloot, 2004).

Yashin and co-authors used Monte Carlo simulations and probabilistic analysis to study the influence of energetic parameters of the interchain homo- and hetero-contacts on a local ordering of both Bernoullian copolymers and products of polymer analogous reaction with accelerating neighbor effect proceeding in confine conditions. It was concluded that when the reaction with intra- and interchain acceleration and local ordering proceed simultaneously in confined conditions, the ordering might affect the process so that the formation of certain nano-structures is possible (Yashin et al., 2004).

Braun and co-authors investigated crystallinity in ethylene/1-hexexe copolymers by Monte Carlo simulations. Minimum crystallite thickness was estimated using the comonomer distributions for the simulated chains and the melting temperatures of real chains. Thickness simulated values were in good agreement with Raman longitudinal acoustic mode (LAM) spectroscopy calculated values except for very low 1-hexene mole fractions. Preliminary results on the effect of varying the comonomer amount on the size and number of polyethylene crystallite was shown (Braun et al., 2004).

Simon and Soares developed a Monte Carlo model to predict the detailed topology of branched polyolefin chains made with two single-site catalysts. Where, one catalyst makes only linear chains and the other makes linear and branched chains (LCB catalyst). The polymer chains were classified into families with different number of long-chain branches per chain. The different configurations within each family were classified as separate family members. The developed model was also able to keep track of the chain-length distribution of each polymer family member, its number of free arms and inner segments, and the seniority and priority of its segments. It was also shown that by varying the ratio of LCB to linear catalyst it is possible to control the overall level of long-chain branching and the relative proportion of the distinct members of a family (Simon and Soares, 2005).

2.8.2 Free-Radical Polymerization

Lu and co-authors described Monte Carlo method for numerically simulating kinetics and chain-length distribution in radical polymerization. The main objective behind this work is to study the kinetic behavior before the steady-state has been reached and for systems in which the steady-state assumption may be violated. Applications of the algorithms were provided. For the case of pseudo-stationary radical polymerization such as rotating-sector and pulsed-laser initiations, the pseudo-stationary radical concentration can be reached after two or three initiation periods (Lu et al., 1993).

Tobita and co-authors carried out free-radical polymerization of styrene in the presence of chain transfer agents. Theoretical and experimental investigations were conducted. Direct observation of the structure of each polymer molecule was achieved with Monte Carlo simulation method. This estimated the elution curve of size exclusion chromatography by using Monte Carlo technique. When the simulated molecular weight distributions was compared with the experimental data, the authors found that up to the functionality $f = 3$, the equal reactivity model could be used to design and control the branched polymer structure (Tobita et al., 1999).

Liang and co-authors applied Monte Carlo method to investigate the kinetic of grafting reaction in free radical copolymerization. The simulation was in agreement with theoretical and experimental results. It proved that the Monte Carlo simulation is an effective method for investigating the grafting reaction of free radical copolymerization (Liang et al., 2000).

Fuentes and his co-authors prepared copolymers of furfurylmethacrylate with N-vinyl-2-pyrrolidone by free radical copolymerization. The reactivity ratios of both monomers were calculated according to the general copolymerization equation using the Fineman-Roess and Kelen-Tuedos linearization methods, as well as the Tidwell-Mortimer non-linear least-squares treatment and the Monte Carlo random method. The values of the reactivity ratios were calculated. Similar results were obtained by both, the Monte Carlo

and the non-linear least square techniques that certified the precision of the proposed method (Fuentes et al., 2002).

Tobita described the molecular weight development during free-radical copolymerization by applying a matrix formula. The probabilistic parameters used in the matrix formula were expressed in terms of the kinetic rate constants and pertinent concentrations involved in free-radical multicomponent polymerization. The calculation results had agreed with the Monte Carlo simulation results. Monte Carlo method provides very detailed structural information; on the other hand, the Markovian approach might be too simple to represent complex molecular buildup processes in free radical polymerization (Tobita, 2003).

Prescott work focuses on free radical polymerization systems. He used a Monte Carlo model to show the importance of the chain-length dependent termination in free-radical polymerization systems containing reversible transfer agents (RTAs) such as RAFT agents and alkyl halides. Prescott concluded that the Monte Carlo model which was presented provided significant insights into the relative importance of the different processes (propagation, transfer to dormant species, and termination). He concluded that in designing RTA-mediated polymerizations, long-chain dormant species provide a considerable advantage, as they lead to an increased lifetime for the radicals compared to short-chain dormant species (Prescott, 2003).

2.8.3 Review Articles

Platkowski and co-authors presented a model concept based on a critical comparison of algorithms already published in the literature. The concept could be used generally and guarantees a high level of formalism. The model concept has been tested on the modeling of several different polymerization reactions, such as a heterogeneous polycondensation, an inverse emulsion polymerization and thermal polymer degradation. The method presented is numerically stable and the precision of the results may be controlled by the size of the simulated volume element (Platkowski, 1999).

Soares conducted a review of the mathematical models developed over the last decade to quantify the microstructure of polymers made with single-site catalysts with special emphasis on the mechanism of long chain branch formation by terminal branching. Powerful polymerization mathematical models for new single-site catalysts are required to fully realize their potential. Their enhanced polymer microstructural control combined with the understanding of structure property relationships will in principle allow the design of products with properties targeted to a given application (Soares, 2004).

Chapter 3 - Mathematical Modeling and Model Description

3.1 Introduction

Monte Carlo simulation model was developed to describe the mechanism of olefins coordination polymerization. Industrial catalysts which are classified as coordination polymerization catalysts are Zeigler-Natta, Phillips and metallocene catalysts. For metallocene single-site-type catalyst single set of kinetic parameters constants is needed whereas with Ziegler-Natta and Philips are multiple-site-type catalysts and two or more sets of polymerization kinetics constants need to be used. If mathematical models are able to predict the polymer molecular structure in terms of molecular weigh and chemical composition, it will give a detailed picture of the molecular structure for homopolymer and copolymer made with coordination reaction mechanisms.

The proposed model is limited to one type of active site (single-site). Multiple-site-types can be obtained by combining several single-site catalysts as long as they behave independently. Multiple-site catalysts are out of the scope of the study. The model proposed here focuses on the homopolymerization of ethylene (monomer A) and on the copolymerization of ethylene (monomer A) and α-olefins (monomer B). It is capable of calculating: a) the complete chain length distribution; b) polydispersity; c) average comonomer (B) composition; d) comonomer composition distribution as function of chain length; e) monomer (A) and comonomer (B) segment length distribution as function of chain length; f) average triads distribution; g) triad distribution as a function of chain length; and h) the distribution of monomer and comonomer as a function of segment length. The developed Monte Carlo Model was used to simulate steady state homopolymerization and copolymerization reactions in semi-batch reactors. Concentration of monomer and comonomer are assumed to be constant during polymerization.

32

The model uses a random number generator which generates random numbers between 0 and 1. The random number is compared with probabilities that are related to the polymerization mechanisms by kinetic equations.

3.2   Reaction Kinetic Constants

The polymerization kinetic parameter constants are directly linked to the characteristics of the catalyst used in the process. The reaction kinetic constants are required in calculating the probability of propagation which leads to predicting the number average chain length (r_n). Here the kinetic parameters could be obtained by knowing the polymer parameters through sample analysis or by calculating the kinetic parameters based on the reaction mechanism. The first case is to analyze a polymer sample using gel permeation chromatography (GPC). Then the number average chain length is calculated from the number average molecular weight (*M*n) values obtained from the GPC. The calculated number average chain length from the polymer information is needed as an input to simulate the model. An example for the first case is shown in Table 3.1.

Table 3-1 Calculated number-average chain length (r_n) for polyethylene

*M*n (g/mol)	r_n
50,000	1700
100,000	3500
150,000	5300
200,000	7000

In the second case we calculate the reaction kinetic constants by satisfying the relationship between the reaction kinetic equations and the calculated values from probability of propagation or probability of termination. Then the number average chain length is calculated as will be described later. The second case uses polymerization kinetic equations based on the reaction mechanism to obtain probability of propagation (P_p), number average chain length (r_n) and the probability of adding monomer B (P_B)

incase of the copolymerization model (Table 3.2). The relationship between the kinetic parameters and probabilities is explained in the next section.

Table 3-2Calculated reaction kinetic parameters (for changing number average chain length and constant number fraction of comonomer)

k_{pA} (L/mole.s)	k_{pB} (L/mole.s)	k_{tA} (L/mole.s)	k_{tB} (L/mole.s)	P_p	r_n	P_B
1210	1910	2.70	1.10	0.99901	1007	0.05
2150	3395	1.35	0.91	0.99967	3005	0.05
3220	5080	1.23	0.80	0.99980	5010	0.05
3420	5340	0.98	0.56	0.99986	7010	0.05

$[Pr^*]=10 \times 10^{-6}$ (mole/L), [A]= 3 (mole/L), [B]= 0.1 (mole/L)

Where

[A] = Concentration of monomer A

[B] = Concentration of comonomer B

$[P_r^*]$ = Concentration of the active species

k_{pA} = Propagation reaction constant for monomer A

k_{pB} = Propagation reaction constant for monomer B

k_{tA} = Termination reaction constant for monomer A

k_{tB} = Termination reaction constant for monomer B

P_p = Probability of propagation

r_n = Number average chain length for branched copolymer

P_B = Probability of adding monomer B

3.3 Homopolymerization Model

3.3.1 Homopolymer-Kinetic Equations

The accepted mechanism for homopolymerization by coordination polymerization was described earlier in Chapter 2 (2.2 Coordination Reaction Mechanism and Kinetic Equations). Catalyst activation with cocatalyst, catalyst initiation with monomer, chain propagation, chain transfer and poisoning and deactivation are the main five steps in the

coordination polymerization reaction. The model assumes initiation to be much fast and the concentration of active sites to be constant during the polymerization.

The model utilizes the polymerization mechanisms to predict the chain length of the polymer chains after termination step. The model is derived from the kinetic equations of the propagation and termination by transfer reaction. The rate of propagation is described in Figure 3.1, where the monomer insertion is repeated to form growing polymer of chain length r, ($P^*_{r=1}$) and increases its length to create ($P^*_{r=1+n}$).

The rate of propagation for the monomer (R_p) is directly proportional to the concentration of the active species ($[P^*_r]$), concentration of the monomer ($[M]$) and the propagation kinetic constant (k_p) for the monomer.

$$P^*_{r=1} + n\,M \longrightarrow P^*_{r=1+n}$$

.

Where
$$R_p = k_p [P^*_r][M]$$

A = transition metal center (Ti, Zr, Ni,...)

L = ligands

R = alkyl group (methyl, ethyl)

Figure 3-1 Propagation reaction kinetic equation for the homopolymer model

The transfer reactions in the model were simplified and lumped to be expressed by one reaction (Figure 3.2). For example only we will consider the β-hydride elimination which is a first order reaction. The hydrogen atom attached to the β-carbon in the living chain is abstracted by the active center forming a metal hydride center (P^*_H) and a dead

35

polymer chain containing vinyl unsaturation ($\overline{\overline{D}}_r$). The polymerization reaction termination rate (R_t) is influenced by the monomer termination reaction constant (k_t) and the concentration of the active species ($[P_r^*]$).

The model proposed here is mainly looking at the short chain branching and did not consider the mechanism for long chain branching formed by macromonomer incorporation as a result of having unsaturated dead polymer chain. Therefore the dead polymer chain with terminal double bond does not incorporate into the new growing chain in our model and is treated as a dead polymer with saturated end.

$$P_r^* \longrightarrow P_H^* + \overline{\overline{D}}_r$$

$$R_t = k_t [P_r^*]$$
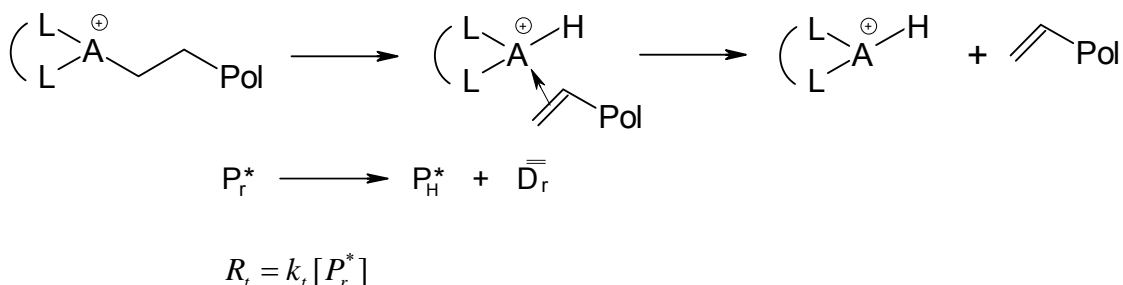
Where

R_t = Rate of termination of monomer M

k_t = Termination reaction constant for monomer M

Figure 3-2 Termination by transfer reaction β-hydride elimination kinetic equation for the homopolymer model

3.3.2 Homopolymer- Probabilities Calculations

The probability of propagation (P_p) and the probability of termination (P_t) are calculated using the reaction kinetic equations of the propagation and termination respectively. The number average chain length (r_n) is related to the propagation rate (R_P) and termination rate (R_t) of each active site using the following equation:

$$r_n = \frac{R_p}{R_t}$$

Therefore reducing the rate of termination of the polymerization process will lead to longer chains produced and greater number average chain length.

The chain length is related to the molecular weight by the molar mass of the monomer unit as the chain length increases the molecular weight increases too. The probability of chain propagation (P_p) is related to the number-average chain length (r_n) by (Simon and Soares, 2002):

$$P_p = \frac{R_p}{R_p + R_t} = \frac{k_p[P_r^*][M]}{k_p[P_r^*][M] + k_t[P_r^*]}$$

$$P_p = \frac{R_p}{R_p + R_t} = \frac{1}{1 + \dfrac{R_t}{R_p}} = \frac{1}{1 + \dfrac{1}{r_n}} \approx 1 - \frac{1}{r_n}$$

The (P_t) is inversely proportional to the number average chain length (r_n) and is given by:

$$P_t = \frac{R_t}{R_p + R_t} = \frac{k_t[P_r^*]}{k_p[P_r^*][M] + k_t[P_r^*]}$$

$$P_t = \frac{R_t}{R_p + R_t} = \frac{1}{\dfrac{R_p}{R_t} + 1} = \frac{1}{r_n + 1} \approx \frac{1}{r_n}$$

Therefore the probability of propagation is expressed through the polymerization reaction kinetics and is related to the number average chain length (r_n) by using the rates of propagation and termination.

The probability of termination determines whether to add more monomer units to the growing polymer chain or to terminate the chain and store the chain length of the terminated reaction for the specific active site.

3.3.3 Homopolymer-Program Flowchart

The model represents a steady-state semi-batch polymerization reactor. It assumes a constant catalyst and monomer concentrations. The initiation step is assumed to be instantaneous as the first monomer insertion is considered to have the same propagation constant as the subsequent monomer propagation steps. For simplicity the model assumes that there is no catalyst deactivation. As polymer chains are formed, they accumulate in the reactor. All kinetic parameters were kept constant during the simulation.

The total number of polymer chains to be simulated and the number average chain length are the parameters needed to run the homopolymerization model. The average chain length can be calculated from the polymerization reaction kinetics or by analyzing a polymer sample. The total number of chains simulated determines the degree of noise present in the final results. This is one of the limitations of Monte Carlo modeling, that is, a large population is needed to provide results with low noise.

The model was developed with the C++ programming language and run on a personal computer with a Pentium 4™ processor. The simulation result is stored as .txt file and the data is processed using Excel™. The homopolymerization schematic flow chart is shown in Figure 3.3. First the model requires parameter data input in order to execute the simulation. The needed parameters are the total number of polymer chains to be simulated and the number average chain length. Once the inputs are fed to the program a random number is generated between 0 and 1 and compared with the probabilities. The probability of termination is compared with the random number generated (RAN). If the random number is less than the probability of termination then the chain would terminate and the chain length size would be store. If the random number was greater than the probability of termination then the chain will propagate and add one more monomer unit to the growing chain.

A new random number is generated in each decision step. The propagation step will repeat itself until the random number is greater than the probability of termination where the chain would be terminated and the chain data stored. After that the program will take

decision whether to create a new chain or to end the program when the total number of chains produced is completed. The model was based on the kinetic equations described earlier for the homopolymer model. The probability of propagation equation could be used for the model and we would get the same outputs. The homopolymer model outputs are the complete chain length distribution and polydispersity index.
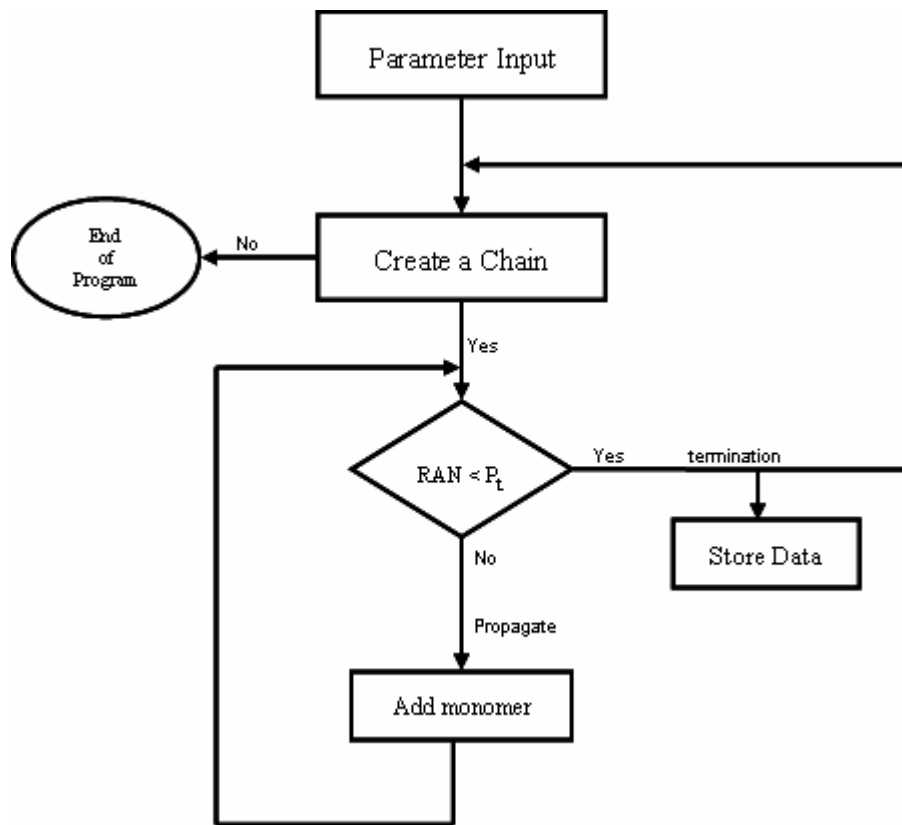
Figure 3-3 Homopolymerization schematic flow chart

3.4 Copolymerization Model

3.4.1 Copolymer-Kinetic Equations

The polymerization reaction kinetic equations are similar to the one described for the homopolymer model except that for the copolymerization model we have monomer A and comonomer B. There is a competition between the monomer and comonomers to coordinate to the active sites and to be inserted into the growing polymer chain. The rate of propagation of monomer A (R_{pA}) and the rate of propagation of comonomer B (R_{pB}) determine the final chemical composition of the copolymer chain.

Figure 3.4 describes the rate of propagation for the copolymer model. The rate of propagation for the monomer A is influenced by the concentration of the active species ($[P_r^*]$), concentration of the monomer ([A]) and the propagation kinetic constant for monomer A (k_{pA}). The rate of propagation for the comonomer B is determined by the concentration of the active species ($[P_r^*]$), concentration of the comonomer B ([B]) and the propagation kinetic constant for comonomer B (k_{pB}).

$$P_{r=1}^* \quad + \quad n\,M \longrightarrow P_{r=1+n}^*$$

$$R_{pA} = k_{pA}[P_r^*][A]$$

$$R_{pB} = k_{pB}[P_r^*][B]$$
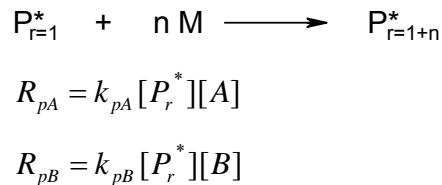
Figure 3.4 Propagation reaction kinetic equations for the copolymerization model

The termination by transfer reactions are lumped into one reaction which is described in (Figure 3.5).

$$P_r^* \longrightarrow P_H^* \quad + \quad \overline{\overline{D}}_r$$

$$R_{tA} = k_{tA}[P_r^*]$$

$$R_{tB} = k_{tB}[P_r^*]$$
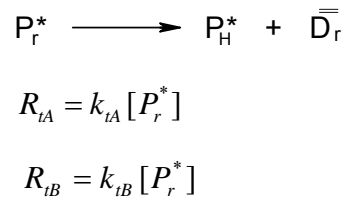
Figure 3.5 Termination reaction kinetic equations for the copolymerization model

The polymerization reaction termination rate for monomer A (R_{tA}) is determined by the termination reaction constant for monomer A (k_{tA}) and the concentration of the active species ($[P_r^*]$). The termination rate for the comonomer B (R_{tB}) is determined by the termination reaction constant for comonomer B (k_{tB}) and the concentration of the active species ($[P_r^*]$). For simplicity, both termination reactions were considered the same.

3.4.2 Copolymer-Probabilities Calculations

The probability of propagation (P_p) is calculated using the propagation kinetic equations for monomer A and comonomer B and the probability of termination (P_t) is calculated using the termination kinetic equations for monomer A and comonomer B. The copolymer model requires the probability of adding comonomer B as an input to simulate a run. The probability of adding monomer B (P_B) is determined by the propagation kinetic equations for monomer A and comonomer B. Note that here we are assuming a Bernoulli process rather than a first order Markov chain; ie end units do not affect which of monomer A or comonomer B are being added.

The number average chain length (r_n) is related to the propagation rate (R_P) and termination rate (R_t) of each active site using the following equation.

$$r_n = \frac{R_p}{R_t} = \frac{(R_{pA} + R_{pB})}{(R_{tA} + R_{tB})}$$

The rate of propagation for the copolymerization is represented by the sum of the rate of propagation for monomer A (R_{pA}) and the rate of propagation for comonomer B (R_{pB}). The rate of termination would be in this case represented by the sum of the rate of termination for monomer A (R_{tA}) and rate of termination for comonomer B (R_{tB}).

The chain length is related to the molecular weight by the molar mass of the monomer unit and the probability of chain propagation (P_p) is related to the number-average chain length (r_n) by:

$$P_p = \frac{R_p}{R_p + R_t} = \frac{(R_{pA} + R_{pB})}{(R_{pA} + R_{pB}) + (R_{tA} + R_{tB})} = \frac{(k_{pA}[P_r^*][A] + k_{pB}[P_r^*][B])}{(k_{pA}[P_r^*][A] + k_{pB}[P_r^*][B]) + (k_{tA}[P_r^*] + k_{tB}[P_r^*])}$$

$$P_p = \frac{R_p}{R_p + R_t} = \frac{1}{1 + \dfrac{R_t}{R_p}} = \frac{1}{1 + \dfrac{1}{r_n}} \approx 1 - \frac{1}{r_n}$$

The termination rate (P_t) would be expressed by the ratio of the rate of termination to the total rates of propagation and termination. The probability of chain termination is related to the number-average chain length (r_n) by:

$$P_t = \frac{R_t}{R_p + R_t} = \frac{(R_{tA} + R_{tB})}{(R_{pA} + R_{pB}) + (R_{tA} + R_{tB})} = \frac{k_{tA}[P_r^*] + k_{tB}[P_r^*]}{(k_{pA}[P_r^*][A] + k_{pB}[P_r^*][B]) + (k_{tA}[P_r^*] + k_{tB}[P_r^*])}$$

$$P_t = \frac{R_t}{R_p + R_t} = \frac{1}{\dfrac{R_p}{R_t} + 1} = \frac{1}{r_n + 1} \approx \frac{1}{r_n}$$

The probability of propagation and probability of termination are expressed through the polymerization reaction kinetics and are calculated using the rates of propagation and termination for monomer A and comonomer B. The link between the number average chain length (r_n) and the polymerization kinetics is shown above.

The probability of termination and the probability of propagation determine which direction the model would proceed. The model will decide whether to add more monomer units to the growing polymer chain or terminate the chain and store the chain length, sequence length distribution, triad distribution and other data-as will be described later in model capability-of the terminated reaction for the specific active site.

The probability of adding monomer B (P_B) is required as an input to run the model. The probability of assign monomer B is calculated through the polymerization kinetic equations. The outcome of the ratio of the rate of propagation of comonomer B to the total propagation rate of monomer A and comonomer B is the probability of adding monomer B.

$$P_B = \frac{R_{pB}}{R_{pA} + R_{pB}} = \frac{k_{pB}[P_r^*][B]}{k_{pA}[P_r^*][A] + k_{pB}[P_r^*][B]}$$

Therefore by increasing the concentration of the comonomer [B] the probability of adding monomer B would increase. The probability of adding monomer B is not a function of the chain length (r).

3.4.3 Copolymer-Program Flowchart

The copolymer model assumptions are similar to those assumptions which were made for the homopolymer model. The copolymer model again represents a steady-state semi-batch polymerization reactor. It assumes constant catalyst and monomer concentrations. The initiation step is assumed to be instantaneous as the first monomer insertion is considered to have same propagation constant as the subsequent monomer propagation steps. For simplicity the model assumes that there is no catalyst deactivation. As polymer chains are formed, they accumulate in the reactor. All kinetic parameters were kept constant during the simulation. The model requires parameter data input in order to execute the simulation. The required parameters are the total number of polymer chains to be simulated, the number average chain length and the probability of adding the comonomer.

Figure 3.4 shows the copolymerization schematic flow chart. The model was based on the polymerization mechanisms described in section 3.4.1. To start the simulation we enter the values for the number of chains that would be produced from the catalyst, the number-average chain length, and the probability of adding comonomer B.

The probability of termination (P_t) is calculated in the beginning of the program from the number-average chain length set in the input. Then a random number is generated

(RAN). The random number is compared with the probability of termination. If the random number is larger than the probability of termination, a monomer has to be added to the growing polymer chain (chain propagation). If the random number is smaller than the probability of termination then the chain would terminate and the chain information would be stored. The model would then decide whether to start the cycle again or end the program. The program would end if the number of chains generated reached the total number of chains desired from the catalyst.

When the random number is larger than the probability of termination then the chain will proceed towards the propagation cycle. Another random number (RAN) is generated and this time the random number is compared to the probability of adding comonomer B (P_B). The probability of adding the comonomer is not a function of the chain length and is set at the start of the program as constant value. If the random number is greater than the probability of adding the comonomer then the model will propagate by adding one monomer unit of (A). While if the random number is smaller than the probability of adding the comonomer then the model will propagate by adding one comonomer unit of (B).

The propagation information is stored and is updated whenever we add a monomer unit to the growing polymer chain. The overall cycle is repeated to the end of the program where the total number of chains produced meets the desired specification of the catalytic system.

The copolymer model outputs are the complete chain length distribution, polydispersity, composition of the monomer and comonomer as function of chain length, monomer and comonomer segment length distribution as a function of chain length, triad distribution as function of chain length, average triad distribution, and the distribution of monomer and comonomer as a function of segment length.
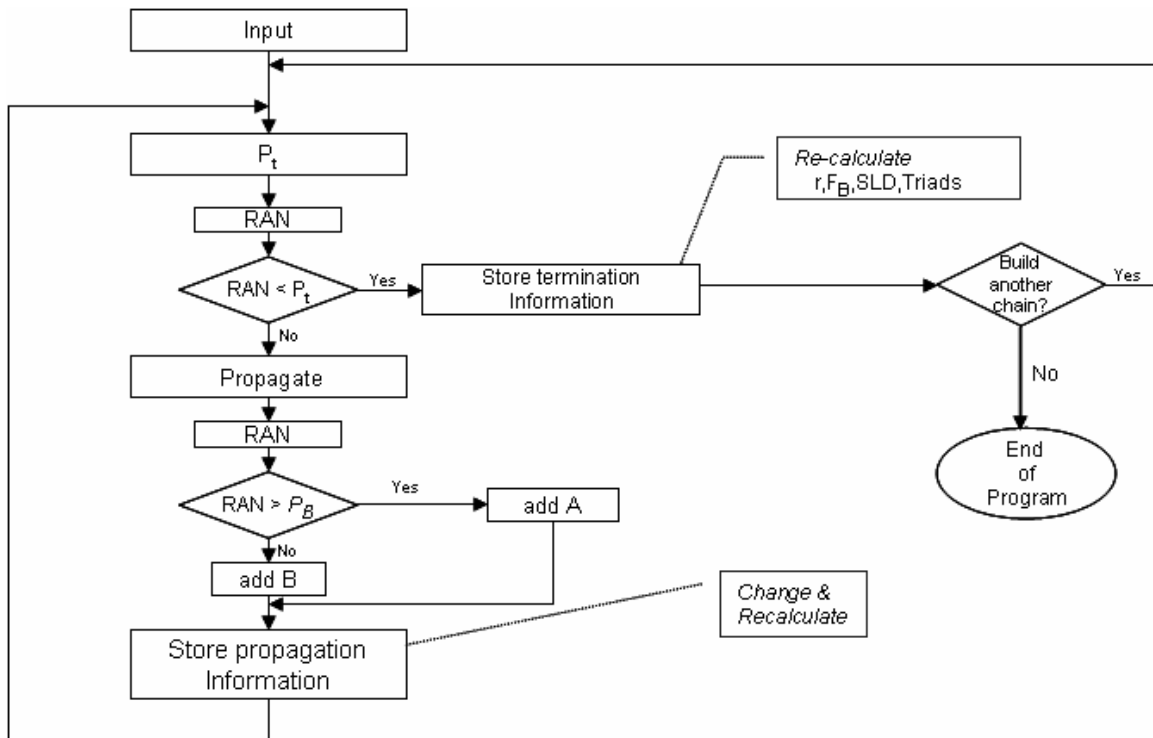
Figure 3-4 Copolymerization schematic flow chart

3.5 Calculation of the Molecular Weight Distribution

According to what was described previously for the homopolymer model and copolymer model, when the random number generated is not less than the probability of termination then the chain would propagate and the chain will add one monomer unit at a time to the growing polymer chain. To store all this information within the program, matrices were created to accommodate the information. All information about the growing polymer chain is kept individually. When the polymer chain stops growing, all its information is stored

The variable which was created to represent the growing polymer chain length was called r_c1. Each time the random number is not smaller than the probability of termination the growing chain length (r_c1) increases by one unit until it terminates and the chain data are stored.

Another variable was created (index_c1) to account for the total number of chains produced at a given chain length size or class (dr-c1). The chain length class/size (dr_c1) is an interval of molecular weight where chains of similar size are lumped together. It is set by the user according to the user preference, generally around 100 to 500. Instead of keeping track of all chain lengths, the chains are grouped within these intervals (classes). The purpose of this step is to allow the program to simplify where to store the data of the terminated chain according to their sizes.

The matrices store different types of information as a function of chain length. The first column of the matrix is the chain length and each subsequent column is attributed to a variable containing information about the chain.

For the copolymer model the program is able to calculate the number fraction of the comonomer as a function of the chain length. The number of comonomer B inserted in the polymer chain is divided by the number of chains produced at that size of chain length to give the number fraction of the comonomer as a function of the chain length.

3.6 Calculation of Sequence Length Distribution

The program is capable of predicting the sequence length distribution (SLD). From the simulation output we can calculate the number fraction of segments for the monomer and comonomer as a function of the segment length and as a function of the chain length.

To predict the segments of the monomer and comonomer as a function of the segment length we created new matrices (sldA[i], sldB[i]) where (i) would represent the segment length. Two variables were created to store the number of monomer A and comonomer B in the growing chain according to their segment lengths called (length_seg_A) and (length_seg_B) respectively.

When the program decides to propagate a random number is generated and compared to the probability of adding comonomer B. The probability of adding comonomer B is defined by the user as a required input data to run the simulation. If the random number is

greater than the probability of adding the comonomer then one unit is added and stored in the variable (length_seg_A) which means an addition of monomer A occurred. But if the random number was smaller than the probability of adding comonomer B then one unit is added and stored in the variable (length_seg_B) which means that we had added comonomer B into the growing chain.

The second way to track the sequence length distribution is as a function of chain length (r). In this part of the model two other matrices (An_rn, Bn_rn) are built as an extension of the original matrix which included the chain length, number of chains produced and fraction of the comonomer. This matrix is made to track sequences of 1 to 19 monomers A_n as a function of molecular weight, where n is the number of consecutive monomers in the sequence (A_{1-19}). Sequences with 20 or more monomers are lumped as A_{20}. The same is calculated for comonomers creating the distribution B_{1-20}. The different sizes for the monomer A and comonomer B sequences are updated and stored according to their chain length.

Once the model proceeds to propagate and the random number is greater than the probability of adding the comonomer we use the (if statement). If the length of segment B was not equal to zero then we add one comonomer B unit to the new variable which is part of the developed matrix (Bn_rn). Also if the length of segment B is greater than twenty ($B_{n>20}$) add it to (B_{20}). Otherwise one monomer A unit will be added to the new matrix (An_rn) as a function of the chain length. Again we ask the program to add any sequence which is greater than twenty ($A_{n>20}$) to (A_{20}) monomer sequence.

3.7   Calculation of the Triad Distribution

The program can track the triad distribution as a function of chain length. This is done by developing a method which enables us to account for the sequence in which the monomers are inserted in the polymer chain. The developed matrix (An_rn) that stores the chain information for the sequence length distribution is extended further to include more six positions. The six positions are used to store the triad information as a function

of the chain length. The triad information that the program is keeping track of are AAA, AAB/BAA, ABA, ABB/BBA, BAB and BBB.

We created variable M1, M2 and M3. Those variables represent the sequence of monomers insertion in polymer chain where M1 is the last monomer updated. As M1 information is updated it is passed to M2 and then M2 to M3 as the propagation continue to occur. If the program decides to add monomer A as the random number is greater than the probability of adding the comonomer then M1 would be identified by another variable called (A). Else the program would add comonomer and consider M1 to be represented by another variable which is called (B). A counter was created and called (Mseq) which has six positions to accommodate the information of the six possible triad sequences.

If M1 is equal to A and M2 equals A and M3 equals A then the counter will add one unit to the AAA sequence which occupies position zero in the (Mseq) counter. If M1 equals B and M2 equals A and M3 equals B then the counter will add one unit to the triad BAB which occupies position four in of the counter and so on. The triad sequence distribution is updated as a function of the chain length. The counter (Mseq) is updated in the (An_rn) matrix and the program keeps track of the triad sequence until the simulation ends.

Chapter 4 - Simulation Results and Discussion

4.1 Introduction

It is not only the average comonomer composition that influences the physical properties of the copolymer but also the microcomposition and monomer sequence distribution along the polymer chain (Mohammadi, 2005). In this chapter we will look at the model output capability where we will present the results for complete chain length distribution, comonomer composition distribution as function of chain length, monomer (A) and comonomer (B) segment length distribution as function of chain length, triad distribution as a function of chain length and the distribution of monomer (A) and comonomer (B) as a function of segment length.

We will start with presenting the simulation results for both the homopolymer model and copolymer model by using the polymer parameters. It is possible to derive the necessary inputs for the model from the polymer parameters by analysis of the polymer sample, those results are shown in Section 4.2. Then we will show simulation results in which we used kinetic parameters to calculate the model inputs in Section 4.3. The results are obtained using the kinetic equations based on the polymerization mechanisms. After that we will present a case study in which we discuss the compositional changes by using four semi-batch reactors in Section 4.4. In the last section of (Chapter 4) we will show results of an attempt to predict the ^{13}C NMR analysis of the simulated polymer. The chemical shift assignments and the intensities equations were explained in (Chapter 2).

4.2 Polymer Parameters

The chain length is related to the molecular weight by the molar mass of the monomer unit. We have explained earlier how the probability of chain propagation is (P_p) and the probability of chain termination ($P_t = 1 - P_p$) are related to the number-average chain length (r_n) in Chapter 3. If we assume that we have polyethylene samples with number

average molecular weights according to Table 4.1 then we are able to calculate the number-average chain length (r_n) for those samples.

Table 4-1 Calculated number average chain length for polyethylene

Mn (g/mol)	r_n
50,000	1700
100,000	3500
150,000	5300
200,000	7000

We used the calculated number-average chain lengths shown in the above Table to simulate the model four times. Figure 4.1 shows the homopolymer model output plots for the number fraction of chains as a function of the chain length.
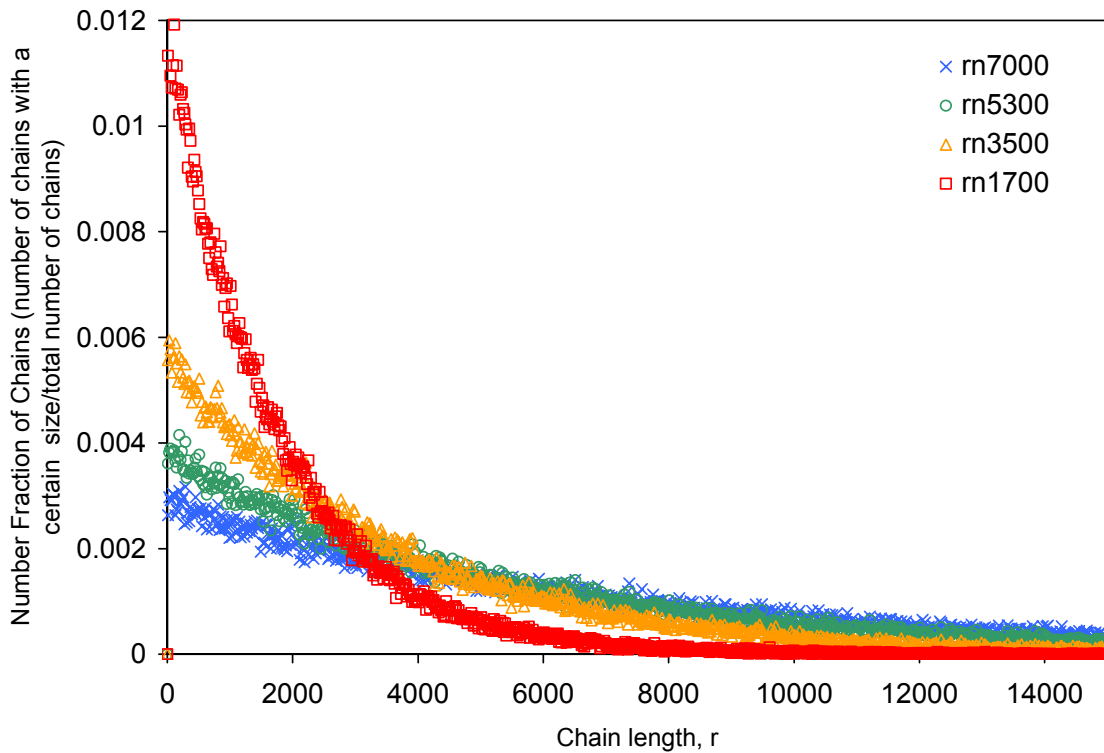
Figure 4-1 Number fraction of chains as a function chain length (r) with homopolymer model

Table 4.2 shows the number average molecular weights (Mn) for potential polyethylene samples and the calculated number-average chain length (r_n). The probability of adding comonomer B (P_B) was set at 0.2 for all the simulation runs. The model was simulated to create 100,000 chains in each run.

Table 4-2 Calculated number average chain length for polyethylene

Mn (g/mol)	r_n	P_B
50,000	1700	0.2
100,000	3500	0.2
150,000	5300	0.2
200,000	7000	0.2

Figure 4.2 shows the results for the copolymer model. Notice that the comonomer incorporation in the polymer chain is not dependent on the size of the chain length (r).
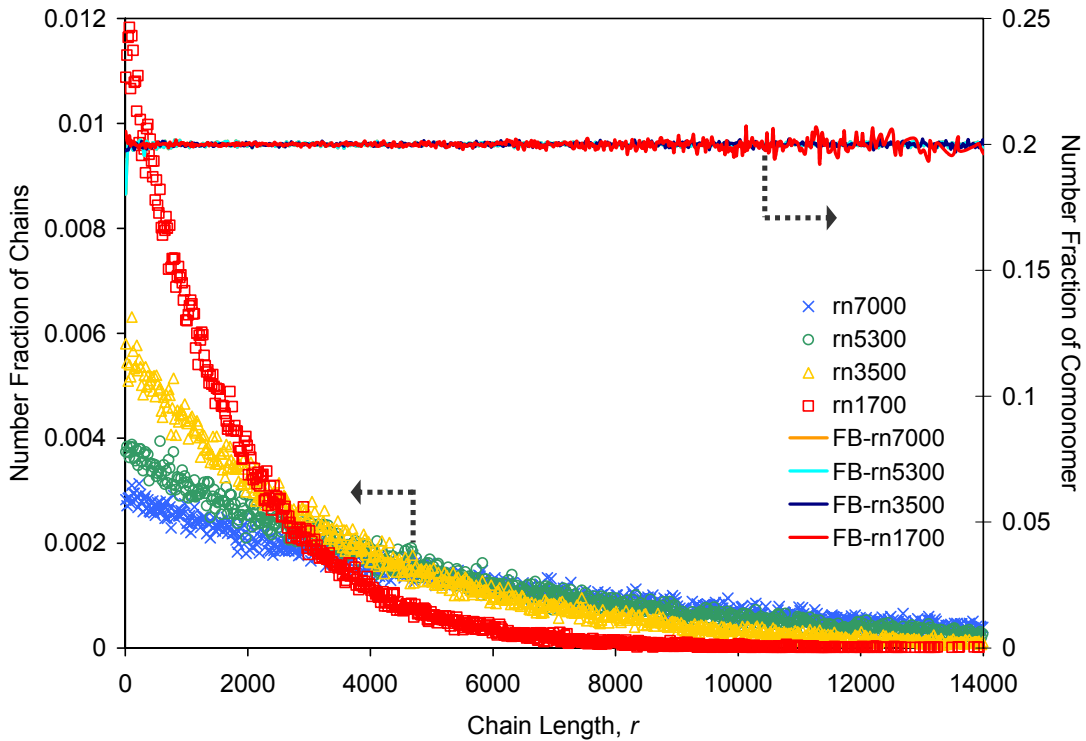
Figure 4-2 Simulation results: number fraction of chains as a function chain length (r) and comonomer distribution with copolymer model

As we run the model with lower number-average chain length we see a higher number of shorter chains. The number-average chain length (r_n) is related to the molecular weight of the material and hence affects the final mechanical properties of the product produced. The noise in the comonomer incorporation curves is due to the small population of chains at the high chain length. This does not change the interpretation of results and can be minimized by increasing the number of chains (longer simulation times) or by lumping the points within a wider range.

4.3 Kinetic Parameters Sensitivity

4.3.1 Homopolymer Model

In this section we will look at the homopolymer simulation results. The simulations will present results for the chain length distribution as a function of the chain length. The simulations are executed using different kinetic parameters that affect the number-average chain length (r_n).

Table 4.3 shows the kinetic parameters used to run the first batch of simulations in this section. The monomer concentration ([M]) and the active species concentrations ([Pr*]) were kept constant whereas the propagation kinetic constant (k_p) and the termination kinetic constant (k_t) were changed after each run. These parameters are within the range of those reported in the literature.

Table 4-3 Kinetic parameters used in the model with changing (k_p, k_t)

k_p (L/mole.s)	k_t (L/mole.s)	P_t	P_p	r_n
3200	1.20	0.00037	0.99963	2668
3600	1.10	0.00031	0.99969	3274
4000	1.00	0.00025	0.99975	4001
4400	0.90	0.00020	0.99980	4890

[Pr*]=10 × 10^{-6} (mole/L), [M]= 3 (mole/L)

The number-average chain length increased from 2668 to 4890 by changing the propagation kinetic constant and the termination kinetic constant (Figure 4.3). In the

coming plots we will change one parameter only and look at the effect on the chain fraction distribution as a function of chain length.

Figure 4-3 Number fraction of chains as a function of chain length (r) influenced by changing kinetic parameter constants (k_p, k_t)

Table 4.4 shows the kinetic parameters used to run the second batch of simulations for the homopolymer model using the kinetic parameters to calculate the simulation inputs. The monomer concentration ([M]), the active species concentrations ([Pr*]) and the termination kinetic constant (k_t) were kept constant whereas the propagation kinetic constant (k_p) was changed after each run.

Table 4-4 Kinetic parameters used in the model with changing (k_p)

k_p (L/mole.s)	k_t (L/mole.s)	P_t	P_p	r_n
3200	0.89	0.00028	0.99972	3597
3600	0.89	0.00025	0.99975	4046
4000	0.89	0.00022	0.99978	4495
4400	0.89	0.00020	0.99980	4945

$[Pr^*]=10 \times 10^{-6}$ (mole/L), $[M]= 3$ (mole/L)

The propagation kinetic constant (k_p) was increased gradually from 3200 (L/mole.s) to 4400 (L/mole.s). This increase resulted in a decrease in the probability of termination which in its turn lead to an increase in the number-average chain length. From Table 4.4 we see that the first run in this batch started with number average chain length of 3597 and last run was 4945. Figure 4.4 shows the chain fraction distribution as a function of the chain length where we were looking at the propagation kinetic constant influence on the chain distribution. Hence by increasing the propagation kinetic constant the number-average chain length increases.
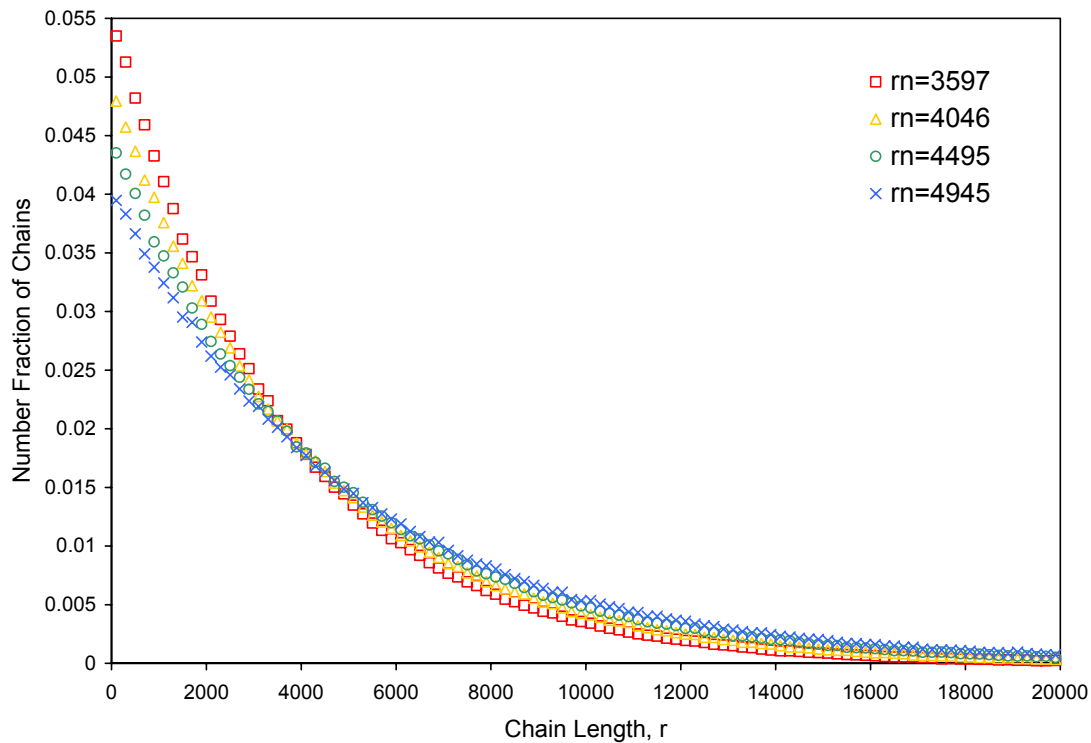
Figure 4-4 Number fraction of chains as a function of chain length (r) influenced by changing kinetic parameter constant (k_p)

Table 4.5 shows the kinetic parameters used in the simulations of the following results. The monomer concentration ([M]), the active species concentrations ([Pr*]) and the propagation kinetic constant (k_p) were kept constant whereas the termination kinetic constant (k_t) was decreased after each run.

Table 4-5Kinetic parameters used in the model with changing (k_t)

k_p (L/mole.s)	k_t (L/mole.s)	P_t	P_p	r_n
3200	1.00	0.00031	0.99969	3201
3200	0.90	0.00028	0.99972	3557
3200	0.80	0.00025	0.99975	4001
3200	0.70	0.00022	0.99978	4572

$$[Pr^*]=10 \times 10^{-6} \text{ (mole/L), [M]= 3 (mole/L)}$$

This time we are looking at the termination kinetic constant (k_t) influence on the chain fraction distribution. It is noticed that by decreasing the termination kinetic constant the probability of termination decreases and the number-average chain length increases. The output from the four simulation runs were plotted and shown in (Figure 4.5).
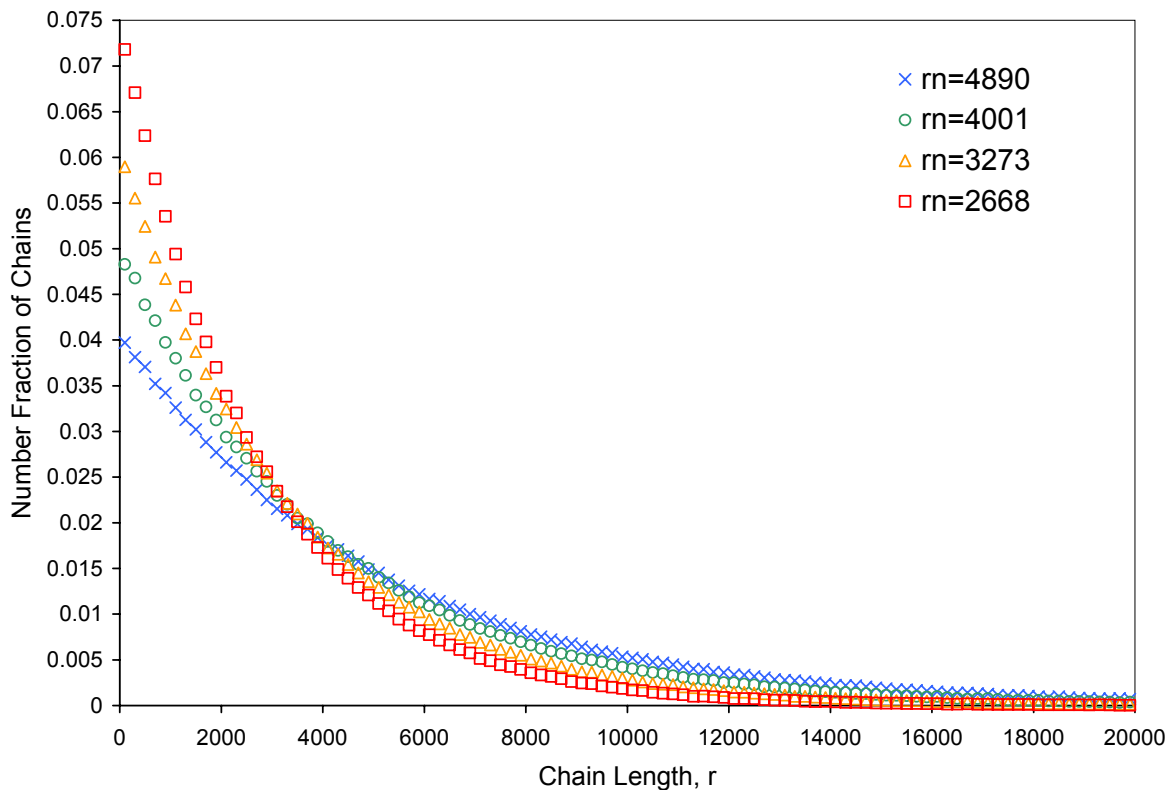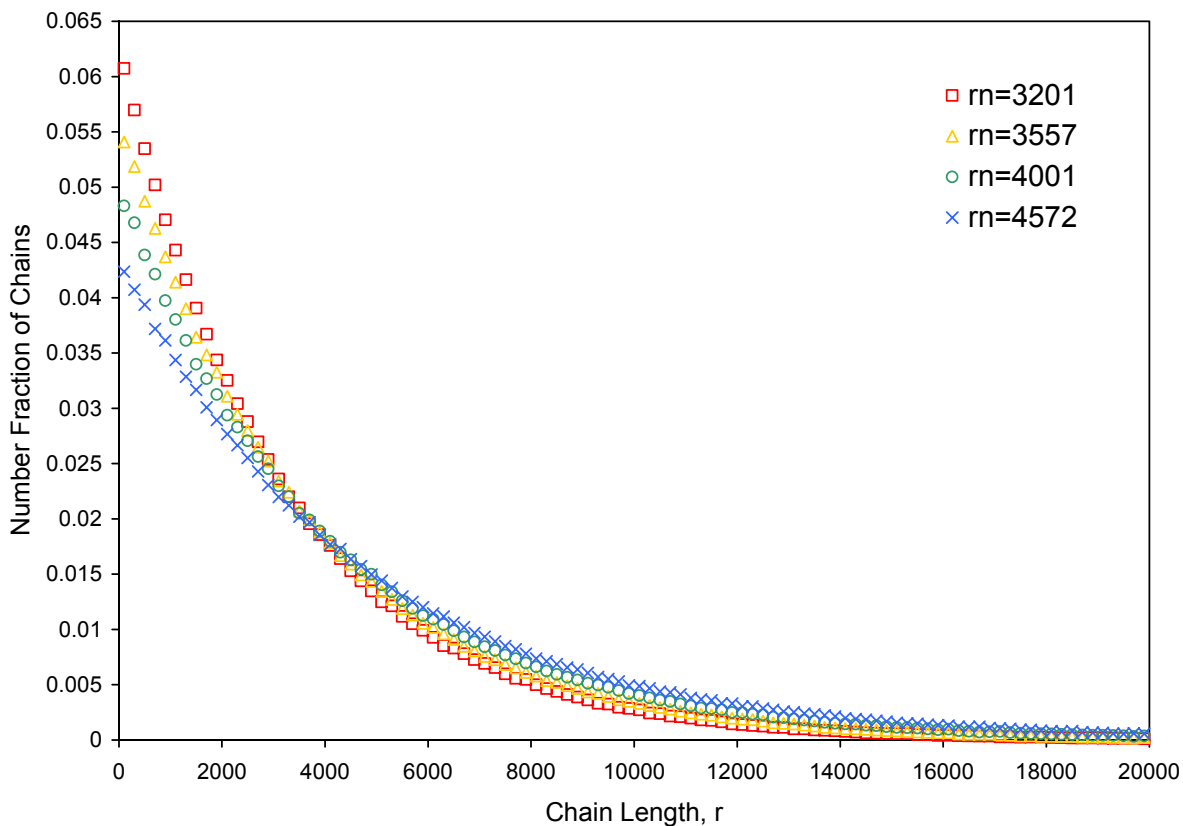
Figure 4-5 Number fraction of chains as a function of chain length (r) influenced by changing kinetic parameter constant (k_t)

Table 4.6 shows the kinetic parameters used to run the last batch of simulations for the homopolymer model. The active species concentrations ($[Pr^*]$), the termination kinetic constant (k_t) and the propagation kinetic constant (k_p) were kept constant whereas the monomer concentration ($[M]$) was decreased.

From the probability of propagation equation described below we see that changing the monomer concentration does not play big role in changing the probability of propagation value (or the probability of termination, $1 - P_p = P_t$) as the second term in the dominator can be negligible due to the presence of very small concentrations of the active species in the reactions.

$$P_p = \frac{R_p}{R_p + R_t} = \frac{k_p[P_r^*][M]}{k_p[P_r^*][M] + k_t[P_r^*]}$$

This will lead to give a constant value for the probability of propagation which in its turn will result in a constant value of the number-average chain length (r_n) according to the following equation.

$$P_p = \frac{R_p}{R_p + R_t} = \frac{1}{1 + \dfrac{R_t}{R_p}} = \frac{1}{1 + \dfrac{1}{r_n}} \approx 1 - \frac{1}{r_n}$$

The monomer concentration could affect the number-average chain length in the case of having multi-site catalyst and high concentration of active species ($[Pr^*]$).

Table 4-6 Kinetic parameters used in the model with changing the concentration of the monomer

[M] (mole/L)	P_t	P_p	r_n
3	0.00030	0.99970	3372
1	0.00030	0.99970	3372
0.1	0.00030	0.99970	3372
0.01	0.00030	0.99970	3372

$[Pr^*]=10 \times 10^{-6}$ (mole/L), k_p= 3000 (L/mole.s), k_t= 0.89 (L/mole.s)

As it was discussed we find that the monomer concentration had no influence on the probability of propagation or the probability of termination and thereby had no influence on the number-average chain length. The chain fraction distributions as a function of the chain length are shown in Figure 4.6.
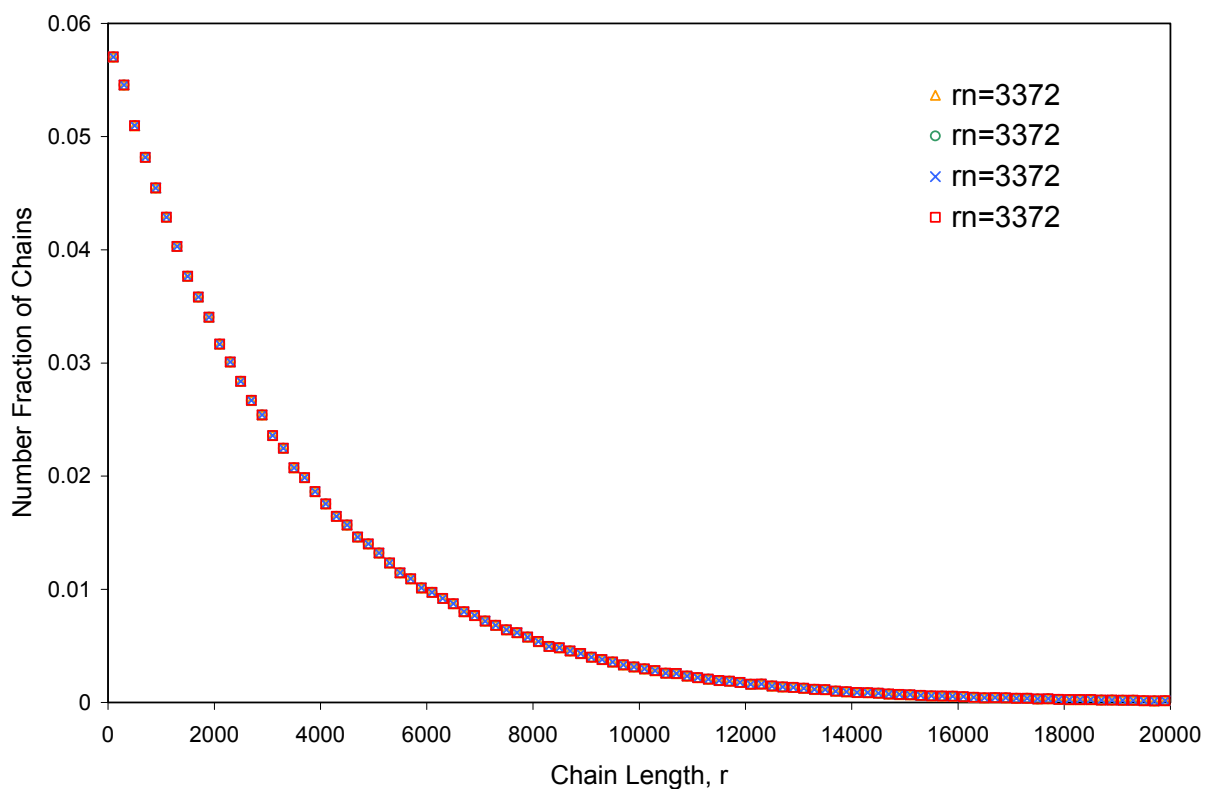
Figure 4-6 Number fraction of chains as a function of chain length (r) influenced by changing the concentration of the monomer [M]

4.3.2 Copolymer Model

In this section we will look at the copolymer simulation results. We will look at monomer (A) and comonomer (B) distribution as a function of the chain length and the segment fraction of monomer (A) and comonomer (B) as a function of the segment length. The simulations are executed using different kinetic parameters that affect the number-average chain length (r_n) with different probabilities of adding comonomer B (P_B).

Table 4.7 shows the kinetic parameters used to look at the influence of changing the concentration of the monomer ([A]). The comonomer concentration ([B]), the active species concentrations ([Pr*]), propagation kinetic constants for the monomer (k_{pA}) and comonomer (k_{pB}), termination kinetic constants for the monomer (k_{tA}) and comonomer

(k_{tB}) were kept constant whereas the concentration of the monomer was changed after each run.

Table 4-7 Kinetic parameters used in the model with changing the monomer concentration [A]

[A] (mole/L)	P_t	P_p	r_n	P_B
1.00	0.00049	0.99951	2041	0.12
1.25	0.00040	0.99960	2491	0.10
1.50	0.00034	0.99966	2941	0.08
1.75	0.00029	0.99971	3391	0.07
2.00	0.00026	0.99974	3841	0.06
2.25	0.00023	0.99977	4291	0.06
2.50	0.00021	0.99979	4741	0.05
2.75	0.00019	0.99981	5191	0.05
3.00	0.00018	0.99982	5641	0.04

$[Pr^*]=10 \times 10^{-6}$ (mole/L), $[B] = 0.1$ (mole/L), $k_{pA}= 3600$ (L/mole.s), $k_{pB}= 4800$ (L/mole.s), $k_{tA}= k_{tB}= 1.0$ (L/mole.s)

Figure 4.7 shows the influence of increasing the monomer concentration on the chain length distribution and comonomer distribution. In the case of the copolymerization we have a competition between the monomer and comonomer to coordinate and be inserted in the polymer chain. The probability of termination decreased with increasing the concentration of monomer (A). Therefore the number average chain length increased with increasing the monomer concentration. On the other hand the probability of adding comonomer B (P_B) decreased by increasing monomer (A) concentration. In the plot presented in Figure 4.7 we see that the comonomer distribution is not changing with the chain length.
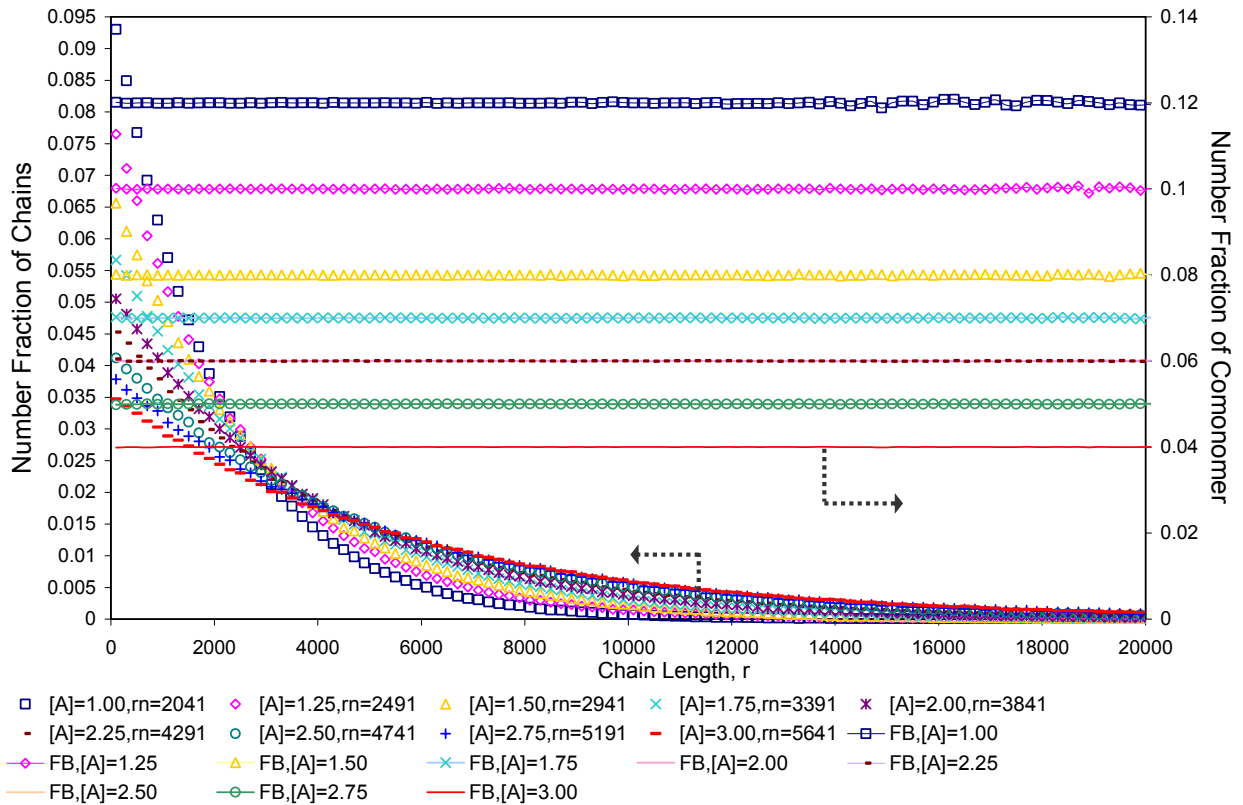
Figure 4-7 Number fraction of chains and comonomer distribution as a function of chain length (*r*) with changing the monomer concentration [A]

The length of the crystallizable monomer sequence is a parameter that determines the degree of crystallinity in polyethylene. Addition of comonomer decreases the length of the segment that can be crystallized, thereby decreasing the degree of crystallinity in these semi-crystalline polymers. Experimental work in the literature has shown segments from 4 up to 18 ethylene units in length do not contribute to the crystalline phase in ethylene copolymers (Randall and Ruff, 1988). Haag and co-workers have previously chosen the value of 20 monomeric as the minimum segment length to be accounted for when simulating the effect of comonomer composition on the degree of crystallinity (Haag et al., 2003). The model developed keeps track of the fraction of monomer and comonomer sequence length A_n and B_n (Figure 4.8).

AAABBAAABAABBBA

$(A)_n$

Segment < 20 monomer units will not crystallize

$$\sum_{n=1}^{n=20} A_n$$

Figure 4-8 Segment length.

Figure 4.9 shows fraction of segments for monomer (A) with different segment length. The purpose of this plot is to show the model capability in predicting the monomer sequence distribution. Figure 4.10 shows the fraction of segments for comonomer (B) as a function of segment length. When the model simulated for number average chain length r_n=2041 with average fraction of comonomer $F_B = 12\%$ we had the longest sequence for isolated comonomer (B_{10}) of ten commoner units.

In the next section of this chapter we will look at the monomer and comonomer segment distribution in more depth and predict it as a function of the chain length.
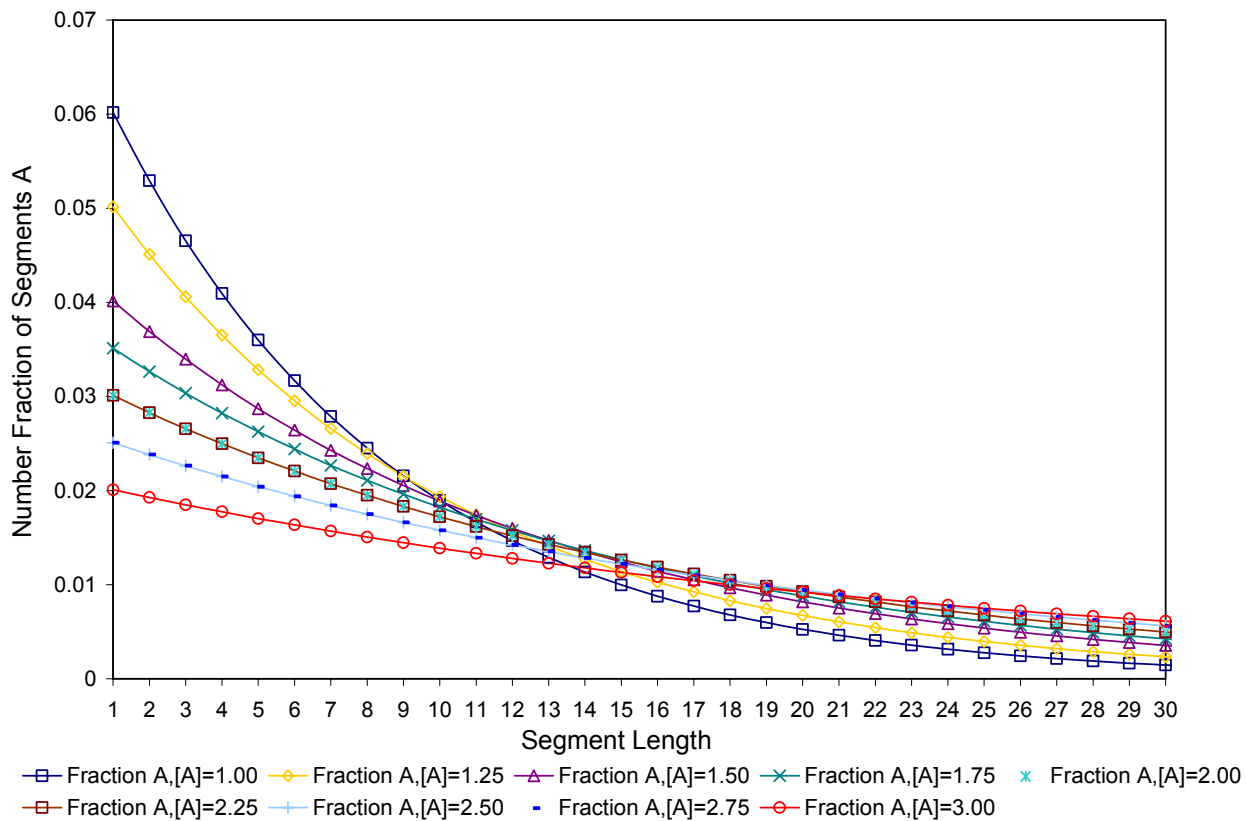
Figure 4-9 Fraction of monomer (A) and comonomer (B) segments as a function of segment length with changing the monomer concentration [A]
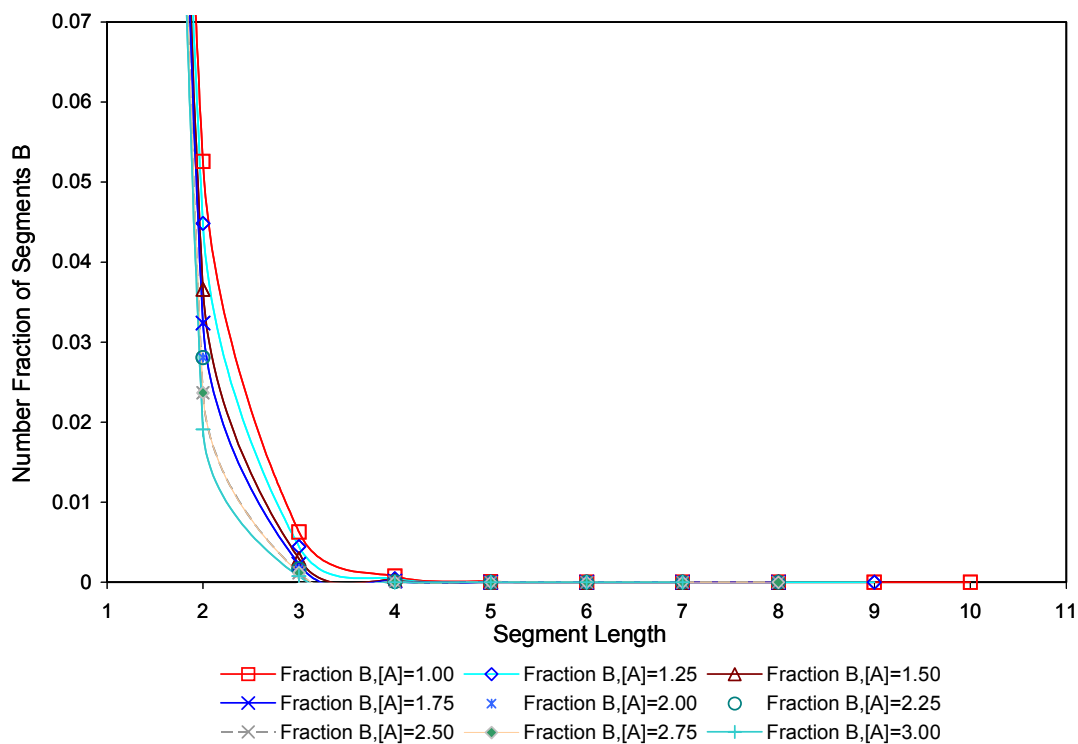
Figure 4-10 Fraction of monomer (A) and comonomer (B) segments as a function of segment length with changing the monomer concentration [A]

Table 4.8 shows the kinetic parameters used to look at the influence of changing the concentration of the comonomer ([B]). The monomer concentration ([A]), the active species concentrations ([Pr*]), propagation kinetic constants for the monomer (k_{pA}) and comonomer (k_{pB}), termination kinetic constants for the monomer (k_{tA}) and comonomer (k_{tB}) were kept constant whereas the concentration of the comonomer was changed after each run.

Table 4-8 Kinetic parameters used in the model with changing the comonomer concentration [B]

[B] (mole/L)	P_t	P_p	r_n	P_B
0.05	0.00027	0.99973	3721	0.03
0.075	0.00026	0.99974	3781	0.05
0.1	0.00026	0.99974	3841	0.06
0.3	0.00023	0.99977	4321	0.17
0.5	0.00021	0.99979	4801	0.25
0.75	0.00019	0.99981	5401	0.33
1	0.00017	0.99983	6001	0.40
2	0.00012	0.99988	8401	0.57

$[Pr^*]=10 \times 10^{-6}$ (mole/L), $[A] = 2.0$ (mole/L), $k_{pA}= 3600$ (L/mole.s), $k_{pB}= 4800$ (L/mole.s), $k_{tA}= k_{tB}= 1.0$ (L/mole.s)

Figure 4.11 shows the influence of increasing the comonomer concentration on the chain length distribution and comonomer distribution. The probability of termination decreased with increasing the concentration of comonomer (B). Therefore the number average chain length increased while the probability of adding monomer B (P_B) increased with increasing comonomer (B) concentration. With comonomer concentration of 0.05 (mole/L) the chain length $r_n = 3721$ and the comonomer fraction was $F_B = 3\%$. When the concentration was increased to 0.3 (mole/L) the chain length increased to $r_n = 4321$ and the comonomer fraction was $F_B = 17\%$. This is explained by looking at the probability of termination equation and studying the relationship between the probability of termination and the number-average chain length (r_n). From the probability of termination equation described below we see that by increasing comonomer B concentration the dominator value will increase resulting in a decrease in the probability of termination.

$$P_t = \frac{R_t}{R_p + R_t} = \frac{(R_{tA} + R_{tB})}{(R_{pA} + R_{pB})+(R_{tA} + R_{tB})} = \frac{k_{tA}[P_r^*]+k_{tB}[P_r^*]}{(k_{pA}[P_r^*][A]+k_{pB}[P_r^*][B])+(k_{tA}[P_r^*]+k_{tB}[P_r^*])}$$

64

As was described earlier the probability of termination is inversely proportional to the number-average chain length and the relationship is given by the following equation:

$$P_t = \frac{R_t}{R_p + R_t} = \frac{1}{\dfrac{R_p}{R_t} + 1} = \frac{1}{r_n + 1} \approx \frac{1}{r_n}$$

Therefore as we increase the concentration of comonomer B the probability of termination decrease which leads to an increase in the number-average chain length.

This could be explained in different way by looking at the relationship between the probability of propagation and the number-average chain length. As the probability of termination decrease the probability of propagation increase ($P_p = 1 - P_t$). Relating the number-average chain length with the probability of propagation from the equations described bellow we find that by increasing the probability of propagation the number-average chain length increases.

$$P_p = \frac{R_p}{R_p + R_t} = \frac{1}{1 + \dfrac{R_t}{R_p}} = \frac{1}{1 + \dfrac{1}{r_n}} \approx 1 - \frac{1}{r_n}$$

$$\Rightarrow \quad r_n \approx \frac{1}{1 - P_p}$$
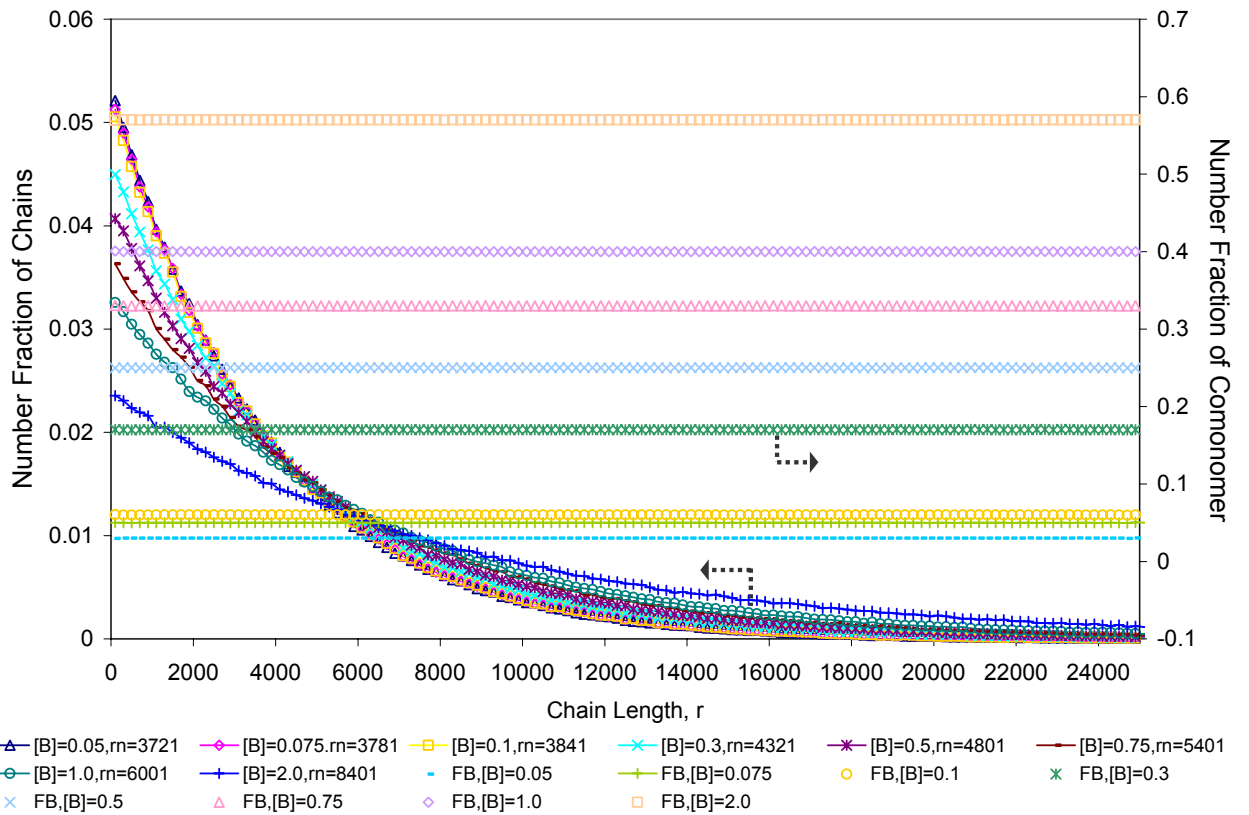
Figure 4-11 Number fraction of chains and comonomer distribution as a function of chain length (*r*) with changing the comonomer concentration [B]

Figure 4.12 shows fraction of segments for the monomer with different segment length. The model simulated for different number average chain lengths shown in Table 4.8 with average fraction of comonomer range from $F_B = 3\%$ to 57%. The copolymer model was capable of predicting the monomer sequence distribution with changing the concentration of comonomer (B).

Figure 4-12 Fraction of monomer (A) segments as a function of segment length with changing the comonomer concentration [B] (units in mole/L)

Figure 4.13 shows the fractions of segments for comonomer (B) with different segment length. The model simulated different number average chain lengths shown in Table 4.8 with average fraction of comonomer range from $F_B = 3\%$ to 57%. This range of average comonomer composition covers the major types of polymer products from linear low density polyethylene (LLDPE) to ethylene propylene rubber (EPR). The copolymer model was capable of predicting the comonomer sequence distribution for different types of potential polymeric materials by changing the concentration of comonomer (B). The longest isolated comonomer sequence was thirty eight comonomer units with comonomer concentration [B] = 2 (mole/L), $r_n = 8401$ and $F_B = 57\%$.
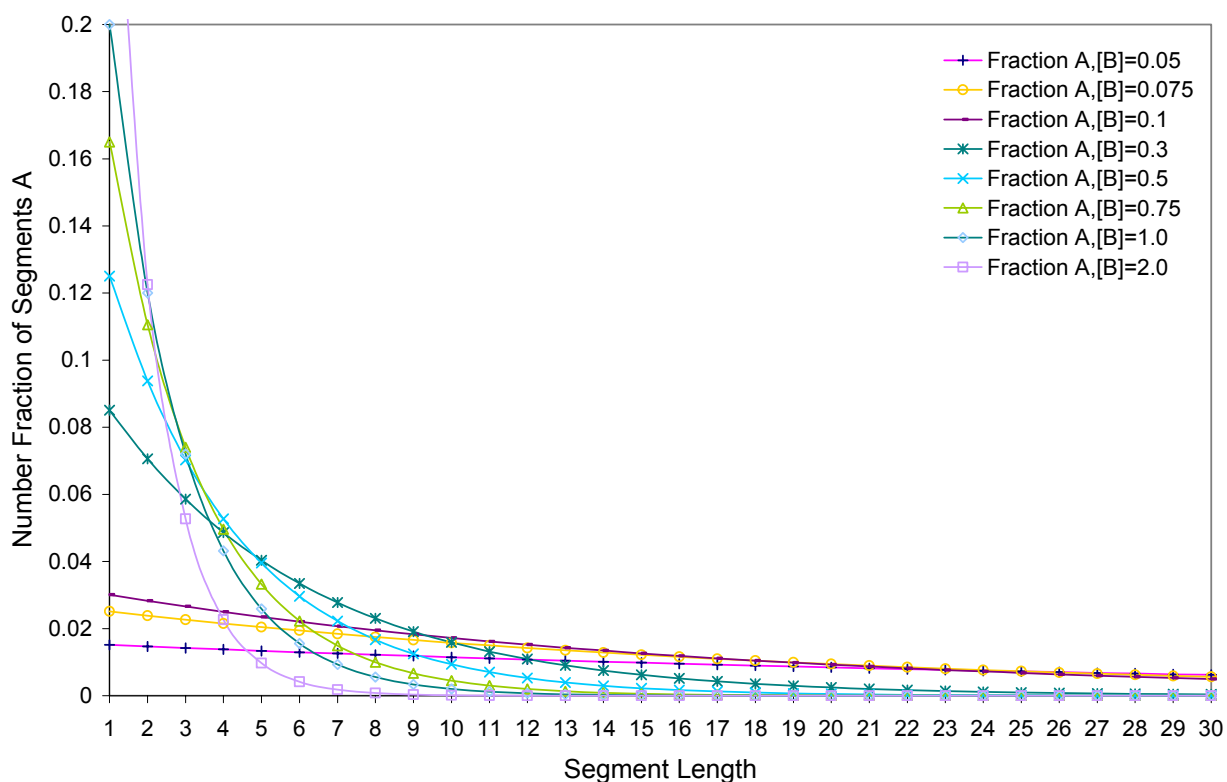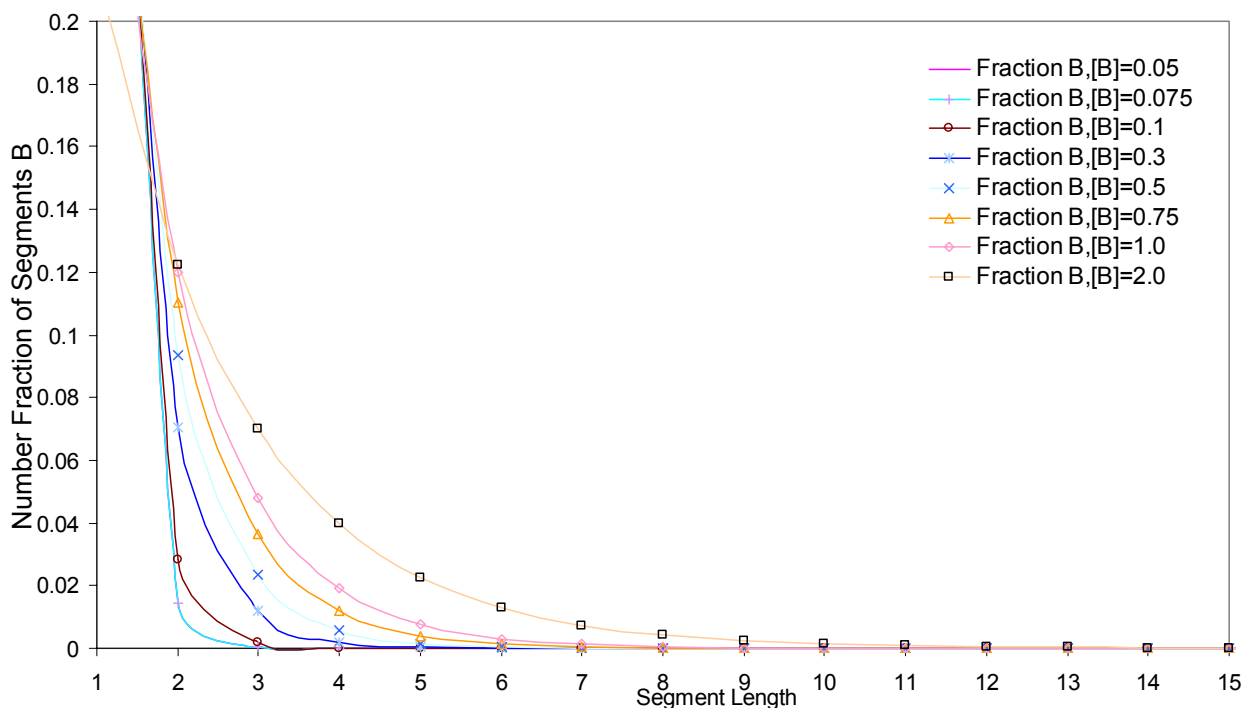
Figure 4-13 Fraction of comonomer (B) segments as a function of segment length with changing the comonomer concentration [B] (units in mole/L)

Now we will change the propagation kinetic constant for the monomer (k_{pA}) and keep the monomer concentration ([A]), comonomer concentration ([B]), the active species concentration ([Pr^*]), propagation kinetic constant for comonomer (k_{pB}), termination kinetic constants for the monomer (k_{tA}) and comonomer (k_{tB}) at constant values. Table 4.9 shows the kinetic parameters used to look at the influence of changing the propagation kinetic constants of the monomer (k_{pA}).

Table 4-9 Kinetic parameters used in the model with changing the propagation kinetic constant for the monomer (k_{pA})

k_{pA} (L/mole.s)	P_t	P_p	r_n	P_B
3600	0.00017	0.99983	5881	0.08
3100	0.00019	0.99981	5131	0.09
2650	0.00022	0.99978	4456	0.11
2100	0.00028	0.99972	3631	0.13

[Pr^*]=10 × 10^{-6} (mole/L), [A] = 3.0 (mole/L), [B] = 0.2 (mole/L), k_{pB}= 4800 (L/mole.s), k_{tA}= k_{tB}= 1.0 (L/mole.s)

Figure 4.14 shows the influence of decreasing the propagation kinetic constant for the monomer (k_{pA}) on the chain length distribution and comonomer distribution. The probability of termination increased with decreasing the propagation kinetic constant for the monomer (k_{pA}). Therefore the number average chain length decreased and the probability of adding monomer B (P_B) increased with decreasing the propagation kinetic constants for the monomer (k_{pA}).

Figure 4-14 Number fraction of chains and comonomer distribution as a function of chain length (r) with changing the propagation kinetic constant for the monomer (k_{pA})

Figure 4.15 shows fraction of segments for monomer (A) with different segment length. The model simulated for different number average chain lengths shown in Table 4.9 with average fraction of comonomer range from $F_B = 8\%$ to 13%. Figure 4.16 shows fraction of segments for comonomer (B) with different segment lengths. The longest isolated comonomer sequence was eleven comonomer units with monomer propagation kinetic constant (k_{pA}) = 2100, $r_n = 3631$ and $F_B = 13\%$.
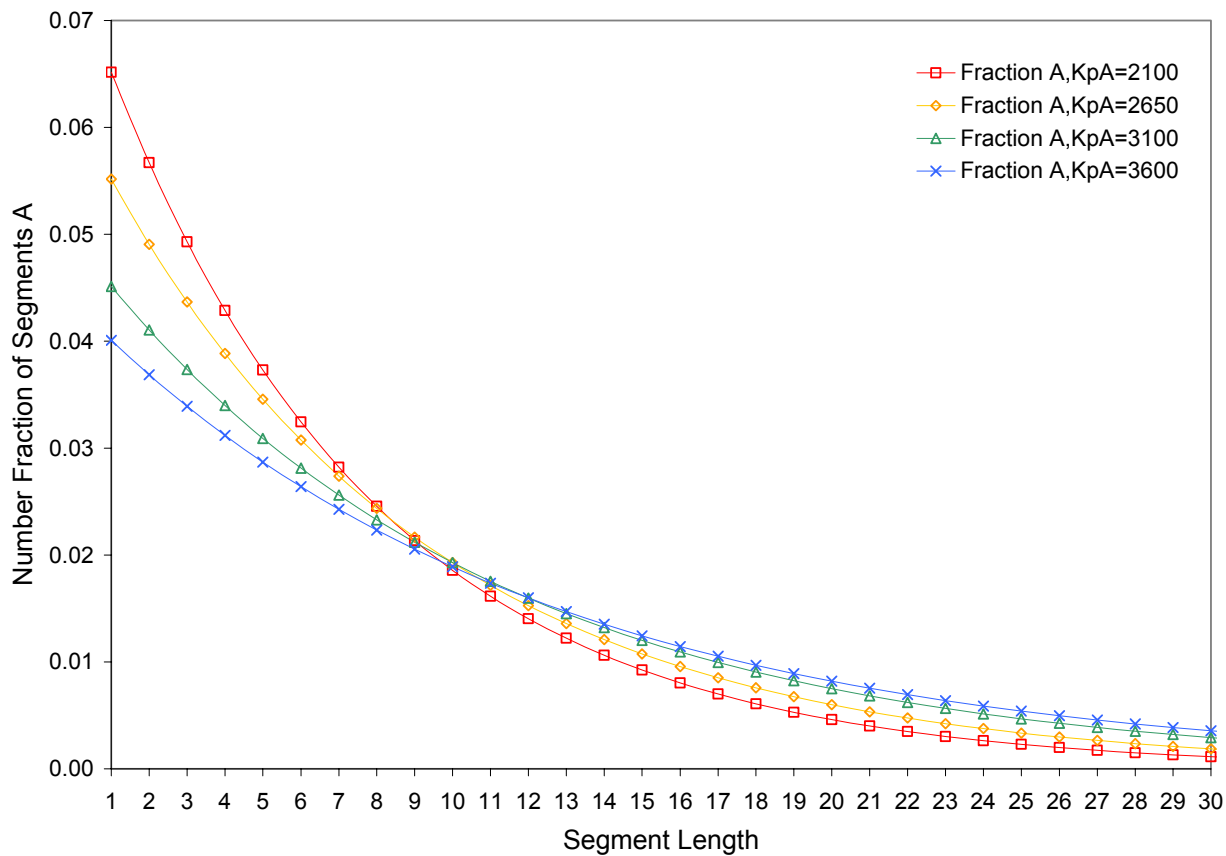
Figure 4-15 Fraction of monomer (A) segments as a function of segment length with changing the propagation kinetic constant for the monomer (k_{pA})

Figure 4-16 Fraction of comonomer (B) segments as a function of segment length with changing the propagation kinetic constant for the monomer (k_{pA})

Finally we will change the propagation kinetic constants for comonomer (k_{pB}) and keep the monomer concentration ([A]), comonomer concentration ([B]), the active species concentration ([Pr*]), propagation kinetic constants for the monomer (k_{pA}), termination kinetic constants for the monomer (k_{tA}) and comonomer (k_{tB}) at constant values. Table 4.10 shows the kinetic parameters used to look at the influence of changing the propagation kinetic constants of the comonomer (k_{pB})

Table 4-10 Kinetic parameters used in the model with changing the propagation kinetic constant for the comonomer (k_{pB})

k_{pB} (L/mole.s)	P_t	P_p	r_n	P_B
4800	0.00017	0.99983	5881	0.08
4300	0.00017	0.99983	5831	0.07
3700	0.00017	0.99983	5771	0.06
3000	0.00018	0.99982	5701	0.05

$[Pr^*] = 10 \times 10^{-6}$ (mole/L), $[A] = 3.0$ (mole/L), $[B] = 0.2$ (mole/L), $k_{pA} = 3600$ (L/mole.s), $k_{tA} = k_{tB} = 1.0$ (L/mole.s)

Figure 4.17 shows the influence of decreasing the propagation kinetic constant for the comonomer (k_{pB}) on the chain length distribution and comonomer distribution. The probability of termination showed a minor increase with decreasing propagation kinetic constant of the comonomer (k_{pB}). Therefore the number average chain length decreased slightly and the probability of adding monomer B (P_B) decreased with decreasing the propagation kinetic constants for the comonomer (k_{pB}).
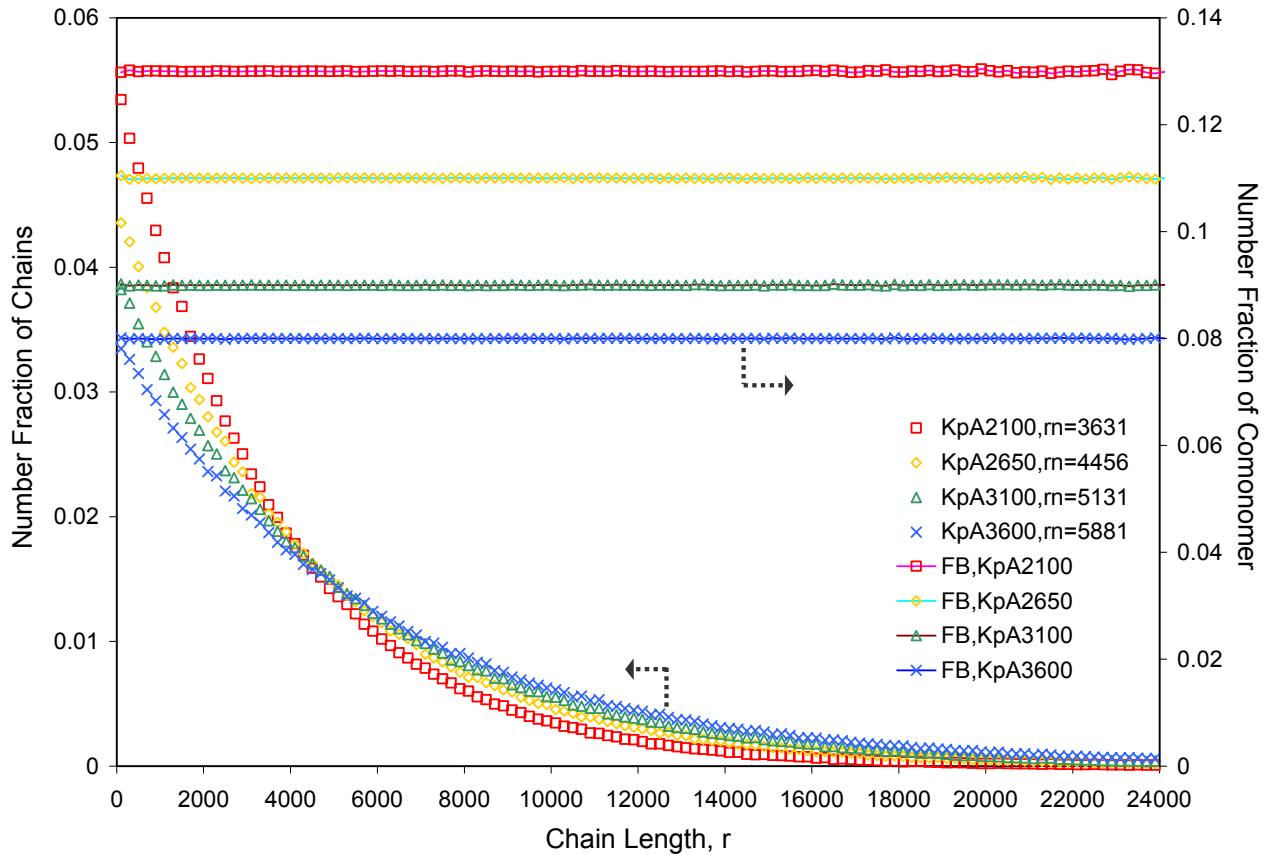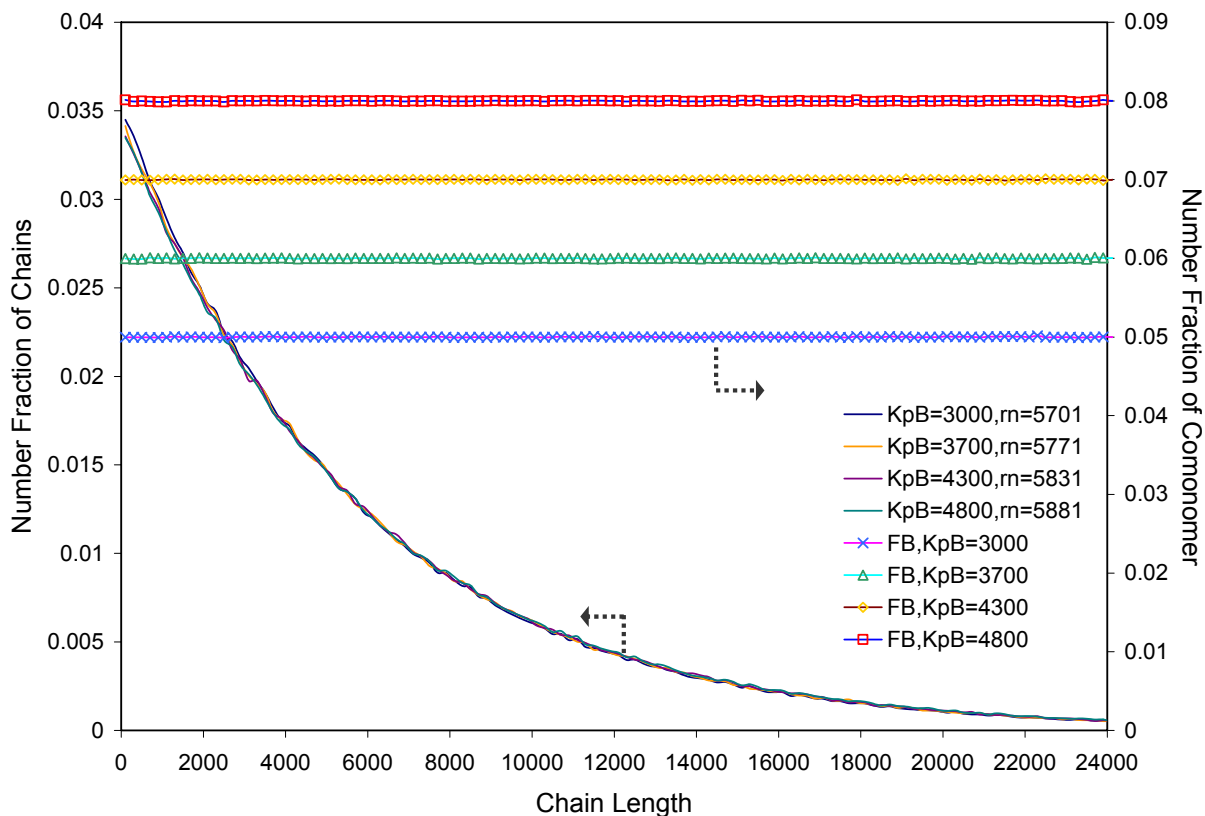
Figure 4-17 Number fraction of chains and comonomer distribution as a function of chain length (r) with changing the propagation kinetic constant for the comonomer (k_{pB})

Figure 4.18 shows fraction of segments for monomer (A) with different segment length. The model was simulated for different number average chain lengths shown in Table 4.10 with average fraction of comonomer range from F_B = 5% to 8%. Figure 4.19 shows the fraction of segments for comonomer (B) with different segment length. The longest isolated comonomer sequence for all the runs were very similar ranging between seven to eight comonomer units.
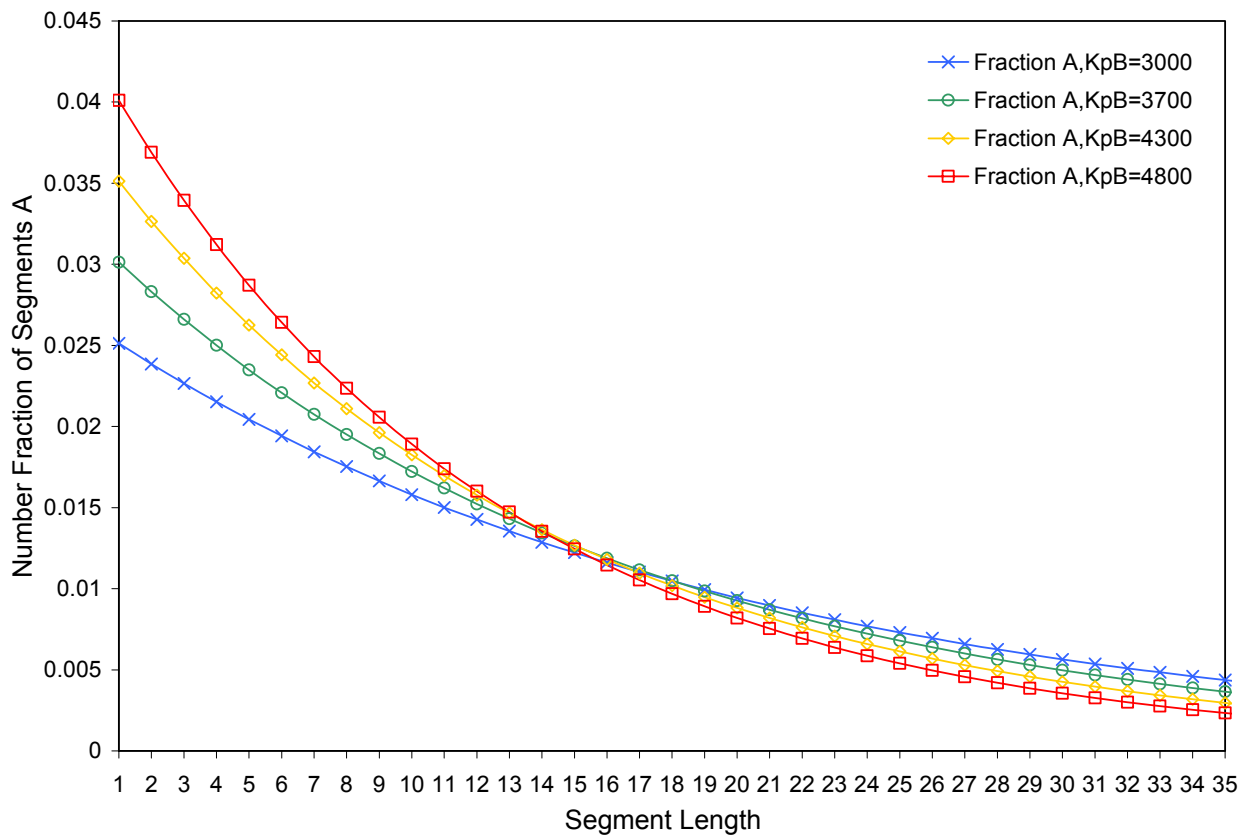
Figure 4-18 Fraction of monomer (A) segments as a function of segment length with changing the propagation kinetic constant for the comonomer (k_{pB})
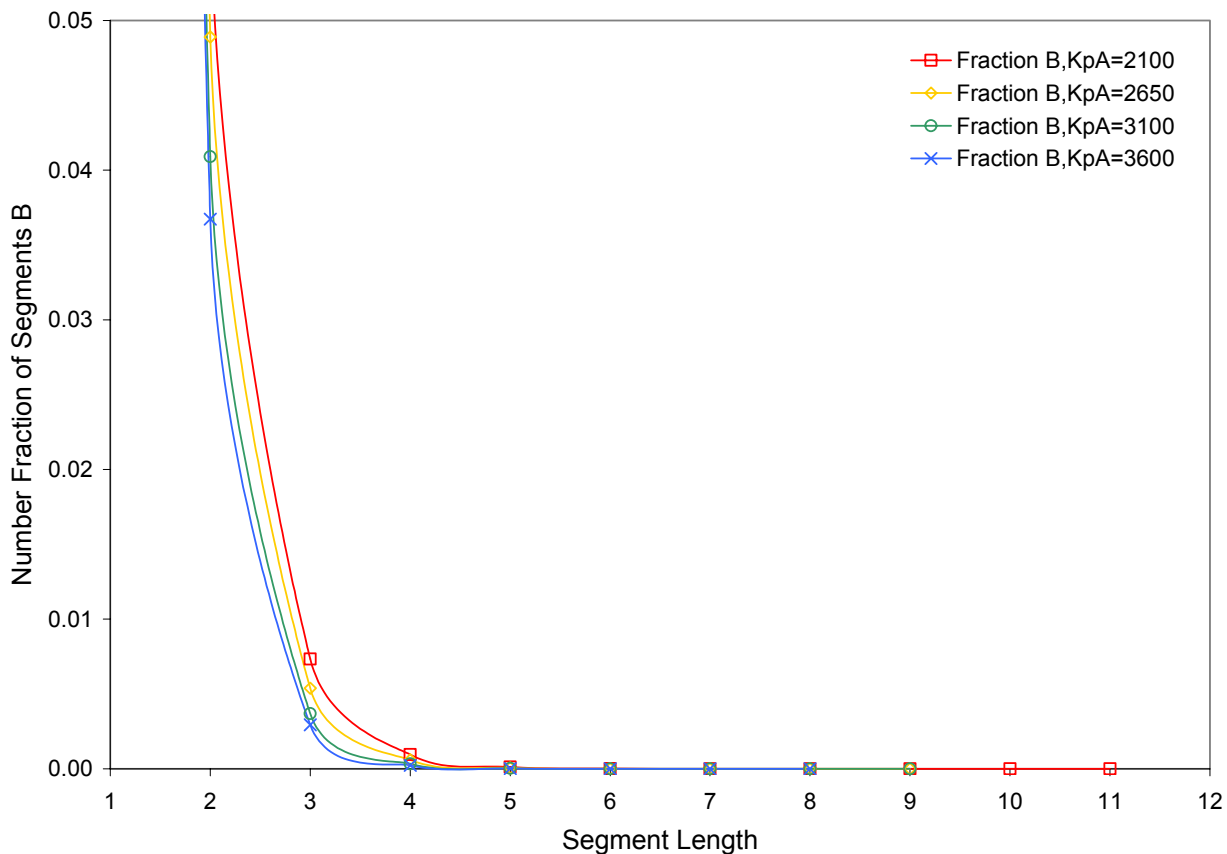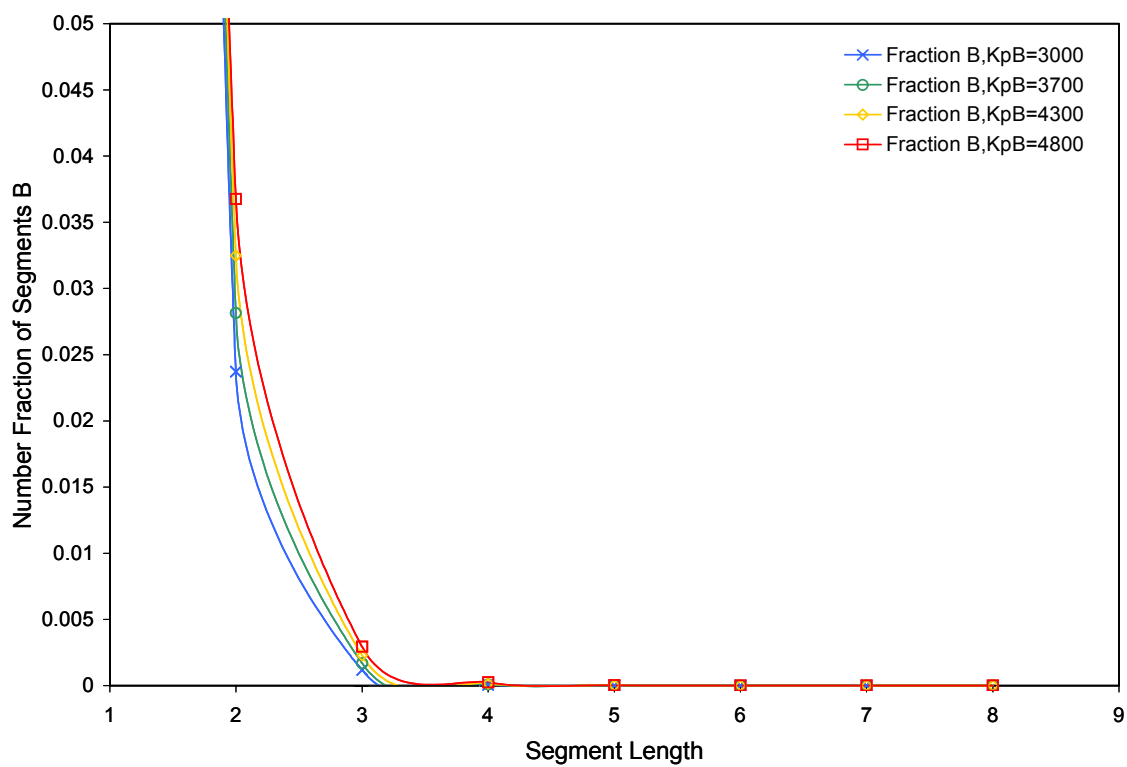
Figure 4-19 Fraction of comonomer (B) segments as a function of segment length with changing the propagation kinetic constant for the comonomer (k_{pB})

4.4 Monomer Sequence Distribution

4.4.1 Detailed Segment Length Distribution

Our discussion will be focused on the segments distribution and triad distribution with parameter input for the copolymer model of r_n=5004 and F_B=3%.The kinetic parameters which were used to simulate the run for the following results of this section are shown in Table 4.11.

Table 4-11 Kinetic parameters used in the model

k_{pA} (L/mole.s)	k_{pB} (L/mole.s)	k_{tA} (L/mole.s)	k_{tB} (L/mole.s)	P_t	Pp	r_n	P_B
2200	2040	0.79	0.57	0.00020	0.99980	5004	0.03

$[Pr^*]$=10 × 10^{-6} (mole/L), [A]= 3 (mole/L), [B]= 0.1 (mole/L)

Figure 4.20 shows fraction of segments with different lengths, for monomer A and comonomer B. Most of the segments of comonomer B are isolated in sequences like ABA, that is $B_{n=1}$, with a fraction equal to 0.9636. There is a monotonic decrease in the fraction of segments B_n when the segment length increases. The longest comonomer segment B_n was six monomers units ($B_{n=6}$ or ABBBBBBA). Most of the segments A_n have lengths between 1 and 100. Surprisingly, segment $A_{n=1}$ representing sequences like BAB where the segment A is isolated by two adjacent segment Bs has the highest fraction. The fraction of segment length of monomer A_n decreases continuously as the segment length increases with an inflection point at around segment length $A_{n=80}$.

76
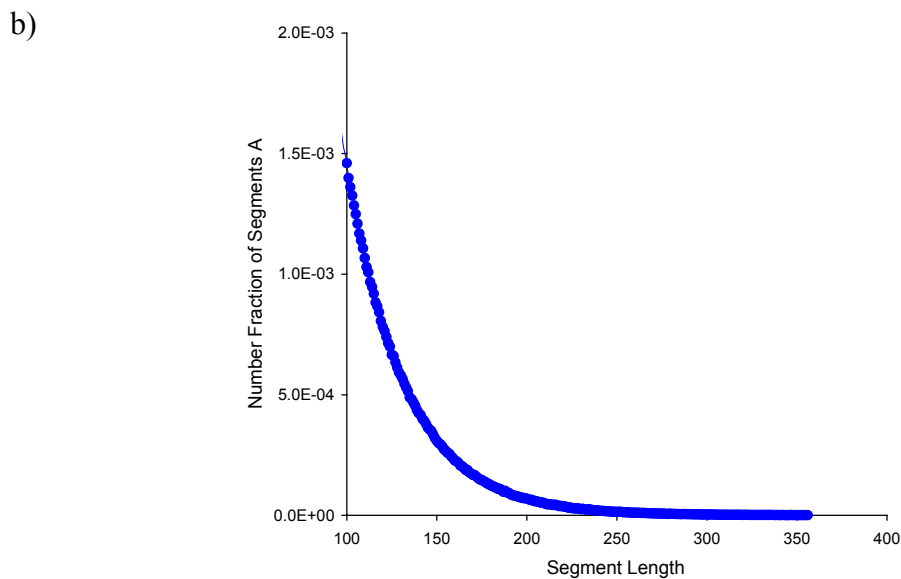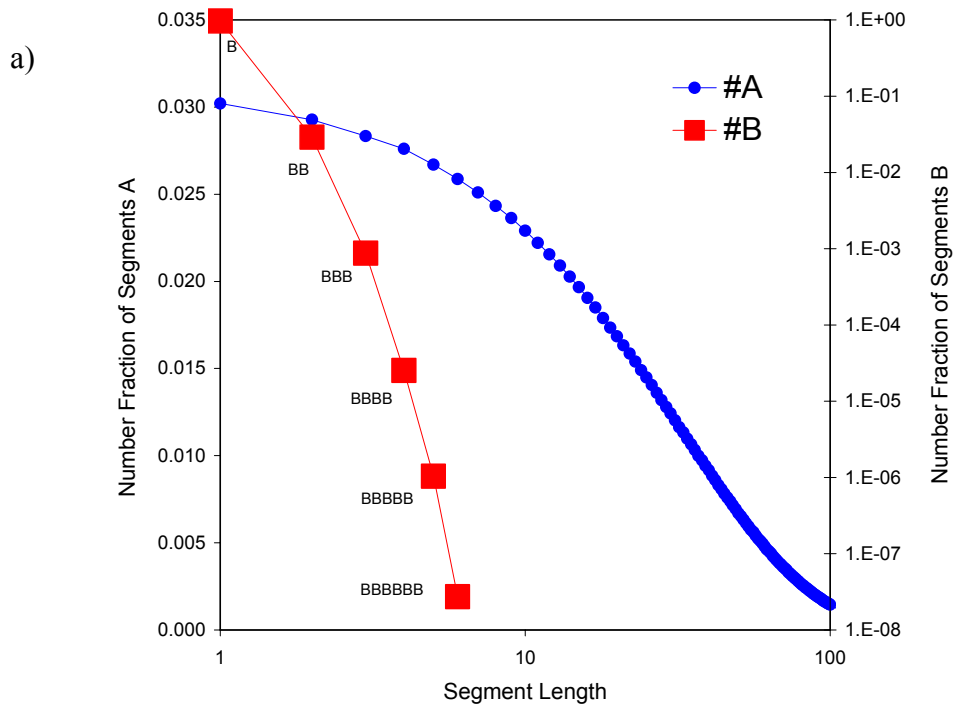
Figure 4-20 a) Fraction of monomer and comonomer segment length, A_n and B_n respectively and b) Tail of fraction for monomer segment length. (r_n=5004, F_B=3%)

As indicated before, the number of segments with length equal or smaller than 20 will be used to indicate the part of a polymer chain that cannot contribute to crystallization. The model is capable of calculating the fraction of all segments with length between 1 and 19,

for monomer A and comonomer B, as a function of chain length. All segments with length 20 or larger are lumped as A_{20+} (or $A_{>19}$). Figure 4.21 shows the distribution of segments that are capable of crystallizing as a function of chain length.

For simplicity, the summation of segments with length from 1 to 19 (A_{1-19} and B_{1-6}) is used to illustrate how this distribution changes as a function of chain length. Although in the case of copolymerization of ethylene (monomer A) with α-olefin (comonomer B) the comonomer sequence is unlikely to crystallize, it is interesting to see how the fraction of segments is distributed as a function of chain length (Figure 4.21). Crystallization of comonomer is possible in the case of ethylene-propylene rubber for example, where long comonomer (propylene) sequences could crystallize if the sequence is isotactic. This case was not considered here.
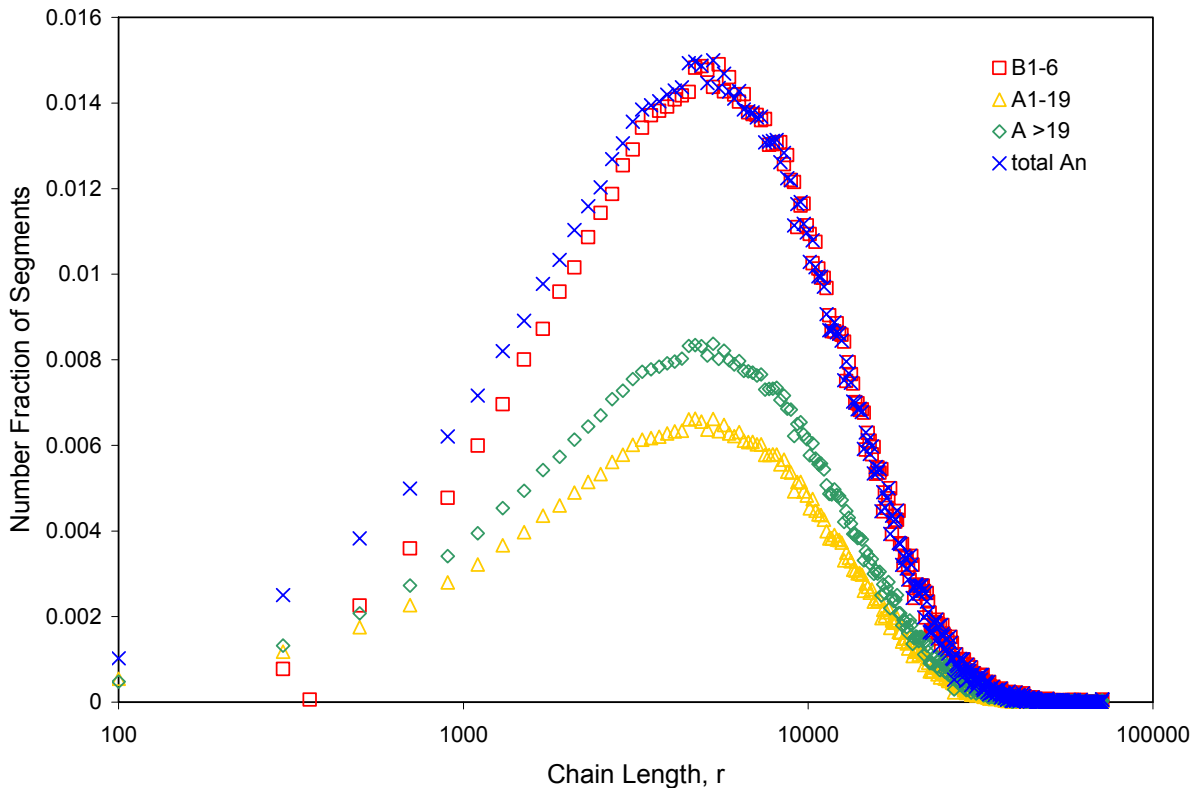
Figure 4-21 Distribution of segments B_{1-6}, A_{1-19}, $A_{>19}$ and total A_n as a function of chain length (r_n=5004, F_B=3%)

Figure 4.22 shows the shows the individual (B_1, B_2,... B_n) distribution for comonomer B segments as a function of chain length. The longest isolated comonomer sequence in this run was six comonomer units. We see in the plot the distribution for comonomer segment length B_1 to B_6. The highest number of segments was for single comonomer units with B_1 which accounted for 96.3% to 97.9% of comonomer segments and B_2 accounted for approximately about 3%. The fraction of segments (population) decreases significantly when the length of the segment increases, which increases the noise in the distribution curve. For example, only a few segments of B_5 were observed. (Noise could be decreased by increasing the simulation time).
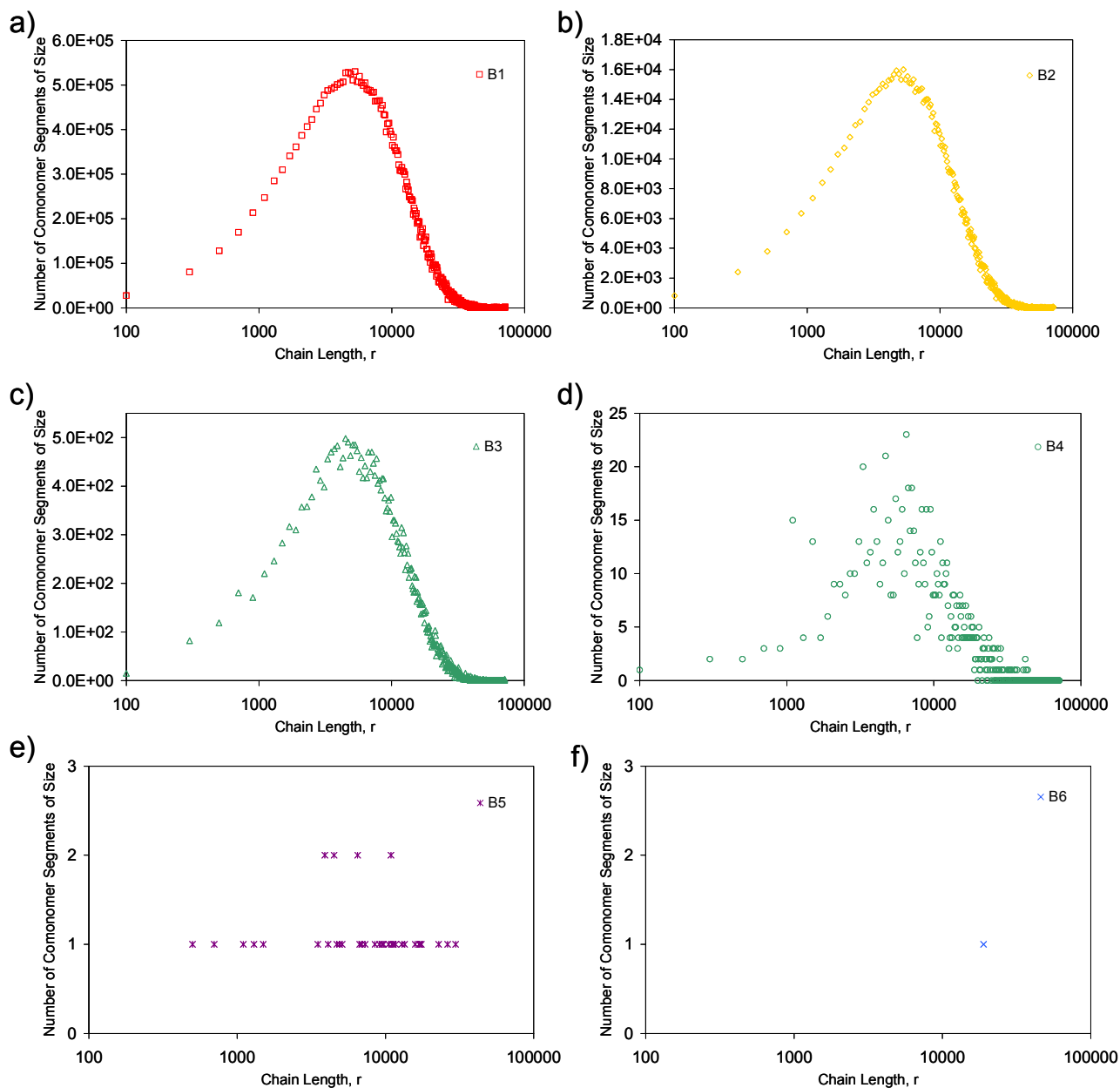
Figure 4-22 Distribution of comonomer segments from B_1 to B_6 represented in graphs from a) to f) respectively as a function of chain length (r_n=5004, F_B=3%)

4.4.2 Triad Distribution

The model is capable of identifying the triad sequence distribution as a function of chain length (Figure 4.23). The calculation of triad sequences distribution for (AAB and BAA), (ABA), (ABB and BBA), (BAB), and (BBB) is an essential step towards predicting the

[13]C nuclear magnetic resonance (NMR) spectra. The triad distribution could be related to the chemical shift assignments for predicating the NMR spectra quantitatively.
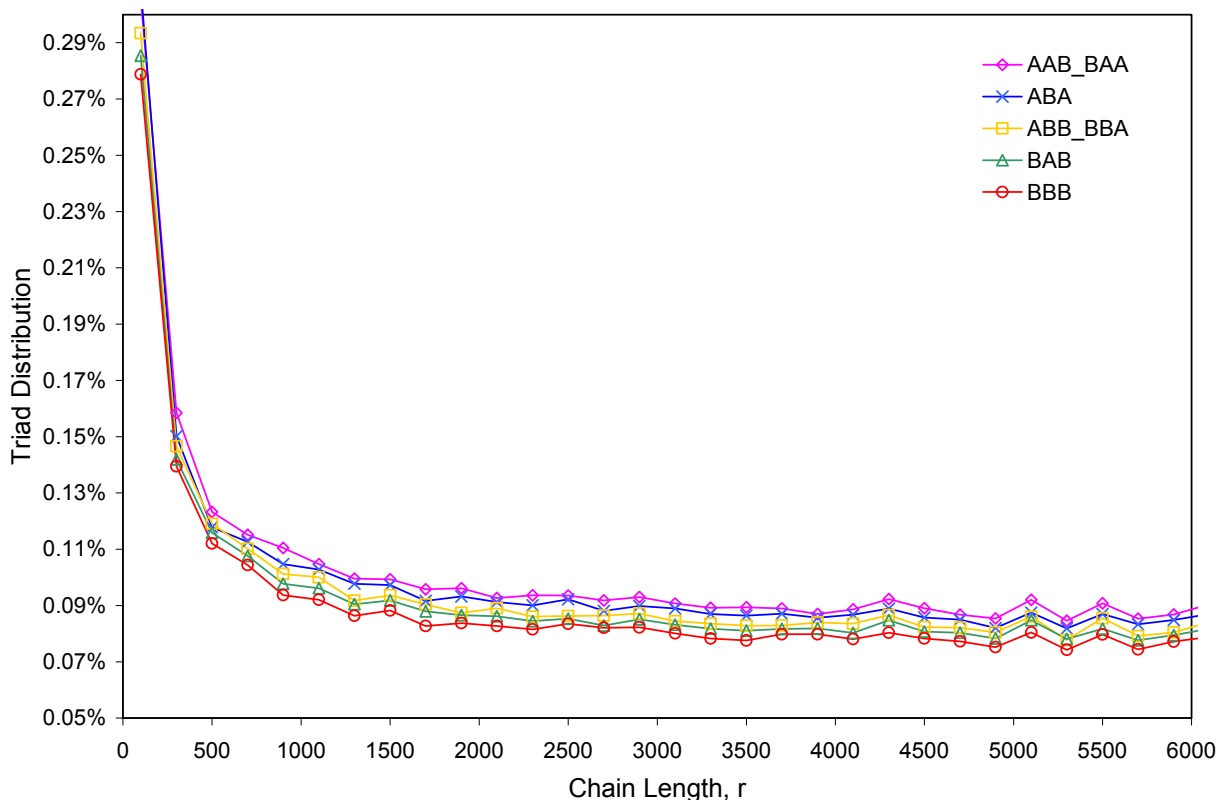
Figure 4-23 Triad distribution as a function of chain length (r_n=5004, F_B=3%)

4.5 Case Study for Semi-Batch Reactors

The model was used to explore the case where four semi-batch reactors with different conditions (kinetic parameters) in each reactor. The purpose of this study is simply to illustrate the model capabilities and potential to understand the distribution of branching as a function of chain length. In this case study, each reactor produces independently 250,000 copolymer chains with different number average chain lengths (r_n) and number fraction of comonomer (F_B). The product from reactor 1 is mixed with reactor 2 to give 500,000 copolymer chains (R_1+R_2). Then mixed product from reactor 1 and 2 is mixed with the product from reactor 3 to give 750,000 copolymer chains (R_1+R_2+R_3). Finally the mixed product from reactor 1, 2 and 3 is mixed with reactor 4 to give a total of 1,000,000 copolymer chains (R_1+R_2+R_3+R_4); see Figure 4.24.

| Reactor 1 (250k chains) | Reactor 2 (250k chains) | Reactor 3 (250k chains) | Reactor 4 (250k chains) |

r_n = 1008 r_n = 3001 r_n = 5004 r_n = 7024

F_B = 5% F_B = 4% F_B = 3% F_B = 2%
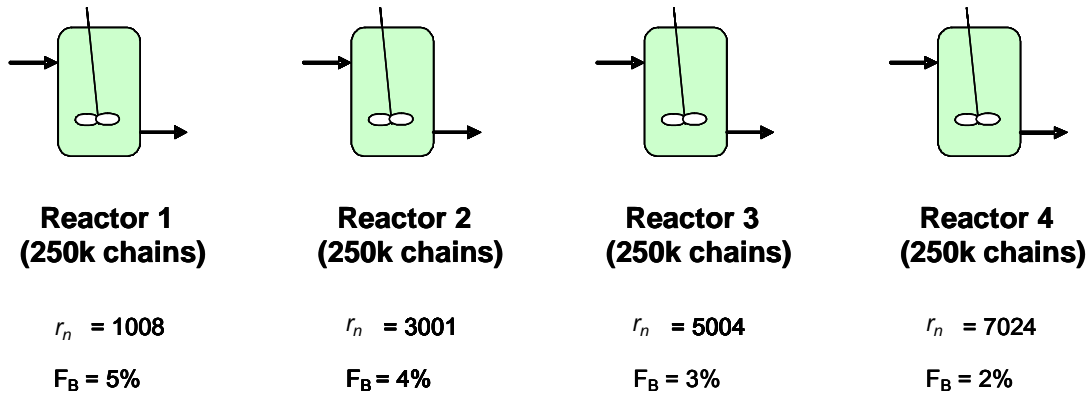
Figure 4-24 Case studies considering 4 semi-batch reactors.

For each reactor the kinetics parameters did not change during each simulation. The number average chain increased from r_n = 1008 to r_n = 7024 (Table 4.12). The average comonomer composition decreased from F_B = 5% to F_B = 2 %.

Table 4-12 Kinetic parameters used in the case study (representing the products with r_n=1007 to 7024 for reactor 1 to reactor 4 simulation run respectively)

	k_{pA} (L/mole.s)	k_{pB} (L/mole.s)	k_{tA} (L/mole.s)	k_{tB} (L/mole.s)	P_t	P_p	r_n	P_B
R_1	1210	1910	2.70	1.10	0.00099	0.99901	1008	0.05
R_2	2160	2700	1.25	1.00	0.00033	0.99967	3001	0.04
R_3	2200	2040	0.79	0.57	0.00020	0.99980	5004	0.03
R_4	3900	2390	0.92	0.78	0.00014	0.99986	7024	0.02

$[Pr^*]$=10 × 10^{-6} (mole/L), [A]= 3 (mole/L), [B]= 0.1 (mole/L)

The number-average chain length (r_n), the weight-average chain length (r_w), polydispersity index (PDI) and the fraction of comonomer B (F_B) for the process of mixing the products from reactor 1 (R_1), reactor 2 (R_2), reactor 3 (R_3) to reactor 4 (R_4) are shown in Table 4.13. The number-average chain length, the weight-average chain length and the polydispersity index are calculated by the following equations respectively:

$$r_n = \frac{\sum n.r}{\sum n}, \quad r_w = \frac{\sum n.r^2}{\sum n.r}, \quad PDI = \frac{r_w}{r_n}$$

where, n is the number of chains and r is the chain length.

Table 4-13 Effect of product mixing from reactor1 to reactor 4 on the polymer parameters

	r_n	r_w	PDI	F_B
R_1	1008	2001	1.98	5.0%
R_1+R_2	2006	4994	2.49	4.5%
$R_1+R_2+R_3$	3007	7777	2.59	4.0%
$R_1+R_2+R_3+R_4$	4009	10513	2.62	3.5%

The effect of mixing the products from reactor 1 to reactor 4 made the number average chain length increase from $r_n = 1008$ to $r_n = 4009$ and the average comonomer composition decrease from $F_B = 5\%$ to $F_B = 3.5\%$ (Table 4.14). The kinetic parameters were calculated backwards by knowing the number average chain length and the probability of adding comonomer B.

Table 4-14 Kinetic parameters used in the case study after mixing (representing the products with r_n= 1008 to 4009 for mixed product from reactor 1 to reactor 4)

	k_{pA} (L/mole.s)	k_{pB} (L/mole.s)	k_{tA} (L/mole.s)	k_{tB} (L/mole.s)	P_t	P_p	r_n	P_B
R_1	1210	1910	2.70	1.10	0.00099	0.99901	1008	0.05
R_1+R_2	1100	1550	0.92	0.80	0.00050	0.99950	2006	0.045
$R_1+R_2+R_3$	1308	1650	0.79	0.57	0.00033	0.99967	3007	0.04
$R_1+R_2+R_3+R_4$	2220	2400	0.94	0.78	0.00025	0.99975	4009	0.035

$[Pr^*]=10 \times 10^{-6}$ (mole/L), $[A]= 3$ (mole/L), $[B]= 0.1$ (mole/L)

The number fraction of chains and the number fraction of comonomer are plotted as a function of chain length. The compositional drift is illustrated in the results. Figure 4.25 shows the impact of mixing the products of reactor 1 to 4 on the number fraction of chains produced. The increase in number average chain length (r_n) could be explained by knowing that the probability of propagation of the mixed product after reactor 4 is greater than the probability of propagation of the product from reactor 1 (Table 4.13) *Pp* reactor1 < *Pp* reactor 1 and 2 < *Pp* reactor 1 and 2 and 3 < *Pp* reactor 1 and 2 and 3 and 4. With larger number average chain length produced in reactor 4 and lower fraction of

comonomer, it is expected that this product would have different final properties than that produced in the other reactors.

Figure 4-25 Number fraction of chains from reactor 1 with 250,000 chain to reactor 4 with 1,000,000 chains as a function of chain length (varying r_n and F_B)

Figure 4.26 shows that the number fraction of comonomer F_B is clearly drifting by increasing the number of chains produced by mixing the products of reactor 1 to 4. Comparing the lines in Figure 4.26, it can be seen that the comonomer fraction F_B decreases from reactor 1 to reactor 4 as the populations of the different reactors are mixed. It is clear that after mixing the products of reactor 1 to 4 the fraction of comonomer drifts to a certain point then it flattens and becomes steady as a function of chain length.

The noise in the comonomer incorporation curves at the high chain length end (right hand side) is due to small population of chains at the high chain length range. This does not

change the interpretation of results and can be minimized by increasing the number of chains (longer simulation times) or by lumping the points within a wider range of chain length.

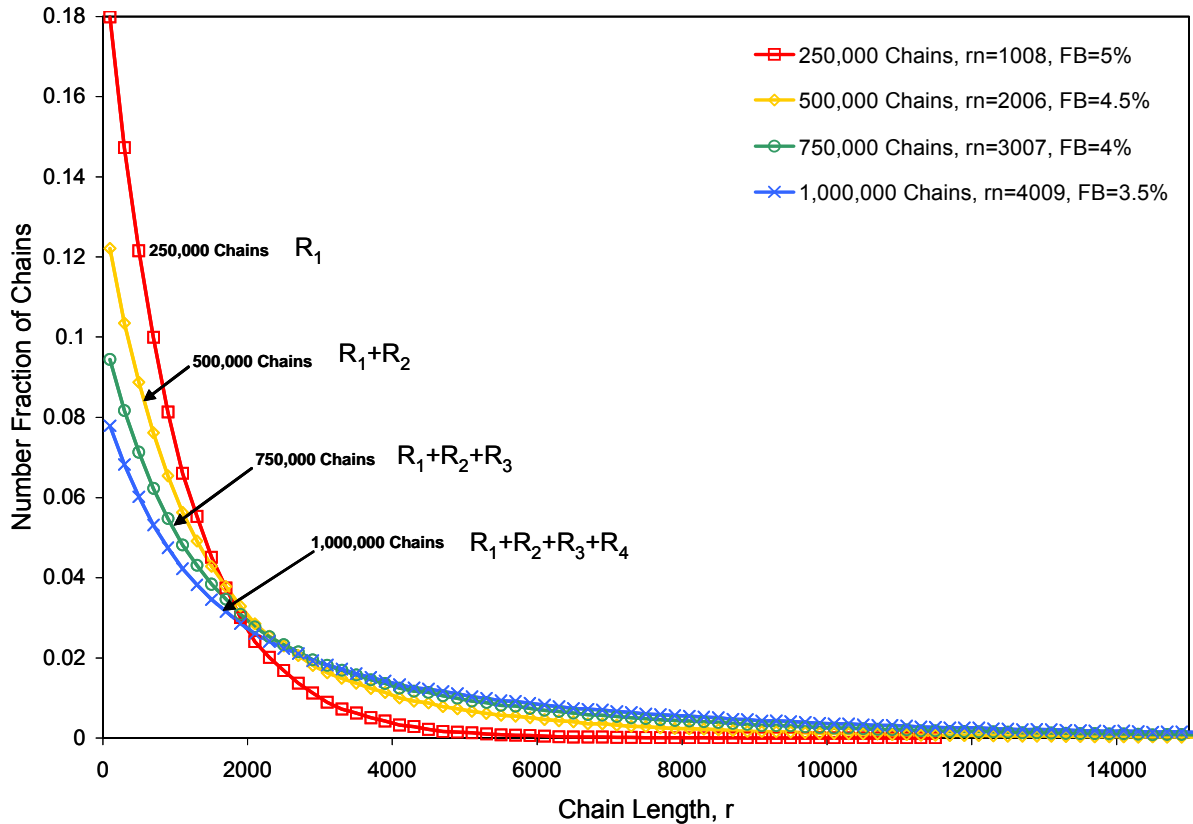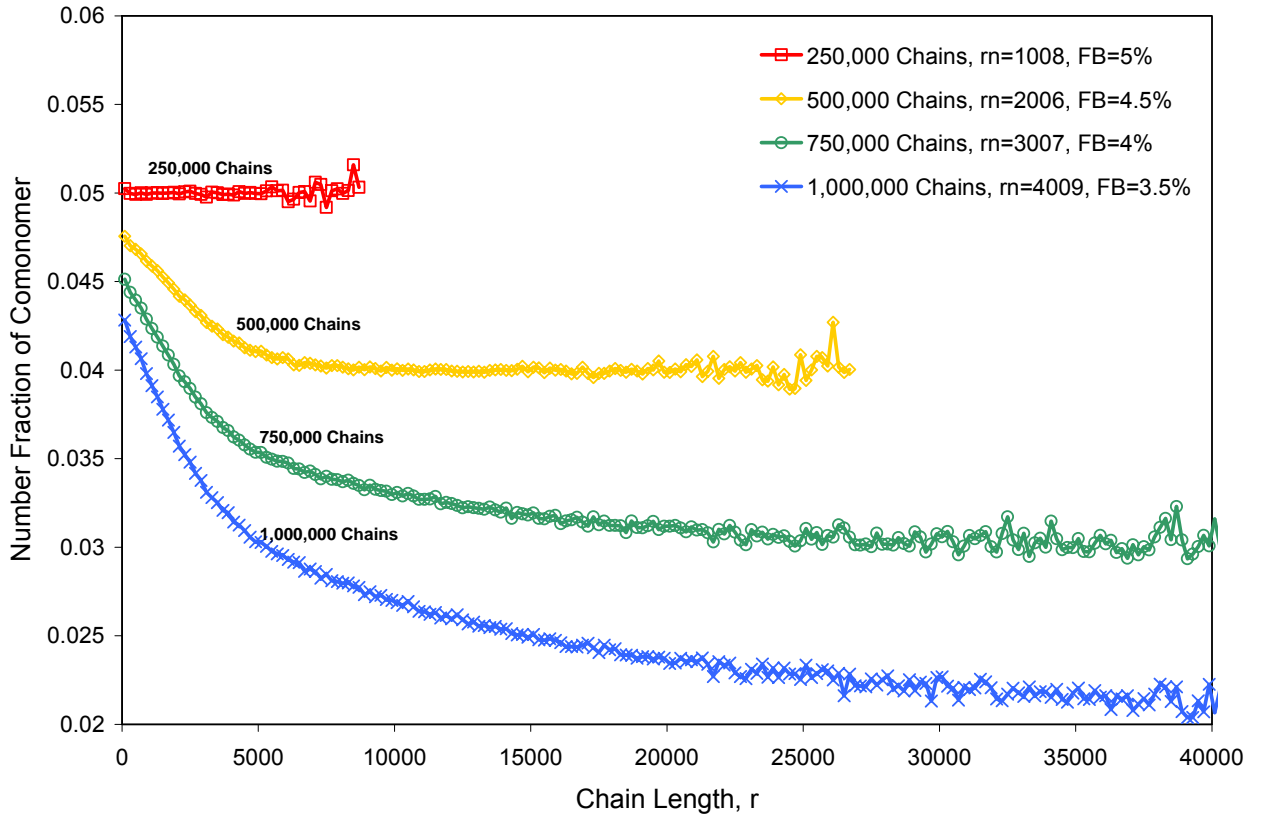

Figure 4-26 Number fraction of comonomer from reactor 1 with 250,000 chains to reactor 4 with 1,000,000 chains as function of chain length (varying r_n, F_B)

Figure 4.27 shows monomer A distribution for segment length from A_1 to A_{19} as a function of the chain length. Those distributions represent the simulation run shown in Table 4.12, that is, each reactor was run independently.
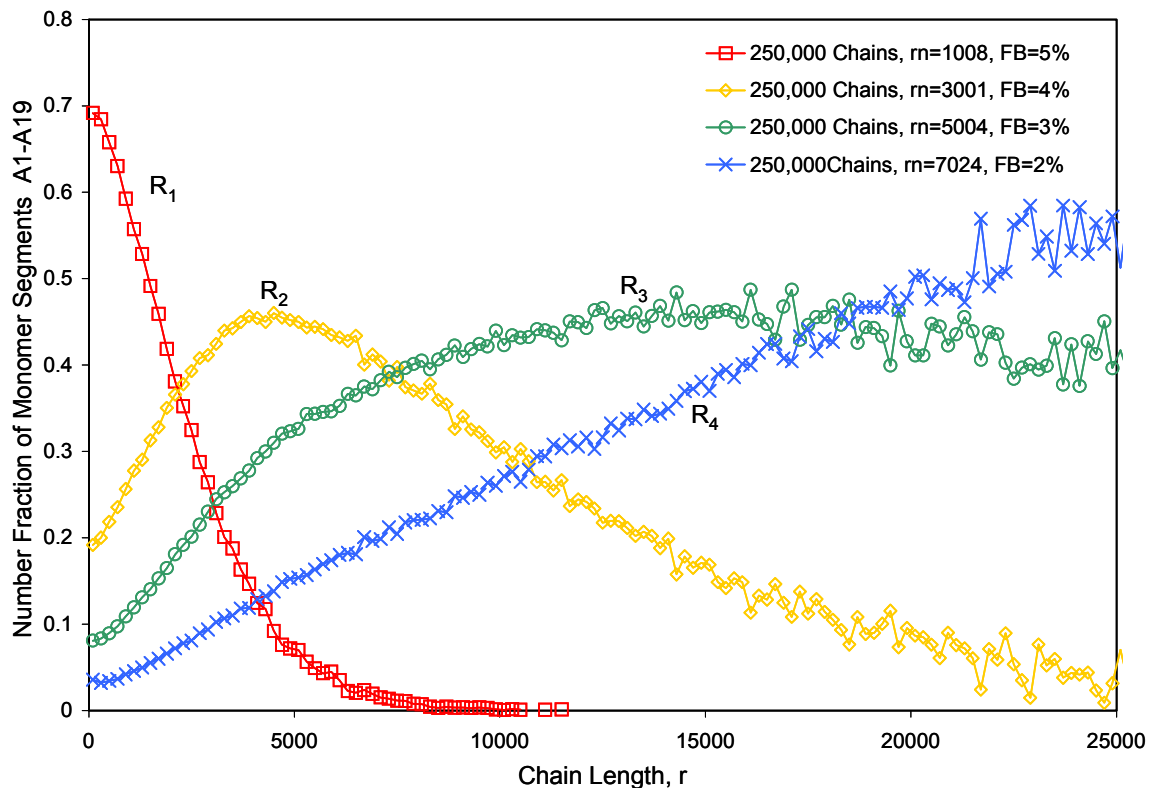
Figure 4-27 Number fraction of monomer segments for A_1 to A_{19} from reactor 1 to reactor 4 before mixing the products as function of chain length (varying r_n, F_B)

The random distribution of the monomer A and comonomer B along the chain is a result of limiting ability of the catalyst to distinguish between the monomer and comonomer as they arrive to the active site. The probability of finding a sequence of N contiguous for monomer A in this random case would be $P_N = prob^N$, where $prob$ is the probability of the catalyst choosing sequence AA rather than BB (Shultz, 2001). The experimentally observed crystal thickness in polyolefins is in the order of several nanometers, that is, it is expected that N should to be 20 or higher. The results in Figure 4-27 represent the fraction of segments in the chain that cannot contribute to the formation of crystalline domains.

Figure 4.28 shows the monomer segment distribution for A_1 - A_{19} as a function of chain length for the final product after mixing reactor 1 to reactor 4. Notice the differences in the distributions from Figure 4.27.
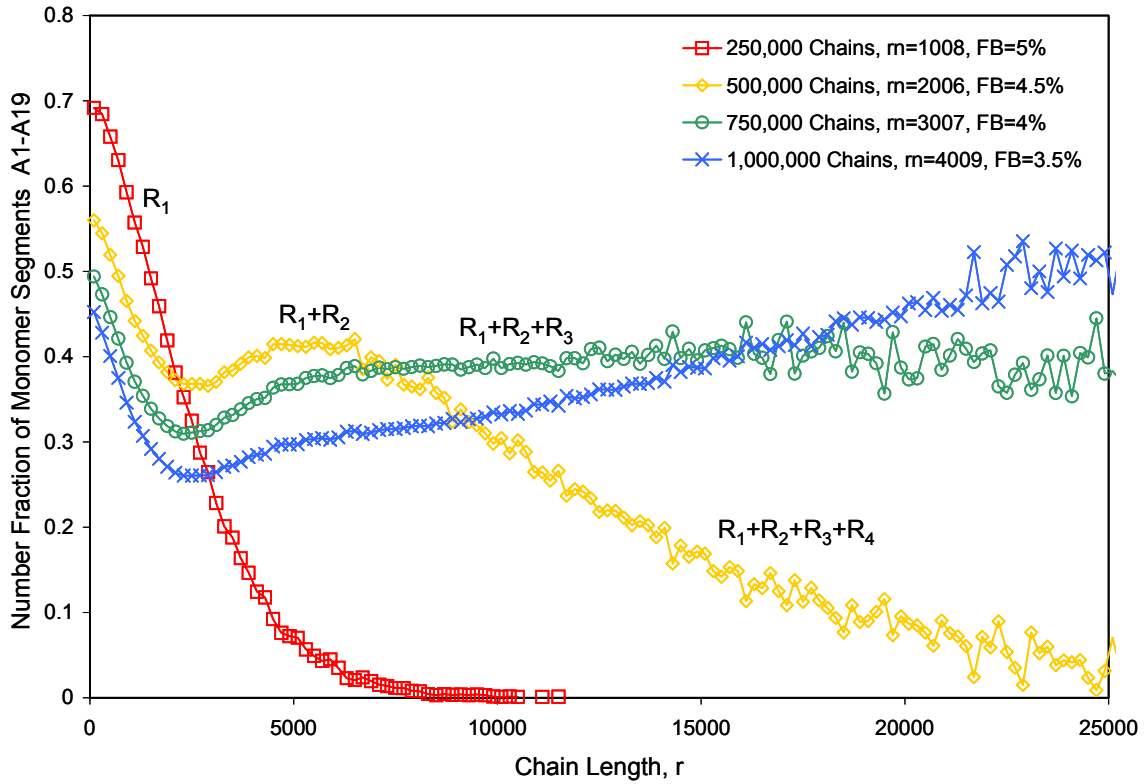
Figure 4-28 Number fraction of monomer segments for A_1 to A_{19} from reactor 1 with 250,000 chains to reactor 4 with 1,000,000 chains as function of chain length (varying r_n, F_B)

Figure 4.29 shows comonomer B distribution for segment length B_{1-6} as a function of the chain length. Those distributions represent the simulation run shown in Table 4.12. In this case each reactor was run separately with different number-average chain length and comonomer incorporation.
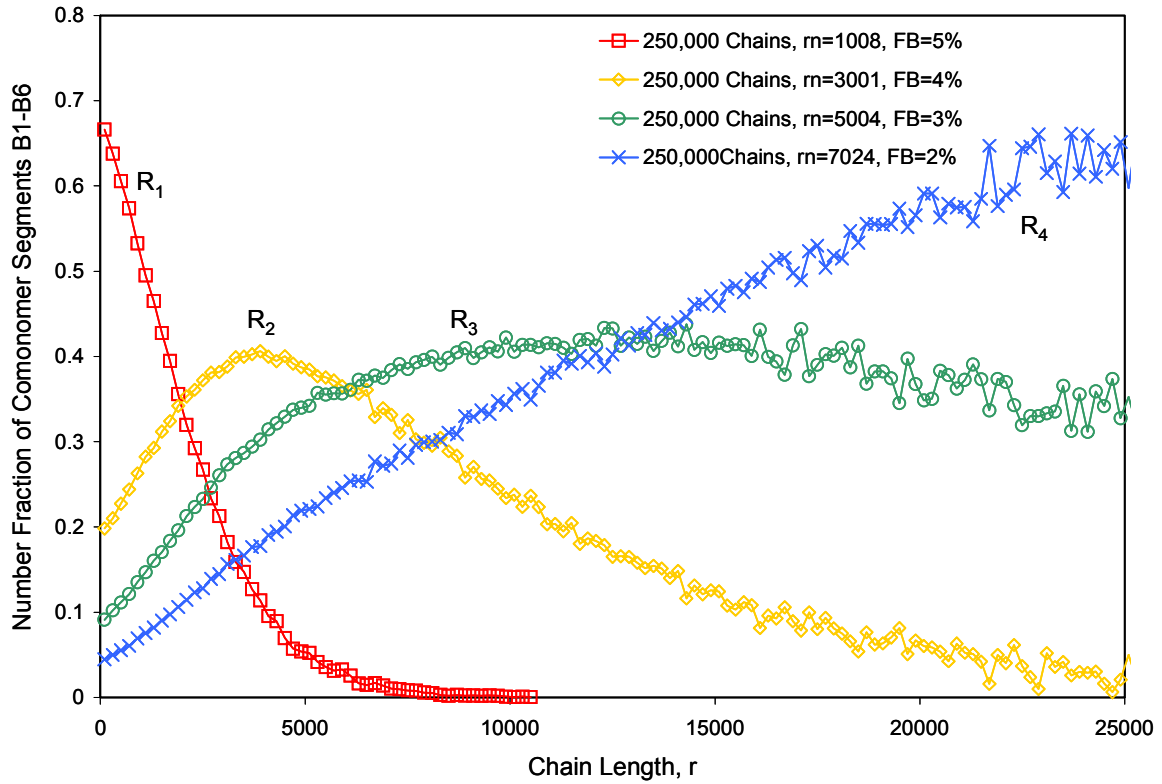
Figure 4-29 Number fraction of monomer segments for B_{1-6} from individual reactor 1 to reactor 4 before mixing the products as function of chain length (varying r_n, F_B)

Figure 4.30 shows the comonomer segment distribution for B_{1-6} as a function of chain length. The distribution showed is representing the product after mixing from reactor 1 to reactor 4. Notice the differences in the distributions from Figure 4.29 where we had the comonomer distribution before mixing the product from each reactor.
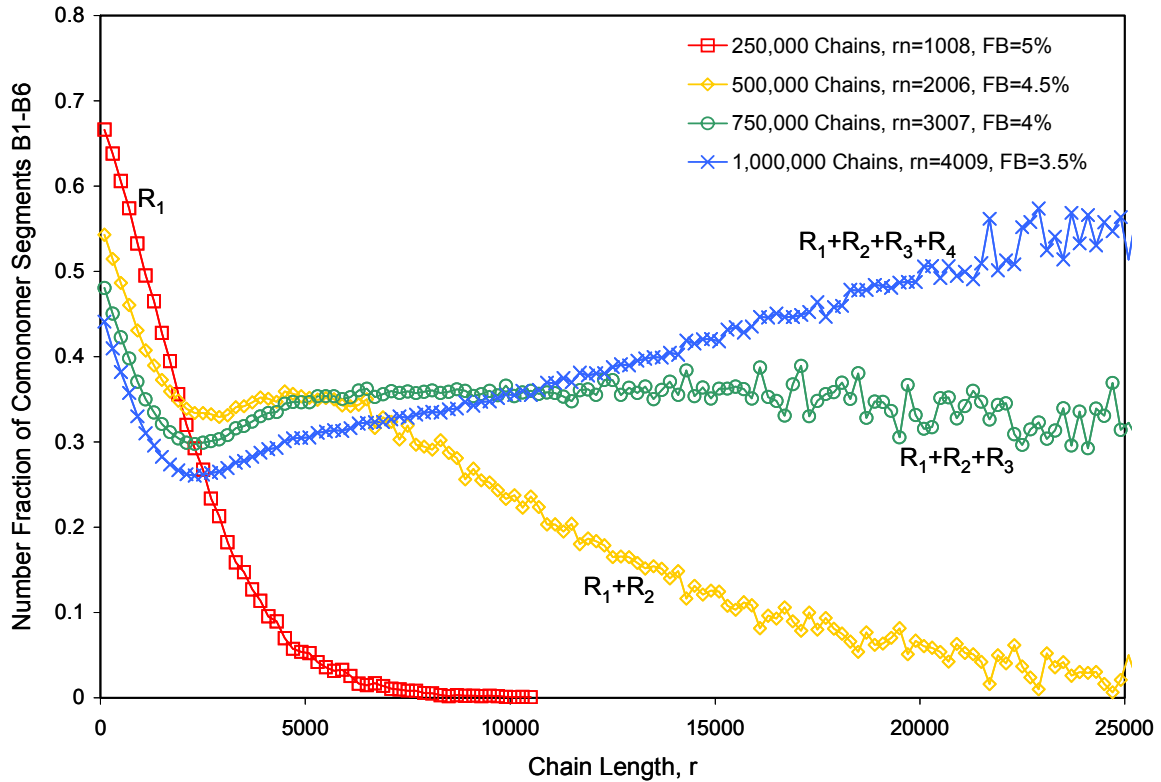
Figure 4-30 Number fraction of comonomer segments for B_{1-6} after mixing the products from reactor 1 with 250,000 chains to reactor 4 with 1,000,000 chains as function of chain length (varying r_n, F_B)

Now we will look at the possible triad distributions as a function of chain length. Being able to quantify the amounts of possible triads is an important step which leads to predicting the ^{13}C nuclear magnetic resonance spectra. Understanding and exploring the monomer and comonomer sequence distributions and the triad distribution enables us to correlate the crystallinity of materials and its thermal and mechanical properties.

Figure 4.31 shows that AAA triad sequence distribution as a function of the chain length. AAA triad increases as the number of chains produced by mixing the products increase from reactor 1 to 4. Having longer chain with more of AAA triad makes more crystalline material possible to be produced. At chain length $r = 3300$ the AAA triad distribution increased after mixing the products from reactor 1 to reactor 4 by 0.46%. This means that the number AAA sequence in the final mixed products from reactor 1 to reactor 4

increased. The encountered increase in the AAA sequence could be explained by knowing that the fraction of comonomer incorporation decreased as we mix the products of reactor 1 to reactor 4.

Figure 4-31 AAA triad distribution from reactor 1 with 250,000 chains to reactor 4 with 1,000,000 chains as function of chain length (varying r_n, F_B)

Figure 4.32 shows ABA sequence distribution drifting by increasing the number of chains produced by mixing the products of reactor 1 to 4. It is noticed that the ABA decreases as the populations of the different reactors are mixed from 250,000 chains to 1,000,000 chains. At chain length $r = 3300$ the ABA triad distribution decreased after mixing the products from reactor 1 to reactor 4 by 0.10%. It is also noticed that the fraction of comonomer incorporation decreased as the products of reactor 1 to reactor 4 are mixed. This explains how we encountered a decrease in the ABA sequence distribution in the mixed products from reactor 1 to reactor 4.

Figure 4-32 ABA triad distribution from reactor 1 with 250,000 chains to reactor 4 with 1,000,000 chains as function of chain length (varying r_n, F_B)

Figure 4.33 shows ABB and BBA sequence distribution drifting by increasing the number of chains produced by mixing the products of reactor 1 to 4. In other words the ABB and BBA decreases as the populations of the different reactors are mixed from 250,000 chains to 1,000,000 chains. At chain length, $r = 3300$ the ABB and BBA triad distribution decreased after mixing the products from reactor 1 to reactor 4 by 0.10%. It is also noticed that the fraction of comonomer incorporation decreased as the products of reactor 1 to reactor 4 are mixed. This explains how we encountered a decrease in the ABB and BBA sequence distribution in the mixed products from reactor 1 to reactor 4.

Figure 4-33 ABB and BBA triad distribution from reactor 1 with 250,000 chains to reactor 4 with 1,000,000 chains as function of chain length (varying r_n, F_B)

Figure 4.34 shows AAB and BAA sequence distribution drifting by increasing the number of chains produced by mixing the products of reactor 1 to 4. At chain length, r=3300 the AAB and BAA triad distribution decreased after mixing the products from reactor 1 to reactor 4 by 0.11%. The fraction of comonomer incorporation decreased as the populations of the different reactors are mixed from 250,000 chains to 1,000,000 chains. This explains how we encountered a decrease in the AAB and BAA sequence distribution in the mixed products from reactor 1 to reactor 4.
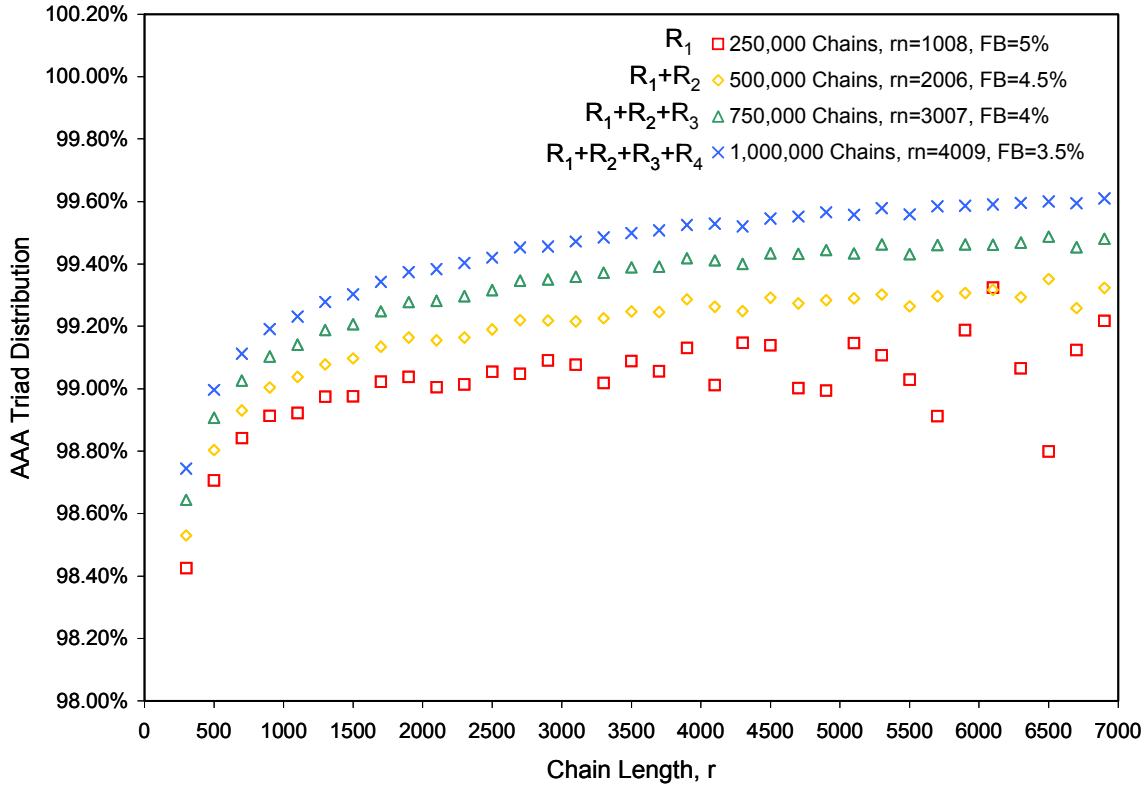
Figure 4-34 AAB and BAA triad distribution from reactor 1 with 250,000 chains to reactor 4 with 1,000,000 chains as function of chain length (varying r_n, F_B)

Figure 4.35 shows BAB sequence distribution drifting by increasing the number of chains produced by mixing the products of reactor 1 to 4. At chain length, $r = 3300$ the BAB triad distribution decreased after mixing the products from reactor 1 to reactor 4 by 0.08%. The fraction of comonomer incorporation decreased as the populations of the different reactors are mixed from 250,000 chains to 1,000,000 chains which explains how we encountered a decrease in the BAB sequence distribution in the mixed products from reactor 1 to reactor 4.
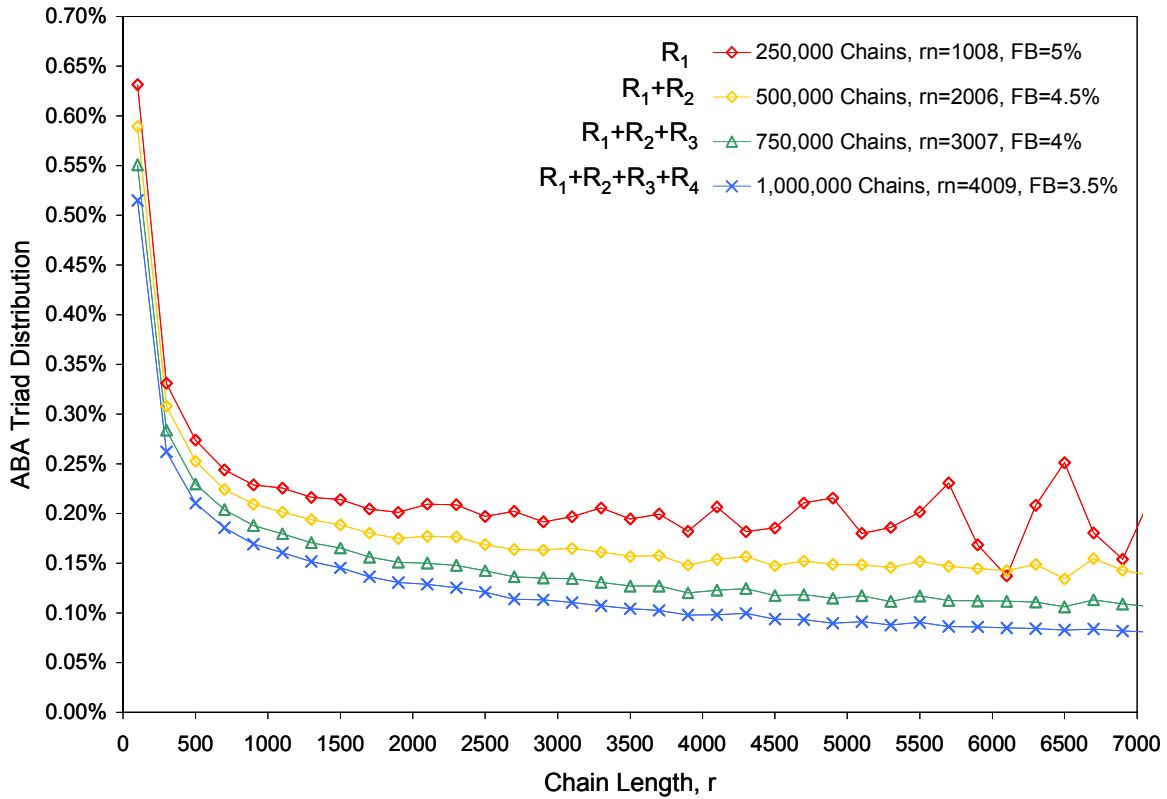
Figure 4-35 BAB triad distribution from reactor 1 with 250,000 chains to reactor 4 with 1,000,000 chains as function of chain length (varying r_n, F_B)

Figure 4.36 shows BBB sequence distribution drifting by increasing the number of chains produced by mixing the products of reactor 1 to 4. At chain length, $r = 3300$ the BBB triad distribution decreased after mixing the products from reactor 1 to reactor 4 by 0.08%. The fraction of comonomer incorporation decreased as the populations of the different reactors are mixed from 250,000 chains to 1,000,000 chains which explains how we encountered a decrease in the BBB sequence distribution in the mixed products from reactor 1 to reactor 4.
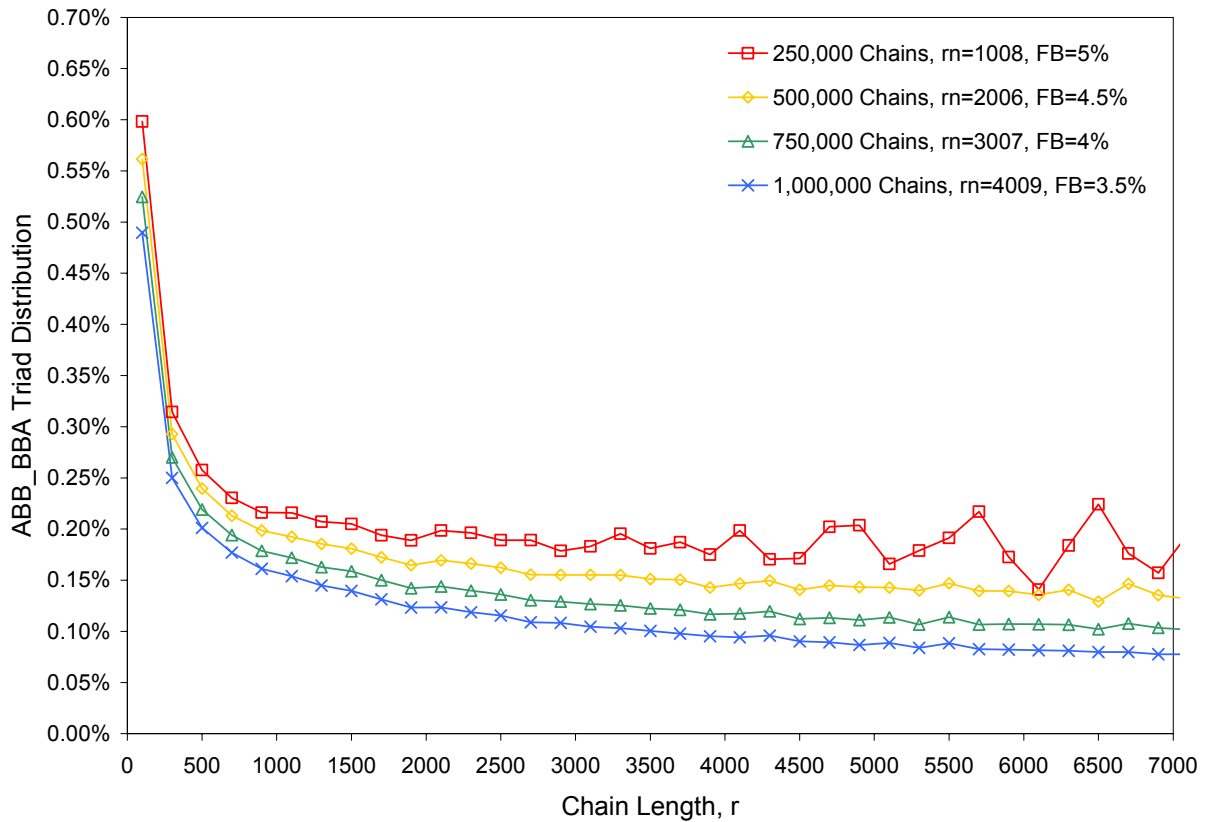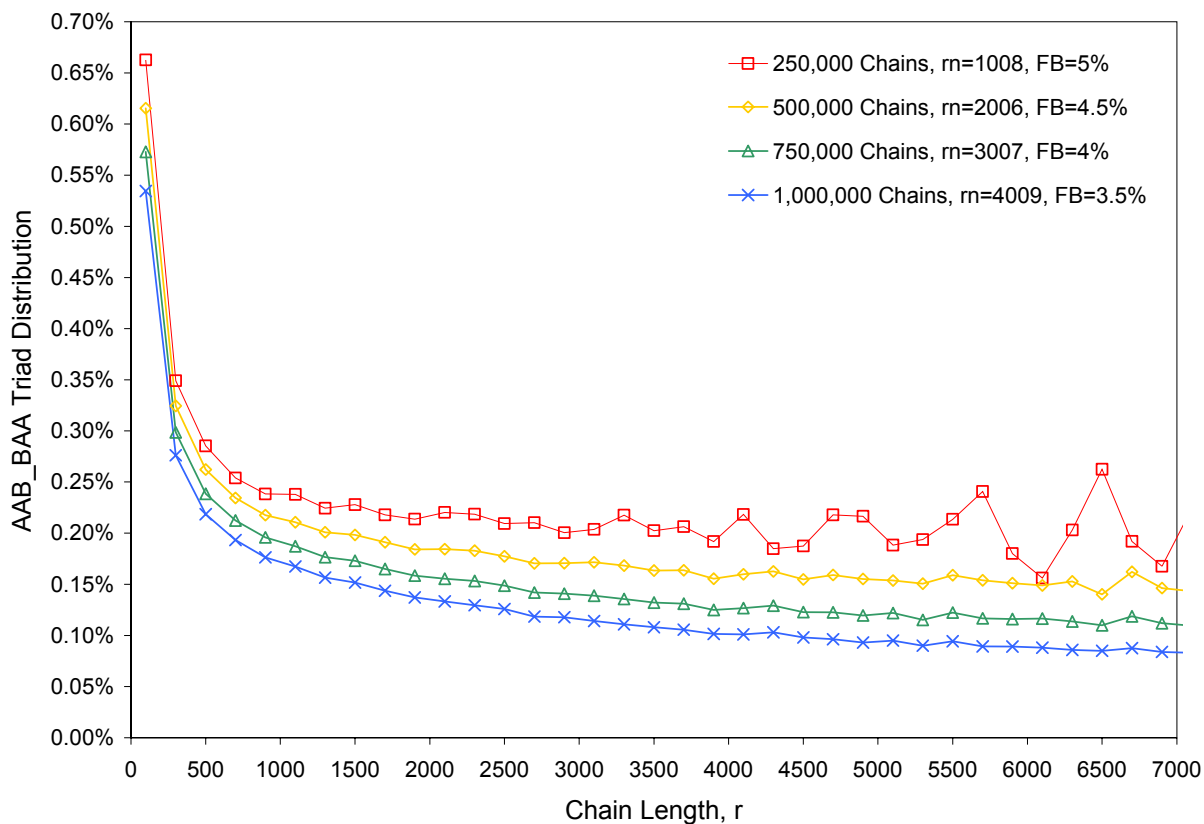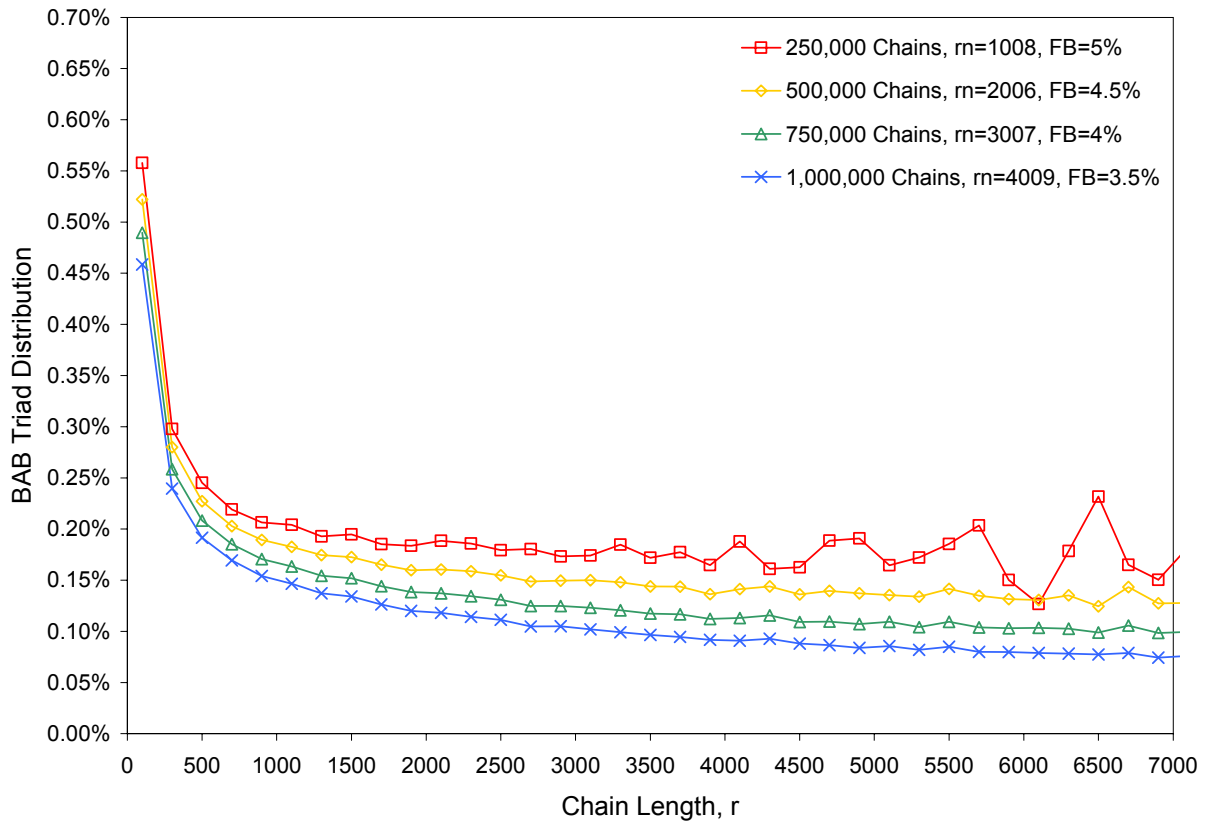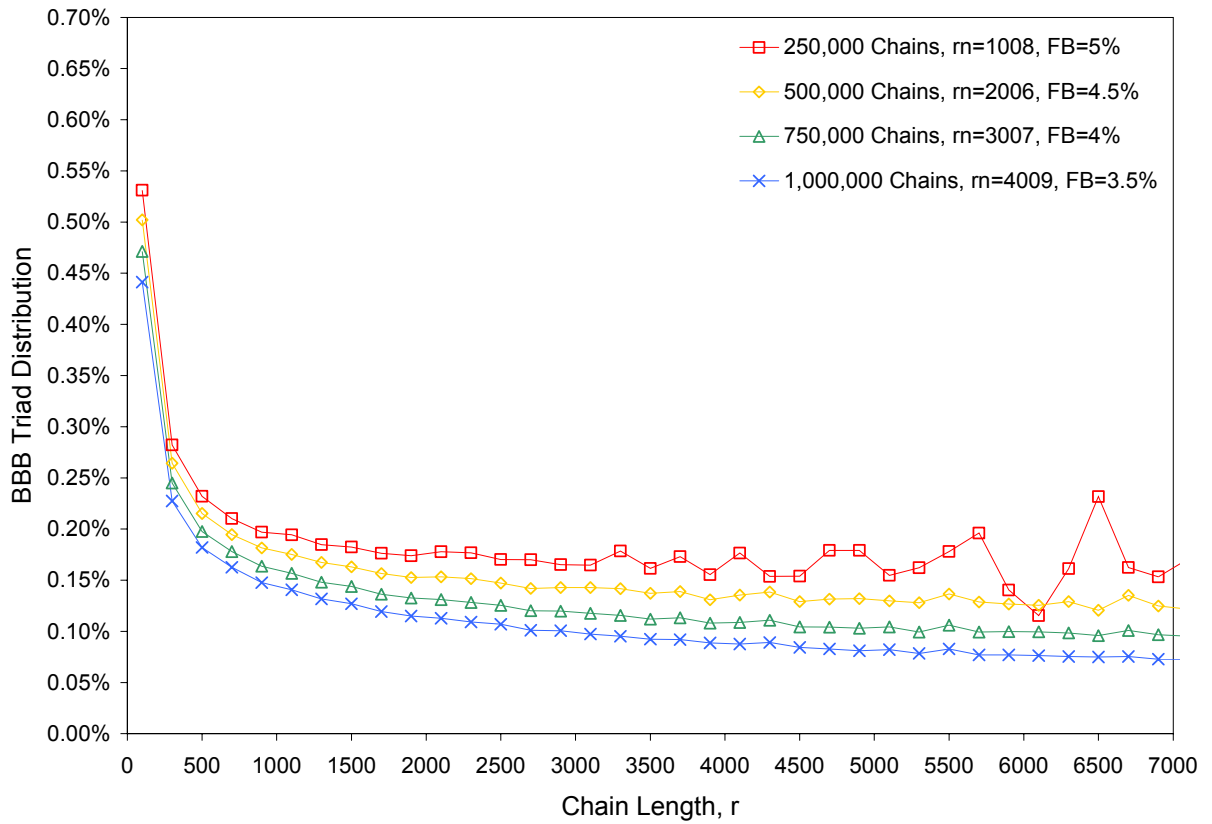
Figure 4-36 BBB triad distribution from reactor 1 with 250,000 chains to reactor 4 with 1,000,000 chains as function of chain length (varying r_n, F_B)

4.6 Calculation of Triad Intensities

We have discussed before, the model can calculate the intensities of the triads which are necessary for predicting the ^{13}C-NMR spectra quantitatively. The model assumes that the polymer chain is made by monomer A and comonomer B. Therefore, different alfa-olefins can play the role of monomer B as long as the appropriate kinetic paramenters are used. Here we will illustrate the ability of using the triad sequence distribution for predicting the ^{13}C-NMR spectra if the case where monomer A is ethylene and comonomer B is 1-hexene. In this case, the sequence ABA will correspond to EHE (ethylene-hexene-ethylene) for instance. First, we will show the major steps to calculate the intensity of each region in the ^{13}C-NMR spectra using the population of reactor 1 (R1 in Table 4-13). Second, we will use the population of the four reactors described in Section 4.5 to illustrate differences in the ^{13}C-NMR spectra.

Table 4.15 shows the total number of triads simulated from reactor 1 with number-average chain length, r_n = 1008 and fraction of comonomer, F_B= 5%. Table 4.16 shows the calculated intensities for each region from region A to region H (Figure 2.11) with the respective equations. The equations are based on the triad values obtained from (Table 4.15).

Table 4-15 Simulation outputs for total possible triads (r_n = 1008 and F_B= 5%)

AAA	AAB_BAA	ABA	ABB_BBA	BAB	BBB
2.51E+08	602346	574038	543913	516421	490599

Table 4-16 Calculated intensities with respective chemical shift assignments (r_n =1008 and F_B= 5%)

Region	Range (ppm) from	to	Contributing Carbons	Intensity Equation	Calculated Intensity
A	39.5	42	αα, Methylene	TA = k(HHH + (1/2) [HHE+EHH])	762556
B	38.1		(Methine)$_{EHE}$	TB = k(EHE)	574038
C	33	36	(Methine)$_{EHH+HHE}$, (Methine)$_{HHH}$, 4B$_4$, αγ, αδ	TC = k(EHE + 2[EHH+HHE] + 2HHH + 2HEH + [HEE+EEH])	4278250
D	28.5	31	δ$^+$δ$^+$, 3B$_4$, γγ, γδ$^+$	TD = k(2EEE + (1/2) [HEE + EEH] + EHE + EHH+HHE + HHH)	502671088
E	26.5	27.5	βδ$^+$	TE = k(HEE+EEH)	602346
F	24	25	ββ	TF = k(HEH)	516421
G	23.4		2B$_4$	TG = k(EHE + EHH+HHE + HHH)	1608550
H	14.1		1B$_4$	TH = k(EHE + EHH+HHE + HHH)	1608550

The intensities and the relative intensities for each region from A to H each reactor 1 and reactor 2 were calculated and presented in Table 4.17. Table 4.18 shows the intensities and relative intensities for reactor 3 and reactor 4 for each region from A to H. The products from each reactor are not mixed with the other.

Table 4-17 Calculated intensities and relative intensities for reactor 1 and reactor 2 with the respective regions for the initial conditions for the reactors before mixing the products

Region	Reactor 1 Calculate intensity	Relative intensity	Reactor 2 Calculate intensity	Relative intensity
A	762555.5	0.149%	1528229	0.100%
B	574038	0.112%	1122226	0.074%
C	4278250	0.835%	8487234	0.557%
D	502671088	98.059%	1.5E+09	98.706%
E	602346	0.118%	1167488	0.077%
F	516421	0.101%	1033002	0.068%
G	1608550	0.314%	3187984	0.209%
H	1608550	0.314%	3187984	0.209%

Table 4-18 Calculated intensities and relative intensities for reactor 3 and reactor 4 with the respective regions for the initial conditions for the reactors before mixing the products

Region	Reactor 3		Reactor 4	
	Calculate intensity	Relative intensity	Calculate intensity	Relative intensity
A	1496155	0.059%	974180	0.028%
B	1072122	0.042%	682393	0.019%
C	8229746	0.326%	5307926	0.151%
D	2.5E+09	99.244%	3.5E+09	99.651%
E	1106152	0.044%	696879	0.020%
F	1010862	0.040%	656752	0.019%
G	3086996	0.122%	1989968	0.057%
H	3086996	0.122%	1989968	0.057%

As expected, there is decrease in the intensity of all the regions associated with branching (A, B, C, E, F, G and H) and an increase in the intensity of region D (which is related to $-CH_2-$ linear segments) when we move from individual populations of reactor 1 towards reactor 4. This trend is in agreement with the average comonomer composition F_B presented in Figure 4-24 and Table 4-12. The simulations results in Tables 4-18 and 4-19 can be correlated with experimental ^{13}C-NMR spectra for the determination of kinetic parameters.

Table 4.19 shows the intensities and relative intensities for reactor 1 and mixture of reactor 1+2. The intensities are divided into the regions from A to H.

Table 4-19 Calculated intensities and relative intensities for reactor 1 and mixture of reactor 1+ 2 with the respective regions for the reactors after mixing the products

Region	Reactor 1		Reactor 1+2	
	Calculate intensity	Relative intensity	Calculate intensity	Relative intensity
A	762556	0.149%	2538724	0.125%
B	574038	0.112%	1892280	0.093%
C	4278250	0.835%	1.4E+07	0.696%
D	502671088	98.059%	2E+09	98.382%
E	602346	0.118%	1978866	0.097%
F	516421	0.101%	1717982	0.084%
G	1608550	0.314%	5331405	0.262%
H	1608550	0.314%	5331405	0.262%

Table 4.20 shows the intensities and relative intensities for the mixture of reactor 1+2+3 and the mixture reactor 1+2+3+4 for the regions from A to H. From Table 4.19 and Table 4.20 we noticed a decrease in all the regions except in region D (linear segments) which increased from 98.059% to 98.913%.

Table 4-20 Calculated intensities and relative intensities for reactor 3 to reactor 4 with the respective regions for the reactors after mixing the products

Region	Reactor 1+2+3		Reactor 1+2+3+4	
	Calculate intensity	Relative intensity	Calculate intensity	Relative intensity
A	4699178	0.103%	6814437	0.084%
B	3476728	0.076%	5019760	0.062%
C	26178871	0.573%	3.8E+07	0.468%
D	4.51E+09	98.668%	8E+09	98.913%
E	3626783	0.079%	5227844	0.065%
F	3179022	0.070%	4608699	0.057%
G	9835386	0.215%	1.4E+07	0.176%
H	9835386	0.215%	1.4E+07	0.176%

Figure 4-37 summarizes the results from Tables 4.19 and 4.20 with the relative intensities in the ^{13}C NMR spectra for the branching regions (all regions except region D). Although the differences look small, they represent the quantitative trend in changing the branching content in this complex mixture of chains. These results can be compared to experimental ^{13}C-NMR spectra as well, for better understanding of the microstructural composition of the polymer sample and for understanding the mechanism of polymerization.
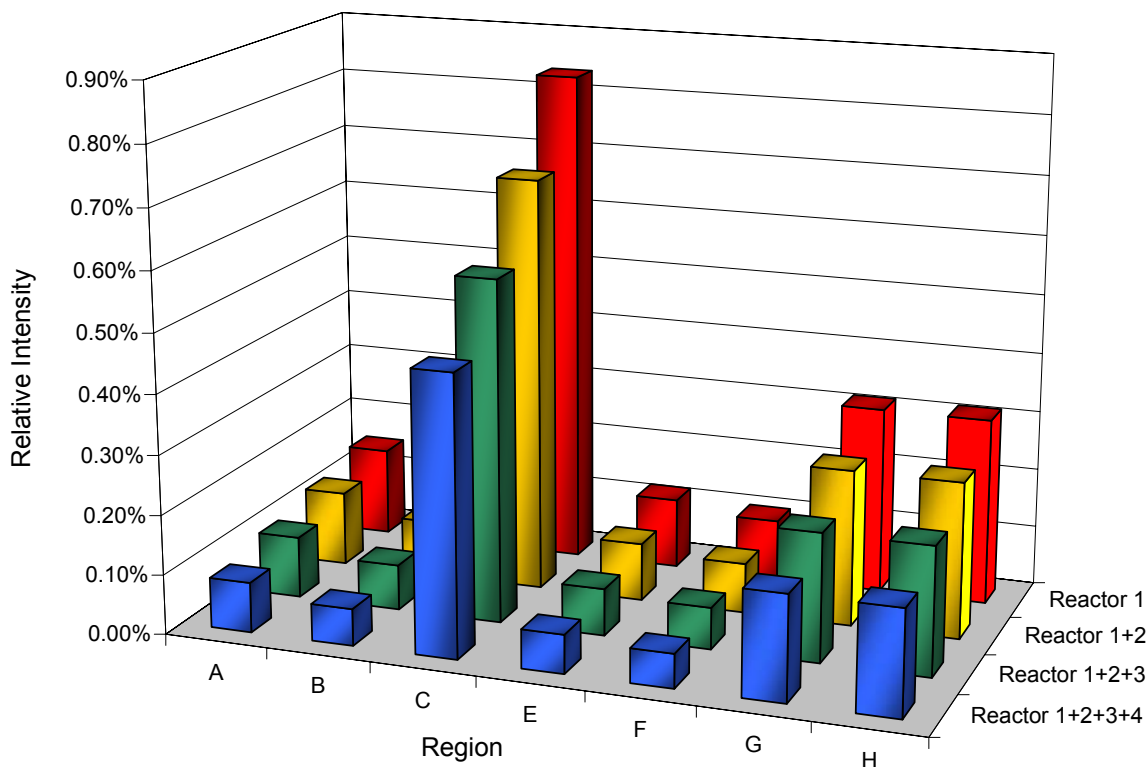
Figure 4-37 Summary of relative intensities of ^{13}C-NMR spectra for different polymer populations simulated in Table 4-13 (region D excluded).

Now we will use the simulation results of triad distribution as a function of chain length to understand contribution in different categories of molecular weight. The objective is to provide a useful comparison with experimental results. In practice, a relatively easy way to obtain a detailed branching distribution as a function of molecular weight involves the fractionation of the polymer sample according to molecular weight followed by ^{13}C-NMR analysis. We will illustrate this by simulation results using the population of reactor 1 (R_1) and the population obtained by mixing all four reactors ($R_1+R_2+R_3+R_4$). The

relative intensities of the ^{13}C NMR spectra will be divided into three categories of chain length: a) low, with chain length < 1100; medium, with 1100 < chain length < 10100; and high, with chain length > 10100. Table 4.21 and Figure 4.38 show fractionated relative intensities for reactor 1. Table 2.22 and Figure 4.39 show the fractionated relative intensities after mixing the product from reactor 1 to reactor 4 (Reactor 1+2+3+4).

Table 4-21 Fractionated population classes for the relative intensities with respective regions of Reactor 1 according to chain length (r)

	Low r<1100	Medium 1100<r<10100	High r>10100
A	0.179%	0.133%	0.102%
B	0.135%	0.100%	0.082%
C	1.004%	0.749%	0.538%
D	97.665%	98.258%	98.717%
E	0.141%	0.106%	0.073%
F	0.121%	0.090%	0.059%
G	0.378%	0.282%	0.215%
H	0.378%	0.282%	0.215%

Table 4-22 Fractionated population classes for the relative intensities with respective regions of reactor 4 after mixing the products from reactor 1 to 4 ($R_1+R_2+R_3+R_4$) according to chain length (r)

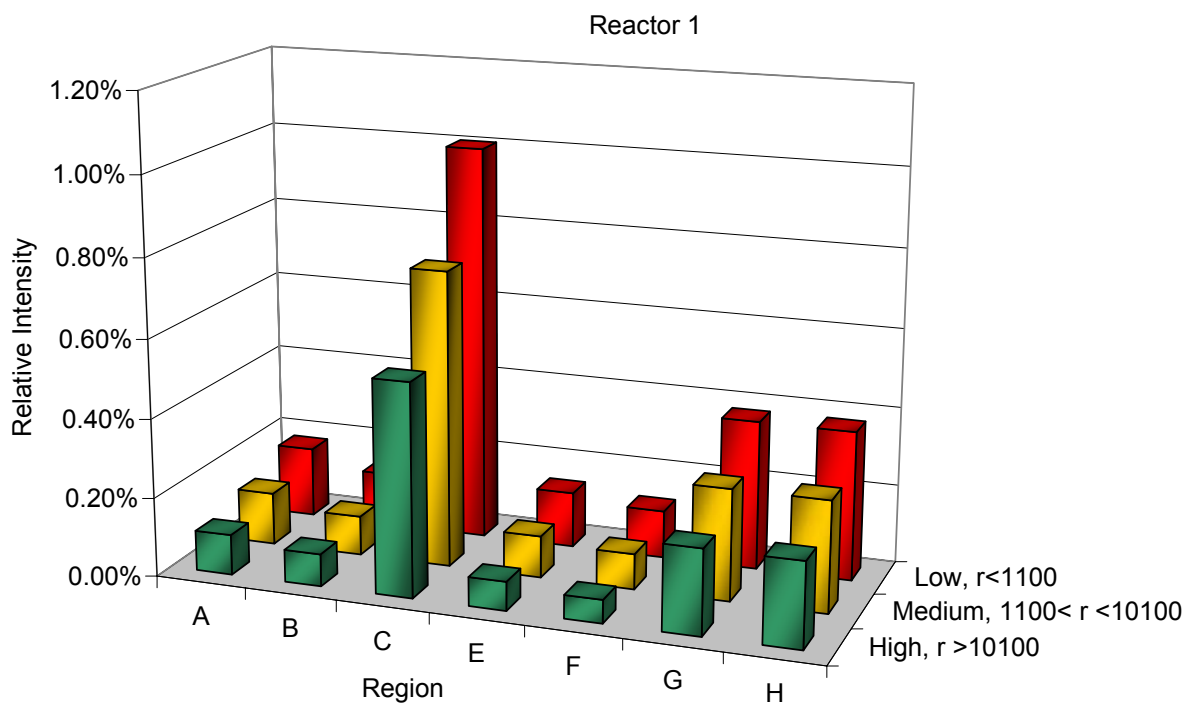|	Low r<1100	Medium 1100<r<10100	High r>10100
A	0.109%	0.080%	0.070%
B	0.080%	0.059%	0.053%
C	0.605%	0.446%	0.381%
D	98.595%	98.964%	99.107%
E	0.083%	0.061%	0.052%
F	0.074%	0.054%	0.045%
G	0.227%	0.167%	0.146%
H	0.227%	0.167%	0.146%

Figure 4-38 Summary of relative intensities of ^{13}C-NMR spectra of the population of Reactor 1 (Table 4.13) for different regions of polymer chain length (Table 4-21, region D excluded).

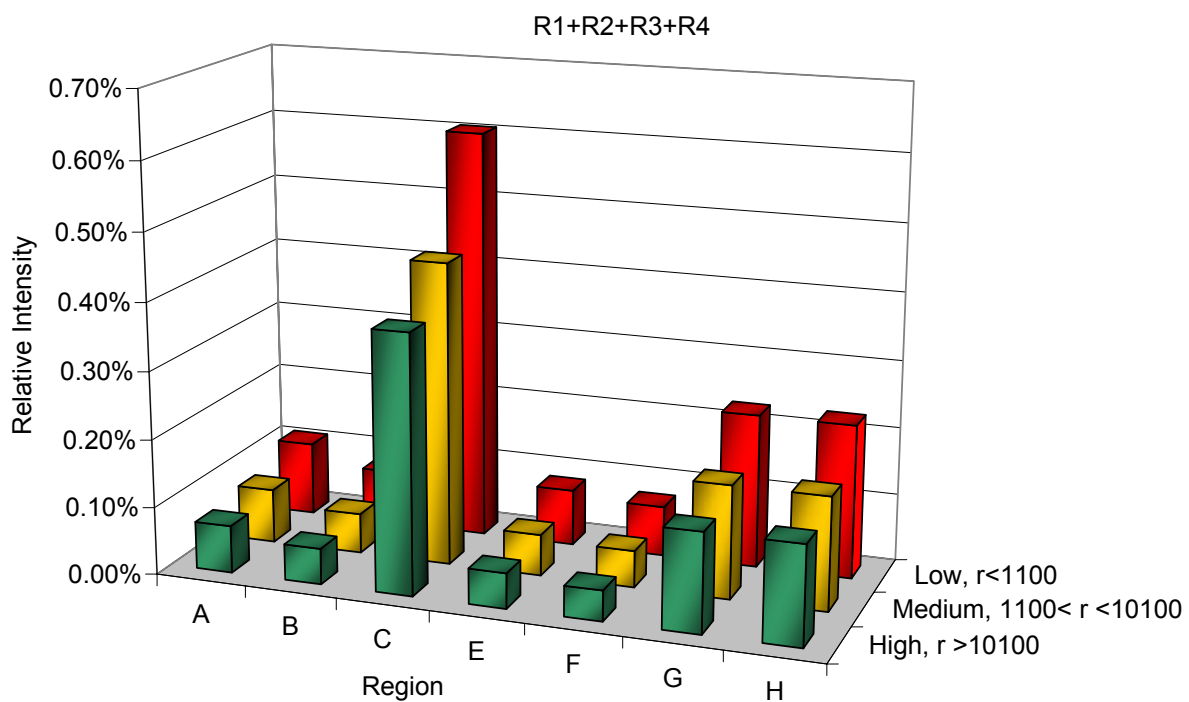Figure 4-39 Summary of relative intensities of ^{13}C-NMR spectra of the mixture of populations ($R_1+R_2+R_3+R_4$) for different regions of polymer chain length (Table 4-22, region D excluded).

Chapter 5 - Conclusions and Recommendations

A comprehensive Monte Carlo model was developed and tested to describe the detailed comonomer distribution in the copolymerization of ethylene and α-olefins. For homopolymerization, the model was able to predict the number fraction of chains produced for a certain chain length. For copolymerization, the model was able to predict chain length and comonomer sequence distribution with great detail. In the case of copolymerization the fraction of monomer B incorporated in the polymer chain was not dependant on the size of the chain, which is in agreement with the polymerization mechanism.

The input information for running the model can be obtained from experimental polymer analysis or through the reaction kinetics. The input information is used to calculate model probabilities that are then used to determine each event of the polymerization mechanism. The probability of propagation is related to the number-average chain length (r_n) and the probability of addition of comonomer is related to the average comonomer distribution (F_B).

The model demonstrated great ability in predicting the detailed segment length distribution as a function of chain length, as well as the relative intensity for the peaks of the ^{13}C NMR. This is a powerful tool to explore the chemical composition of the polymer in more detail. Knowing the segment lengths and triads distribution as a function of chain length is an advantage that allows us to study the polymerization mechanism and the properties of the polymer (like crystallinity).

Some of the suggestions that we would recommend for future work are:

- Account for the different steps in the polymerization mechanism, such as types of transfer reactions, macromonomer incorporation for long chain branching, use of

bifunctional comonomers (dienes for cyclization, branching or functionalization), or catalyst deactivation.

- Include an option in the model for multi-site catalyst. This option will allow the program to cover more types of catalyst systems. As was discussed before metallocene single-site-type catalyst requires single set of kinetic parameters constants whereas with Ziegler-Natta and Philips which are multiple-site-type catalysts require two or more sets of polymerization kinetics constants.

- Expand the use of Monte Carlo simulation to address non-steady state problems for semi-batch experiments on lab scale.

- Develop the model to predict the tetrad distribution and extended further to enable the program to predict the nuclear magnetic resonance spectra.

- Validate the model with laboratory polymerization experiments.

- Use the model to simulate polymer chemical structure.

Reference

Askeland, D.; Phule, P. 2003, The Science and Engineering of Materials, Fourth Edition, Brooks/Cole, Thomson Learning Inc.

Beigzadeh, D., 2003, Monte Carlo Simulation of Long-Chain Branched Polyethylene Chains Synthesized with Dual-Site-Type Catalyst Systems, Macromolecular Theory and Simulation, 12, 174–183

Braun, J.; Madkour, T.; Mark, J. 2004, Some Simulations on Crystallinity in a Typical Linear Low-Density Polyethylene, European Polymer Journal, 40, 245–249

Bruce, M.; Waymouth, R., 1998, Statistical Analysis and Simulation of Pentad Distributions of Stereoblock Polypropylenes, Macromolecules, 31, 2707-2715

Bubeck, R., 2002, Structure–Property Relationships in Metallocene Polyethylenes, Materials Science and Engineering, R 39, 1–28

Cerruti, L., 1999, Historical and Philosophical Remarks on Ziegler-Natta Catalysts, HYLE-International Journal for Philosophy of Chemistry, 5 (1), 3-41

Costeux, S., 2003, Statistical Modeling of Randomly Branched Polymers Produced by Combination of Several Single-Site Catalysts: Toward Optimization of Melt Properties, Macromolecules, 36, 4168-4187

Costeux, S.; Anantawaraskul, S.; Wood-Adams, P.; Soares, J., 2002, Distribution of the Longest Ethylene Sequence in Ethylene/α-Olefin Copolymers Synthesized with Single-Site-Type Catalysts, Macromolecular Theory and Simulation, 11, 326-341

Epacher, E.; Krohnke, C.; Pukanszky, B., 2000, Effect of Catalyst Residues on the Chain Structure and Properties of a Phillips Type Polyethylene, Polymer Engineering and Science, 40 (6), 1458-1468

Fuentes, G.; Monett, D.; Peniche, C.; Arcis, R. W.; Soto, A.; San Roman, J., 2002, Application of a Monte Carlo Method for the Evaluation of Reactivity Ratios in the Copolymerization of Furfurylmethacrylate with N-vinyl-2-pyrrolidone, Latin American Applied Research, 117-122

Galli, P.; Vecellio, G., 2004, Polyolefins: The Most Promising Large-Volume Materials for the 21st Century, Journal of Polymer Science: Part A: Polymer Chemistry, 42, 396–415

Haag, M.; Simon, L.; Soares, J., 2003, Comparing Strategies for the Synthesis Polyolefinic Thermoplastic Elastomers via Macromonomer Incorporation, Macromolecular Theory and Simulation, 12, 142–152

Hoffman, P., 1998, The Man Who Loved Only Numbers: The Story of Paul Erdos and the Search for Mathematical Truth. New York: Hyperion, 238–239

Iedema, P.; Hoefsloot, H., 2004, A Conditional Monte Carlo Method to Predict Branched Architectures from Molecular Weight and Degree of Branching Distribution of Polyethylene for Single and Mixed Systems with a Constrained Geometry Metallocene Catalyst in Continuous Reactors, Polymer, 45, 6071–6082

Kashiwa, N., 2004, The Discovery and Progress of $MgCl_2$-Supported $TiCl_4$ Catalysts, Journal of Polymer Science: Part A: Polymer Chemistry, 42, 1–8

Kou, B.; McAuley, K.; Hsu, C.; Bacon, D.; Yao, K., 2005, Gas-Phase Ethylene/Hexene Copolymerization with Metallocene Catalyst in a Laboratory-Scale Reactor, Industrial Enginering Chemistry Research, 44, 2443–2450

Liang, H.; Li, F.; He, X.; Jiang, W., 2000, Monte Carlo Simulation for the Modification of Polymer via Grafting, European Polymer Journal, 36, 1613–1617

Ling, J.; Ni, X.; Zhang, Y.; Shen, Z., 2000, Monte Carlo Simulation of Gas Phase Polymerization of 1,3-Butadiene Part I. Modeling and Programming, Polymer , 41, 8703–8707

Ling, J.; Ni, X.; Zhang, Y.; Shen, Z., 2003, Monte Carlo Simulation of Gas Phase Polymerization of 1,3-Butadiene. Part II: Kinetics Optimization and Confirmation. Polymer International, 52, 213–217

Ling, J.; Zhang, Y.; Shen, Z.; Nie, J., 2001, Kinetic Simulation of High Viscous Styrene Bulk Polymerization System, European Polymer Journal, 37, 2407–2411

Lu, J.; Zhang, H.; Yang, Y., 1993, Monte Carlo Simulation of Kinetics and Chain-Length Distribution in Radical Polymerization, Makromol. Chem., Theory and Simulation., 2, 747-760

Mohammadi, Y.; Najafi, M.; Haddadi-Asl, V., 2005, Comprehensive Study of Free Radical Copolymerization Using a Monte Carlo Simulation Method, 1 Both Reactivity Ratios Less than Unity (r_A<1 and r_B<1), Macromolecular Theory and Simulation, 14, 325–336

Ohshima, M.; Tanigaki, M., 2000, Quality Control of Polymer Production Processes, Journal of Process Control, 10,135–148

Pasch, H., 2001, Recent Development in Polyolefin Characterization, Macromolecular Symposia, 165, 91–98

Platkowski, K.; Reichert, K., 1999, Application of Monte Carlo Methods for Modelling of Polymerization Reactions, Polymer, 40, 1057–1066

Prescott, S., 2003, Chain-Length Dependence in Living/Controlled Free-Radical Polymerizations: Physical Manifestation and Monte Carlo Simulation of Reversible Transfer Agents, Macromolecules, 36, 9608–9621

Randall, J. C.; Ruff, C. J., 1988, A New Look at the "Run Number" Concept in Copolymer Characterization, Macromolecules, 21, 3446-3454

Randall, J., 1989, A Review of High Resolutuin Liquid ^{13}Carbon Nuclear Magnetic Resonance Characterization of Ethylene-Based Polymers, Macromolecular: Chemistry and Physics, C29 (2-3), 201-317

Salzer, S., 1999, Nomenclature of Organometallic Compounds of the Transition Elements, Pure Applied Chemistry, 71(8), 1557-1585

Schultz, J., 2001, Polymer Crystallization The Development of Crystalline Order in the thermoplastic Polymers, American Chemical Society, Oxford University Press, Chapter 2, 9-25

Seger, M.; Maciel, G., 2004, Quantitative ^{13}C NMR Analysis of Sequence Distributions in Poly(ethylene-co-1-hexene), Analytical Chemistry, 76 (19), 5734-5747

Simon, L.C.; Soares, J.B.P., 2002, Polyethylene Made with Combinations of Single-Site-Type Catalysts: Monte Carlo Simulation of Long-Chain Branch Formation, Macromolecular Theory and Simulation, 11(2), 222-232

Simon, L.C.; Soares, J.B.P., 2005, Monte Carlo Simulation of Long-Chain Branched Polyolefins Made with Dual Catalysts: A Classification of Chain Structures in Topological Branching Families, Industrial Engineering Chemistry Research, 44, 2461–2468

Simon, L.C.; Williams, C.; Soares, J.B.P.; de Souza, R., 2001, Effect of Polymerization Temperature and Pressure on the Microstructure of Ni-Diimine-Catalyzed Polyethylene: Parameter Identification for Monte-Carlo Simulation, Chemical Engineering Science, 56, 4181–4190

Soares, J.B.P., 2004, Polyolefins with Long Chain Branches Made with Single-Site Coordination Catalysts: A Review of Mathematical Modeling Techniques for Polymer Microstructure, Macromolecular Materials and Engineering, 289, 70–87

Soares, J.B.P.; Simon, L.C., 2005, Coordination Polymerization, Chapter 8, Meyer, Keurentjes, Handbook of Polymer Reaction Engineering, Volume 1, Wiley-VCH, 365-428

Tobita, H., 2003, Molecular Weight Development during Simultaneous Chain Scission, Long-Chain Branching and Crosslinking, 2 Free-Radical Polymerization, Molecular Theory and Simulation, 12, 32–41

Tobita, H.; Hamashima, N., 2000, Monte Carlo Simulation of Size Exclusion Chromatography for Randomly Branched and Crosslinked Polymers, Polymer Science: Part B: Polymer Physics, 38, 2009–2018

Tobita, H.; Mima, T.; Okada, A.; Mori, J.; Tanabe, T., 1999, Molecular Weight Distribution Formed during Free-Radical Polymerization in the Presence of Polyfunctional Chain Transfer Agents. Polymer Science: Part B: Polymer Physics, 37, 1267–1275

Whiteley, K.S., 2002, Polyolefins - Polyethylene. Ullmann's Encyclopedia of Industrial Chemistry, InterScience Wiley-VCH

Yashin, V.; Kudryavtsev, V.; Kriksin, A.; Litmanovich, D., 2004, Monte Carlo Simulation of Polymer Analogous Reaction in Confined Conditions: Effects of Ordering, Macromolecular Symposia, 210, 31–40